Measurement of lung mechanics during spontaneous tidal breathing in out-patient care

Sarah Howe

A thesis presented for the degree of
Doctor of Philosophy
in
Mechanical Engineering
at the
University of Canterbury,
Christchurch, New Zealand.

11 August 2020

ABSTRACT

Respiratory disease is a major public health problem worldwide. In New Zealand alone, it costs the economy 5.5 billion NZD annually (∼1.8% GDP), with 1 in 6 New Zealanders affected. Respiratory diseases can be classified as either obstructive or restrictive. Obstructive lung disease is characterized by airway obstruction and increased resistance in the airways. Examples of obstructive lung diseases include asthma, COPD, and cystic fibrosis. Restrictive lung disease is characterised by an inability to inhale due to an increase in lung elastance (a stiff lung), weakness in the muscles controlling respiration, or due to external pressure on the lungs. Examples of restrictive diseases include fibrotic diseases of the lung, neuromuscular disorders and obesity. The different effect the two classes of respiratory disease have on breathing implies a need to assess lung function in terms of both airway resistance and lung elastance.

The most commonly performed lung function test is spirometry. Lung function testing is required to diagnose the type and severity of respiratory disease. Spirometry is able to guide outpatient respiratory care, but does not provide information about the underlying lung mechanics, which change in response to lung condition. These mechanics could provide a true and potentially more accurate assessment of lung condition. However, the underlying lung mechanics are not typically monitored in outpatient care due to the additional cost and specialised equipment required. As such there is a need for an easily accessible, cost effective lung function test to measure lung mechanics.

This thesis develops a novel, model-based lung function test, and an associated testing device, all designed for use in monitoring outpatients with chronic respiratory disease. This test aims to meet the following criteria:

- Measure lung mechanics during spontaneous tidal breathing, to give deeper insight into lung condition while minimising patient effort during testing.

- Test should be easily accessible, able to be performed on widely available testing equipment
- Accurate measurements must be easily obtained, emphasising tidal breathing measurements because peak effort lung testing can be inconsistent, especially in patients with insufficient expiratory ability, which affects ongoing care.

To begin, this thesis assesses whether lung mechanics can be accurately measured during expiration as well as inspiration. This was assessed using data from mechanically ventilated (MV) respiratory failure patients in intensive care. Typically, lung mechanics of MV are calculated during inspiration, since the inspiratory phase has greater potential for ventilator induced lung injury. However, spirometery and other lung function tests in outpatient care typically focus on expiration.

The single compartment lung model was used to assess the inspiratory and expiratory lung mechanics of retrospective data from MV patients. Analysis of the decay rate of airflow showed the lung model was able to capture the lung mechanics of passive expiration. The final modelled expiratory lung elastance showed a strong, linear relationship with inspiratory elastance. There was no relationship between inspiratory and expiratory resistance. This method of measuring expiratory lung mechanics was able to provide reasonable estimates of respiratory mechanics of spontaneously breathing (SB) patients, when no large end-inspiratory SB efforts were present. This study shows that when conventional methods fail, expiratory data may provide clinicians with the real-time lung mechanics measurements needed guide MV therapy.

However, a second measurement of lung mechanics is required to separate mechanics from the decay rate. Because expiration during tidal breathing is not an entirely passive process, a shutter was used to induce exponentially decaying flow during expiration. This technique also allowed lung elastance to be calculated from the alveolar pressure measured during the occlusion. Separation of the flow decay rate using the measured lung elastance showed airway resistance to the airflow was minimal. The volume of air affected by the decaying flow was very small. As such, the resistance component of the decay rate only represents a minimal resistance area in the upper airways. Monitoring the decay rate over time would only give information about lung elastance trends overtime, but not direct values to assess severity.

A better estimation of airway resistance can be obtained by calculating the occlusion resistance. This resistance is calculated from the change in mouth

pressure at the start of occlusion. A human trial of the novel lung function test in Villingen-Schwenningen, Germany, used state-of-the-art medical equipment to analyse lung elastance and resistance. The test briefly occludes airflow during expiration while a subject breathes normally into a spirometer with built-in shutter. This study assessed the tidal breathing lung mechanics of healthy subjects, and showed lung elastance and resistance calculated by breath occlusion were within the expected range for healthy subjects.

When resistance was added to the spirometer mouthpiece to mimic upper airway obstruction, the result was increased measured resistance and a slight increase in elastance for some subjects as work of breathing increased. These outcomes are expected for upper airway obstruction, showing the potential of this breath occluding lung function test to differentiate obstructive and resistive lung diseases. Future work is needed to validate this test with different disease states.

Lung diseases are often not homogeneous, with some regions of the lung being affected by disease, while other regions remain healthy. As such, monitoring average lung mechanics may not provide the detailed level of insight needed clinically, with large and small airways responding differently as the lung tissue expands and contracts during breathing.

The single compartment lung model assumes lung mechanics are constant over time, and calculates the average lung mechanics. More complex lung models are needed to assess lung heterogeneities. Mechanics of the small airways are able to be modelled with multi-compartment lung mechanics models. Comparison of mechanics from these models and the single compartment lung model show the single compartment lung model is unable to capture the mechanics of small airways resistance and lung tissue viscoelasticity. As a result, using the single compartment lung model alone to monitor changes in lung condition over time may miss information about changes in condition of small airways and lung tissue.

Patients undergoing breath-occluding lung function tests are required to support their cheeks to ensure the results correctly represent their underlying respiratory lung mechanics. Cheek support is typically provided by patients placing their hands on their cheeks with thumbs under the chin. This support prevents rapid expansion of the cheeks when pressure builds up in the mouth during breath occlusion. If the cheeks were able to expand, the test would require less patient input, but an additional elastic component would be added to the respiratory

system. This extra elastic component alters the pressure measured at the mouth, and, consequently, affects the measured lung mechanics.

Previous research has shown that measured airways resistance reduced when cheeks were not supported, with the variability of resistance remaining the same regardless of whether cheeks were supported or not. These trends in airway resistance were observed in the data recorded for this thesis. Elastance and lung viscoelasticity were also assessed using the same data. Both of these mechanics were also found to be underestimated when cheek support was missing. The amount of change in each mechanic was subject dependent. As such, no rule-of-thumb to account for missing cheek support could be identified.

An identified limitation to the breath occluding lung function test developed in this thesis was accessibility. The test requires a spirometer with built-in shutter, which is not a typical feature outside of plethysmography. Plethysmographs are the "gold standard" for intrathoracic gas volume measurements and the measurement of specific airway resistance, and, consequently, have heavy clinical use. This limits access to the devices for research. To simplify model development and validation, a desktop spirometer with built-in shutter was developed. This device is a prototype for a spirometer able to measure lung mechanics in a clinical environment, or potentially as a take-home device. The device was able to measure mouth pressure and airflow at a sufficient level required for development and validation of novel breath occluding lung function tests during tidal breathing. It was able to occlude airflow for the 100 ms required by the lung function test, and it was able to repeatedly occlude airflow during a single breath. For use outside of a research environment, or for higher flow rates than found in normal tidal breathing, the device will need slight modification.

Overall the lung function test and methods described in this thesis show promise. They are able to produce reasonable measurements of lung mechanics in healthy subjects during tidal breathing. Clinically, the lung function test could impact current practise, as it does not require high levels of cooperation from patients, allowing a wider cohort to be assessed. Additionally, this test was designed to be widely accessible as it can be implemented with either a small standalone device, or with standard lung function testing equipment. Future work is needed to assess how well lung mechanics can be measured in patients with lung disease, and perhaps to integrate more complex lung mechanics models into the lung function test to give more detailed insight into lung condition.

CONTENTS

ACKNOWLEDGEMENTS

I would like to thank a number of people who supported me along the journey of completing this thesis.

To my primary supervisor, Geoffrey Chase. Thank you for giving me the idea to pursue a PhD in the first place. For letting me work through this thesis at my own pace, and encouraging me to present my work and attend conferences I would otherwise never have been confident enough to.

To my co-supervisor Chris Pretty, thank you for your brilliant insights, and for patiently answering my slightly chaotic questions on your visits down to the Bioeng office. And to my co-supervisor Thomas Desaive, for supplying the data which made me choose this thesis path in the first place.

To Dr Geoff Shaw, for your invaluable advice and guidance throughout this research. And for the introduction to the intensive care unit, which brought home the impact my research could have.

To the team at Furtwangen University, for all the help and support you gave me, and for the compliments even though my German is pretty awful.

To the entire crew in the Bioeng office, for the laughs, distractions, and week-long debates on "what makes soup soup?", and "can a plane on a treadmill fly?".

To my family, thank you always being there to support me in everything I do, and for the guaranteed supply of good food when I visit home.

Finally, thank you to my office plants for bringing life to my desk, and for surviving when I forget to water you for weeks on end.

ABBREVIATIONS

The following are common abbreviations used in this thesis:

Acute respiratory distress syndrome (ARDS)

Chronic obstructive pulmonary disease (COPD)

Total driving elastance (E_d)

Time-varying lung elastance (E_{drs})

Elastance representing muscular breathing effort (E_{dy})

Respiratory system elastance (E_{rs})

Forced expired volume in first second (FEV1)

Functional residual capacity (FRC)

Mechanical ventilation (MV)

Pressure (P(t))

Airway pressure (P_{aw})

Positive end-expiratory pressure (PEEP)

Airflow (Q(t))

Airlow vs volume plot (QV loop)

Airway resistance (R_{aw})

Occlusion resistance (ROCC)

Respiratory system resistance (R_{rs})

Residual volume in the lungs (RV)

Spontaneous breathing (SB)

Total lung capacity (TLC)

Upper airway obstruction (UAO)

Volume (V(t))

Chapter 1

HOW AND WHY DO WE BREATHE?

1.1 PULMONARY ANATOMY

The body needs oxygen to survive. After only four minutes without oxygen, brain cells begin to die. When oxygen is inhaled, it is transported to parts of the body that need it by red blood cells. The same cells will collect carbon dioxide, the waste product produced by cells, and return it to the lungs to be exhaled.

The respiratory system consists of all organs involved in breathing, and is responsible for gas exchange between the air and bloodstream. The main organ of the respiratory system is the lungs. Each lung is enclosed by a membrane called the pleura, which consists of two layers: the visceral layer and the pleural layer. The space between these layers is called the pleural cavity, and is filled with pleural fluid (Patton and Thibodeau [2010]). A cross-section of these layers is shown in Figure 1.1.

The pleural fluid serves two main purposes. It acts as a lubricant, allowing the two layers to easily slide over each other, and it acts as an adhesive, keeping the surface of the lung in contact with the thoracic wall. Pleural fluid is vital for respiration because it allows the lungs to expand by transmitting the driving pressure generated by the diaphragm and intercostal muscles, while minimising trauma due to friction.

Small airsacs called alveoli make up the blood-gas interface in the lungs. The walls of alveoli are extremely thin, less than 0.5 μm, and are tightly wrapped by small blood vessels to allow easy diffusion of gas into and out of the blood. The average lung contains around 300 million alveoli, making up a total surface area of 50-100 m^2 available for diffusive gas exchange.

The shapes of alveoli are highly variable, as shown in Figure 1.2. However, each

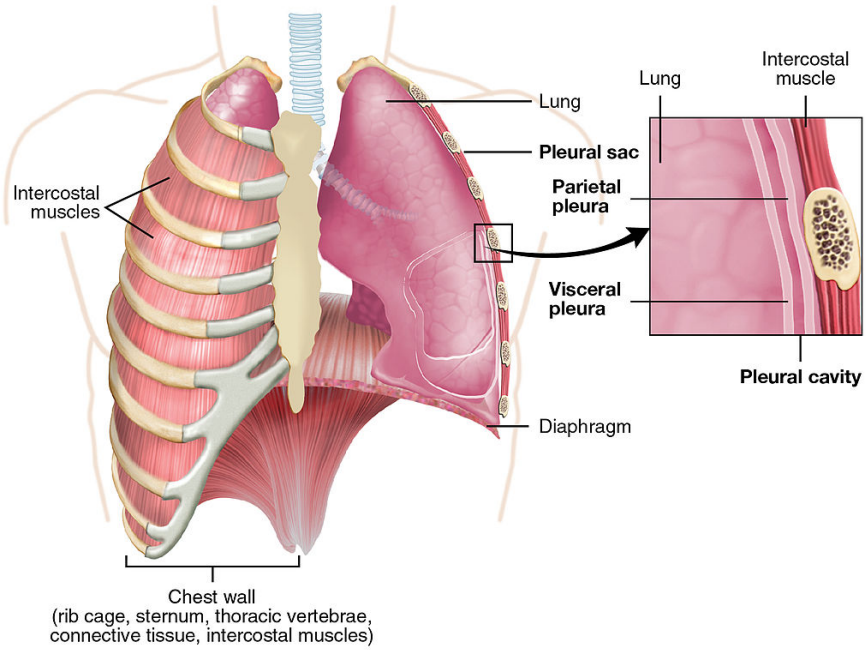

Figure 1.1 The pleura surround the lungs, and are surrounded by the rib cage and intercostal muscles. Liquid inside the pleural cavity helps reduce friction caused by breathing (Illustration from Anatomy & Physiology, Connexions Web site Jun 19, 2013).

alveolus has a diameter of about $\frac{1}{3}$ mm (West [1974]). If alveoli were perfect spheres with their whole surface area available for gas diffusion, their total functional surface area would be approximately 85 m^2 with a combined volume of around 4 L. In comparison, the surface area of a single sphere with a 4 L volume would be only 0.001 m^2. Hence, the division of the lung into smaller units is the factor allowing such a large area for gas diffusion.

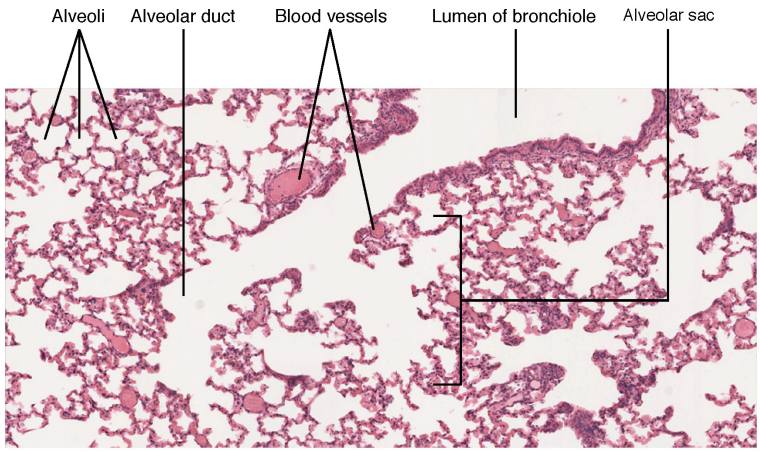

Figure 1.2 A micrograph shows the alveolar structures within lung tissue. (Micrograph from the Regents of University of Michigan Medical School © 2012)

The airways transfer gasses between the alveoli and atmosphere. The respiratory

system contains a system of branching airways, illustrated in Figure 1.3. Each generation of these airways branches to give roughly twice the number of airways as the previous generation (Patton and Thibodeau [2010]).

The trachea is the largest airway, and divides into the left and right primary bronchi, which further divide into segmental bronchi. The bronchi continue to divide in this fashion down to the terminal bronchioles, which are the last airways without alveoli. These first 16 of the total 23 generations do not take part in gas exchange, and make up the anatomical dead space which has a volume of roughly 150 ml (West [1974]). These first 16 generations of airways are important for warming, humidifying and filtering the air, and for speech (Ward [2005]).

The terminal bronchioles divide into respiratory bronchioles, which have occasional alveoli appearing from their walls. The final four generations of the lungs are the alveolar ducts, which are completely lined with alveoli for gas exchange. The final generation has an alveolar sac at the end.

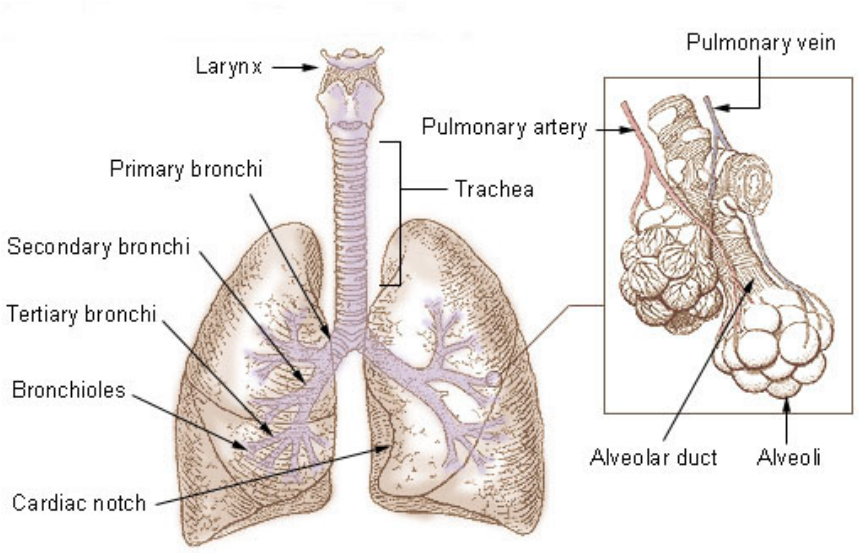

Figure 1.3 The airways have a branching structure, dividing 23 times from the trachea down to the alveolar sacs (Illustration from public domain, from http://training.seer.cancer.gov/anatomy/respiratory/passages/bronchi.html).

The structure of the alveoli is inherently unstable, just like a system of bubbles connected together. Large elastic forces develop in the alveoli due to the surface tension of alveolar lining fluid, which tends to make them collapse. Furthermore, smaller alveoli will tend to empty into larger ones.

Laplace's law shows how the pressure, P, within a bubble is related to the radius,

r, and surface tension, T, of the bubble:

$$P = 2T/r \tag{1.1}$$

This law predicts that as the alveoli begin to empty and reduce in size, the pressure within the alveoli increases. This behaviour creates a positive feed-back loop, speeding up the rate of emptying and causing alveolar instability and collapse. To break this cycle, special cells lining the alveoli secrete surfactant, an oily mixture of phospholipids and apoproteins. Surfactant reduces surface tension, and is more effective in smaller alveoli. The reduction in surface tension caused by surfactant more than offsets the reduction in radius, greatly improving alveolar stability.

1.2 PULMONARY PHYSIOLOGY

The main function of the respiratory system is gas exchange. In addition, the lungs also have other jobs. These include breaking down microthrombi (small blood clots) carried by the veins, filtering toxins from circulation, metabolizing some substances, and acting as a blood reservoir (Ward [2005]). The lungs must draw air into the body for gas exchange to take place. For there to be any airflow, a pressure difference must be created between the inside of the lung and the surrounding air.

During respiration, the diaphragm and respiratory muscles in the chest wall contract and relax, as shown in Figure 1.4, which changes the volume of the lungs. The change in volume leads to a change in pressure, driving airflow. The relationship between pressure, P, and volume, V, in a gas at constant temperature is described by Boyle's law:

$$P_1V_1 = P_2V_2 \tag{1.2}$$

Pressure and volume are inversely proportional. An increase in volume will lead to a decrease in pressure, likewise if volume decreases, pressure increases. As a result, when the diaphragm and respiratory muscles contract during inspiration, expanding the chest cavity, a sub-atmospheric pressure is created in the lungs, drawing air into the airways. Conversely, when the respiratory muscles relax during expiration, lung volume is decreased and air is driven from the lungs.

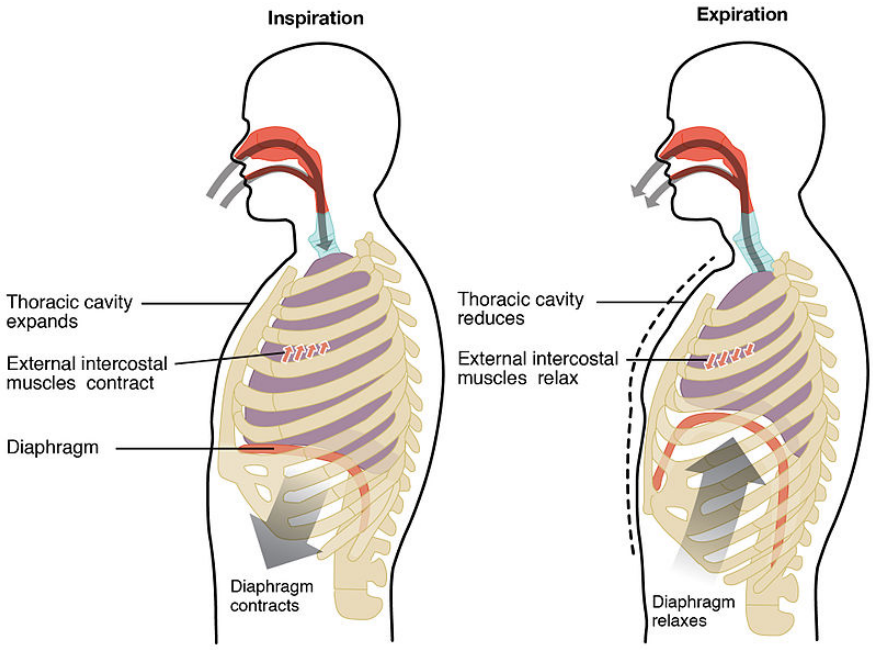

Figure 1.4 Movement of the diaphragm and intercostal muscles cause changes in lung volume during respiration (Illustration from Anatomy & Physiology, Connexions Web site. Jun 19, 2013.)

Expansion of the chest is opposed by the elastic recoil of the lung. Intrapleural pressure is the pressure generated in the pleural cavity by the opposing elastic forces of the lung and chest wall (Lai-Fook and Rodarte [1991]). This pressure is typically negative, acting like a suction cup to keep the lungs from collapsing. However, it can be greater than atmospheric pressure when the intrapleural space is compressed by large expiratory efforts, such as coughing

This behaviour is shown in Figure 1.5, where as the thoracic wall is pulled outward during inspiration, the volume of the pleural cavity increases slightly, decreasing the intrapleural pressure. This pressure decrease is transferred through the pleural wall to expand the lungs, driving airflow. As the thoracic wall recoils during expiration, the volume of the pleural cavity decreases, returning the pressure to its resting value and allowing the lung volume to decrease.

1.3 PULMONARY PATHOPHYSIOLOGY

Pathophysiology is the meeting point of pathology and physiology. Pathology is the study of disease and physiology is the study of the how the body functions. Combining these two areas of research, pathophysiology describes how disease disrupts normal body function.

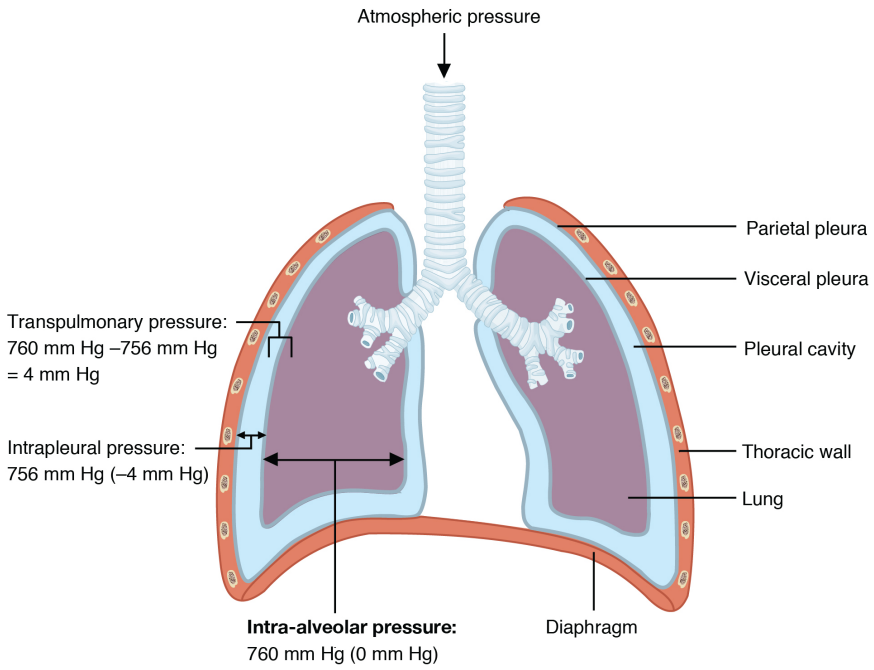

Figure 1.5 The pleural pressure is the pressure in the pleural space, created by the tension between the lung and thoracic wall.

Respiratory failure occurs when the lungs cannot perform their main functions of blood oxygenation and removal of carbon dioxide. It is divided into two categories. Type I respiratory failure is defined by low O_2 and normal or low CO_2 levels. Type II respiratory failure is defined by low O_2 and high CO_2 levels.

Type I respiratory failure is caused by diseases which damage lung tissue, such as pneumonia, acute respiratory distress syndrome (ARDS), and pulmonary oedema. The lung tissue damage leads to reduced blood oxygenation (hypoxaemia). However, removal of CO_2 requires less functional lung tissue, resulting in normal CO_2 levels.

The most common lung diseases which cause type II respiratory failure are chronic obstructive pulmonary disease (COPD) and asthma. Other rarer causes include respiratory muscle weakenss, chest-wall deformities, and severe obesity. These diseases affect the whole lung, reducing its ability to fully expand. The result is the retention of CO_2 in the blood (hypercapnia) and hypoxaemia.

COPD is a prominent cause of mortality and morbidity world wide (Hill et al. [2010], Rabe et al. [2007]). It is a chronic and slowly progressive lung disease, characterized by obstruction to airflow which does not improve over several months (Arne et al. [2010]). The main cause of COPD is inhalation of irritants, namely cigarette smoke (Yang et al. [2017]). Other causes include exposure to air

pollutants, chronic asthma, impaired lung growth and genetic predisposition.

Because of the link between COPD and smoking, it is regarded as a preventable and treatable disease. Thus, early detection and diagnosis are crucial. New Zealand guidelines state that COPD diagnosis requires spirometry (Yang et al. [2017]). However, there is debate about the benefit of using spirometry to guide COPD care, as spirometry-based estimates of COPD prevalence can vary by a factor of two, depending on the definition of mild COPD used (Arne et al. [2010], Rabe et al. [2007], Vollmer et al. [2009]).

Respiratory diseases are classified as either obstructive or restrictive (Pellegrino et al. [2005]). Obstructive lung disease is characterized by airway obstruction. Many obstructive diseases are the result of narrowing of the smaller bronchi and larger bronchioles in the lung, often due to contraction of the smooth muscle itself. The increased resistance to airflow in these narrowed airways makes it difficult to fully exhale. Examples of obstructive lung diseases include asthma, COPD, and cystic fibrosis. Obstructive lung diseases are commonly treated with inhalers and steroids to relax smooth muscles (Antus [2013]).

Restrictive diseases reduce the lung's ability to inhale and bring more oxygen into the lung due to an increase in lung elastance (a stiff lung), weakness in the muscles controlling respiration, or due to external pressure on the lungs. Examples include fibrotic diseases of the lung, neuromuscular disorders and obesity. Treatments for restrictive diseases are often unable to reverse the effect of the disease, but aim to improve quality of life. Typical treatments can include antibiotics, immunosuppressants, oxygen therapy, or non-invasive mechanical ventilation to assist or replace the work of breathing (Ambrosino et al. [2009], Caronia [2016]).

The different effect the two classes of respiratory disease have on breathing implies a need to assess lung function for inhalation and exhalation separately: Restrictive diseases limit lung volume, affecting inspiration, and obstructive diseases reduce airflow, affecting expiration. In both cases, blood oxygen levels drop and the body is starved of oxygen.

Notably, the mechanics of the two breathing phases are different. Inhalation is driven by muscular ability to create negative pressure in the lungs. Expiration is a function of lung and muscle relaxation, and when forced is a function of chest wall stiffness and muscular contraction to create lung pressure and drive out air.

1.4 SUMMARY

Lungs are complicated organs. As a result, they can be affected by numerous, and vastly varied diseases. In order for clinicians to correctly and quickly diagnose the specific type of disease affecting a patient's lungs, it is necessary for them to have access to reliable, real-time lung function tests.

Chapter 2

HOW IS LUNG HEALTH MEASURED?

2.1 PULMONARY WAVEFORM MEASUREMENT

2.1.1 Pressure

Respiratory pressures are commonly measured using piezoresistive pressure transducers. The voltage produced by these sensors will vary depending on the amount of deformation of the sensor from the air pressure. Many of these sensors are able to measure a pressure difference between two pressure ports. The pressure difference can be uni-directional, meaning one port must have a higher pressure, or bi-directional. When used in spirometry, pressure sensors measure the pressure drop between the mouth and atmosphere. This pressure drop across the spirometer can be translated into a flow-rate, if the resistance of the spirometer is known.

Measurements of the intrathoracic pressure are useful for determining lung mechanics and the work of breathing. The difference between the intrapulmonary pressure and the pressure at the airway opening is the transpulmonary pressure. This value is the pressure required to inflate the lung. The airway opening pressure is the pressure at the the mouth for unintubated, quiet breathing. However, direct pressure measurements in the pleural cavity are highly invasive and risky because they typically involve puncturing the chest wall, which comes with a high risk of pneumothorax (lung collapse due to air in the pleural space).

Studies in the 1950s showed intra-oesophageal pressure reflects changes in intrathoracic pressure (M. B. McIlroy and E. S. Thomlinson [1955]). To have the best estimate of the intrapleural pressure, the pressure sensor must be placed close to

the pleural wall so the pressure in the pleural space is transmitted through to the sensor. An oesophageal balloon placed in the lower third of the oesophagus will closely match the pleural pressure (Hofmann et al. [2016]), allowing the driving pressure of respiration to be estimated. These types of pressure measurements are highly invasive so they are not often used clinically.

2.1.2 Flow

Airflow is measured by the addition of sensors to the breathing circuit made up of the lungs, airways, and any resistance to airflow external to the body. Common flow sensors used clinically are hot-wire anemometers, ultrasound flow meters, orifice plate flow meters, and linear resistance pneumotachometers (Schena et al. [2015]). Orifice plates and pneumotachometers are popular in research applications due to their simplicity. Airflow through one of these sensors will create a pressure drop over the sensor's known internal resistance, allowing the flowrate to be calculated from Ohm's law:

$$Pressure = Flow \times Resistance \tag{2.1}$$

2.1.3 Volume

Integrating flowrate with respect to time will give the volume of air inspired/expired. Typically, volume is measured with the reference volume, $V = 0$, at the start of inspiration, yielding a tidal volume for the breath. More invasive techniques are required to measure the residual amount of air left in the lungs at the end of expiration, denoted function residual capacity (FRC).

2.1.4 Functional residual capacity

FRC is the amount of air remaining in the lungs after expiration during normal, quiet breathing. Measurements of FRC are useful for distinguishing different types of lung disease. Direct measurements of FRC are much more difficult and can be more invasive than tidal volume measurements, because the entire volume of the lungs cannot be exhaled through a spirometer. The measurement of FRC requires body plethysmography or a helium gas dilution test (Stocks et al. [2001]).

FRC is affected by disease. Lung fibrosis, a restrictive disease where the lungs have abnormally high elastic recoil, causes a decrease in FRC. The reduction is

due to the highly elastic lungs balancing with the opposing recoil of the chest wall at a lower lung volume. However, restrictive diseases caused by weakness of respiratory muscles do not affect FRC because the elastic forces are normal. This difference helps distinguish restrictive disease caused by lung fibrosis and muscle weakness. In emphysema, lung tissue involved in gas exchange is destroyed. This destruction reduces the lung's elastic recoil, increasing FRC. FRC can also be increased in obstructive diseases with high airway resistance (E.g. COPD and severe asthma). These diseases slow the rate of expiration, and the patient must breathe in before breathing out fully, causing air trapping and leading to a rise in FRC.

2.1.5 Summary of waveform measurement

Lung condition cannot be accurately assessed without taking measurements of the respiratory system. Common measurements include airflow, lung volume, and pressure. The shape and magnitude of these waveforms can inform clinicians whether lung capacity or the output of the lung is abnormal, which may indicate disease.

2.2 LUNG FUNCTION TESTS

2.2.1 Spirometry

Spirometry is a simple pulmonary test and an important tool in monitoring lung condition. The patient breathes into a small device which measured airflow from the mouth, as shown in Figure 2.1. Breathing manoeuvres are used to assess whether a patient has reduced air flow or lung capacity, which would indicate possible respiratory disease.

The results of spirometry are highly dependent on the patient's ability to cooperate or participate in the test (Miller et al. [2005]). However, misdiagnosis can occur if the required breathing manoeuvres are performed poorly or are unable to be repeated reliably, which is particularly difficult to achieve in maximum effort spirometry tests. For this reason, elderly and children may not be able to participate effectively (Ruppel and Enright [2012]). Some of the major parameters measured by spirometry are outlined in Table 2.1.

Spirometry results are compared against reference values to diagnose respiratory disease (Stanojevic et al. [2010]). A widely accepted standard for diagnosing

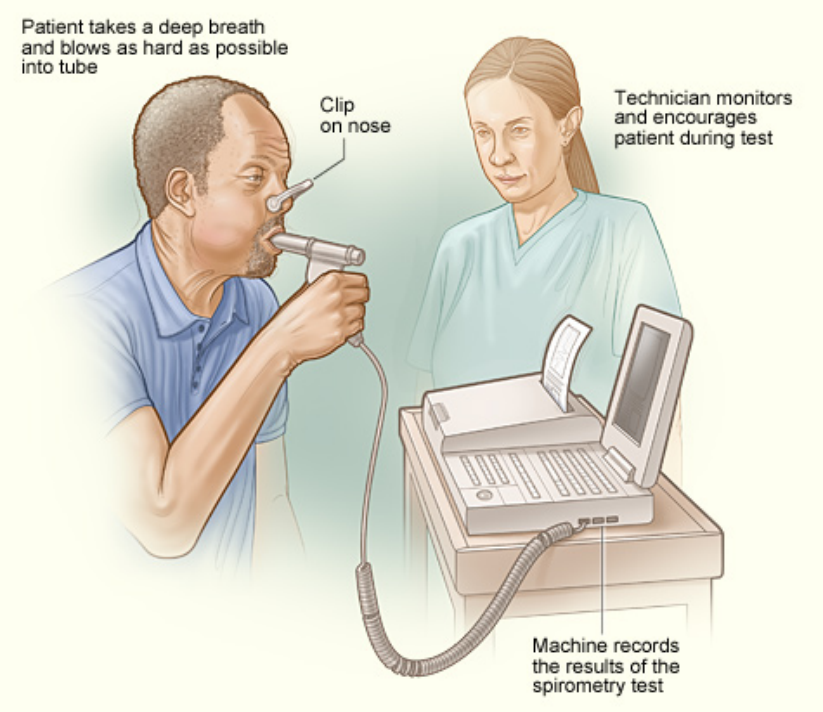

Figure 2.1 An example of forced expiration in spirometry. The spirometer measured the rate of airflow and volume of air passing through the mouthpiece. Image sourced from National Heart Lung and Blood Insitute (NIH)

COPD is the Global Initiative for Chronic Obstructive Lung Disease (GOLD) classification. GOLD uses fixed cut-off values for FEV1/FVC to diagnose the severity of COPD by placing patients into one of four categories, from mild to very severe COPD. Additionally, GOLD specifies a recommended treatment plan for each level of COPD (Rabe et al. [2007]).

A rule-of-thumb is a FEV1/FVC ratio below 0.7 indicates an obstructive condition (Mohamed Hoesein et al. [2011]). Examples of volume traces for normal and diseased lungs are shown in Figure 2.2. However, the use of fixed cut-offs can cause misclassification of spirometry results, with a tendency to over diagnose airway obstruction in the elderly and under diagnose in children (Gólczewski et al. [2012], Miller et al. [2011], Ruppel and Enright [2012], Stanojevic et al. [2010]). This issue has lead to debate around the efficacy of current spirometric standards to predict asthma, COPD and other obstructive conditions affecting breathing function (Arne et al. [2010], Coates et al. [2014], Owens et al. [1991], Vollmer et al. [2009]).

Intermittent measurement of lung function is another limiting factor in diagnosis of some respiratory diseases. Asthma is a disease with reports of significant

Table 2.1 Parameters measured in spirometry

Vital Capacity (VC)	Volume exhaled after full inspiration
Forced Vital Capacity (FVC)	Volume forcibly exhaled after full inspiration
Forced Expiratory Volume in 1 second (FEV1)	Volume forcibly exhaled the first second after full inspiration
Functional Residual Capacity (FRC)	Volume of air remaining in the lungs after forced expiration
Residual Volume (RV)	Volume of air remaining in the lungs after normal expiration
Peak Expiratory Flow (PEF)	Maximum flow rate in a forced expiration. Measured with a peak flow meter
Total Lung Capacity (TLC)	Total volume of the lungs after full inhalation. Is the sum of RV and VC

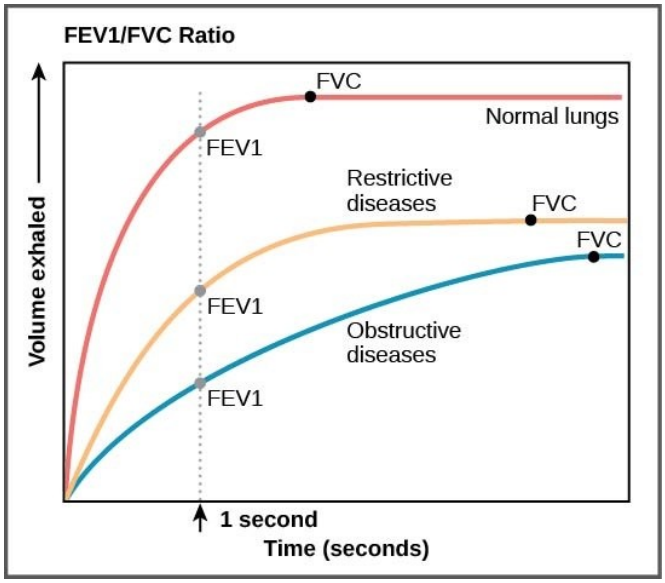

Figure 2.2 Volume traces measured for healthy and diseased lungs. As lung function decreases due to disease, the FEV1/FVC ratio also decreases. This decrease indicates airflow reduction. Reproduced from Physiology of breathing I - Jane Ward

misdiagnosis (Magnoni et al. [2015], Pakhale et al. [2011], Stanbrook and Kaplan [2008]). Lung mechanics can appear normal in asthmatics between exacerbation events, further complicating diagnosis with spirometry (Schifano et al. [2014]). As a consequence, physicians often recommend patients monitor peak expiratory flow at home as an alternative to spirometry (Ignacio-Garcia and Gonzalez-Santos [1995]), which is itself highly variable (Ignacio-Garcia and Gonzalez-Santos [1995]).

Finally, the metrics in Table 2.1 notably focus on expiration. Spirometry is thus more suited to assessing and monitoring obstructive diseases than the less common

restrictive diseases. Lung volume measurements, requiring a full pulmonary function testing laboratory, are needed to confirm restrictive diseases (Johnson and Theurer [2014]), adding difficulty and cost.

2.2.1.1 Difficulty with direct lung mechanics measurements

Spirometry measures pressure and flow at the mouth. These values are the expected outputs from a lung model. The main problem preventing the use of lung models in standard spirometry is the driving pressure created by the diaphragm and chest muscles is not known or easily measured. Without a driving pressure, lung mechanics cannot be easily determined. Nevertheless, numerous pulmonary tests able to measure respiratory resistance and reactance are available (Ranu et al. [2011], Ruppel and Enright [2012]).

2.2.1.2 Occlusion techniques

Resistance may also be assessed during spirometry using an interrupter technique (Panagou et al. [2004]). This method blocks airflow during tidal breathing to estimate alveolar pressure. The technique is based on the assumption that when the airway is suddenly occluded during the tidal breathing, there is a pressure change in the mouth, equaling the resistive pressure drop across the airways. Interrupter resistance (Rint) can be estimated by dividing this pressure difference by the pre-occlusion flow. The measured resistance (Rint) relates alveolar pressure to pressure at the mouth. Although this test is able to simply measure lung mechanics, it is not easily used in regular daily care due to the limited availability of specialised equipment.

Respiratory mechanics can be evaluated through passive measurements when the respiratory muscles are relaxed. Passive respiratory mechanics give information about elastance and resistance of the whole respiratory system, and may be obtained through single or multiple occlusion techniques. Hence, there is a need to provide better access to clinical devices able to measure these easily obtained lung metrics.

2.2.1.3 Weighted spirometer technique

The weighted spirometer technique is a variation of spirometry which is able to measure lung elastance during tidal breathing without occluding breathing. This test is simple and non-invasive enough to be carried out on sleeping infants with

no sedation (Tepper et al. [1984]).

The spirometer used in this test is a water-sealed spirometer. This is a closed circuit system with CO_2 absorber. Figure 2.3 shows the actual setup used in studies (Tepper et al. [1984]).

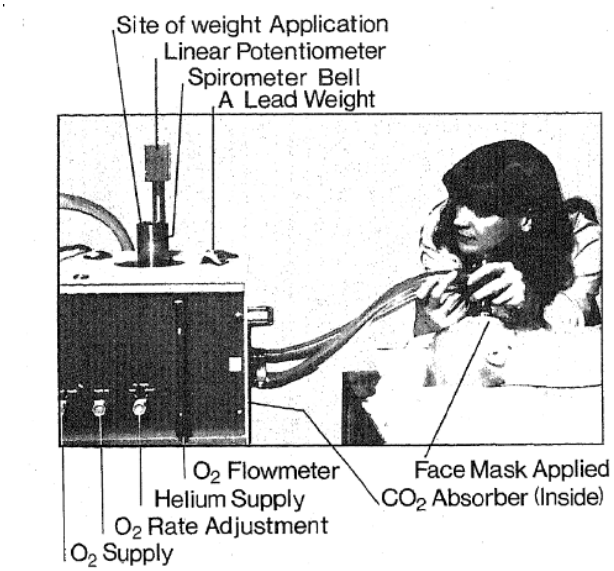

Figure 2.3 Illustration of the spirometer closed-circuit system as applied to an infant. Image sourced from Tepper et al. [1984]

Weights are placed on the bell while the patient breathes into the sealed spirometer system. The resting lung volume would increase when the weight was added due to the increased end-expiratory pressure in the system. The lung compliance can then be measured by relating the change in lung volume to the change in pressure. In this technique, a number of breaths must be allowed to give time for the system to equalise. The lung complaince, C_{rs}, obtained from this method is "quasi-static" because the subject still breaths spontaneously during the measurements.

An assumption of this method is that the chest wall muscles are completely and equally relaxed at the end of each breath. Figure 2.4 shows the recorded volume and pressure from the spirometer during lung mechanics testing. Compliance recorded with this method were shown to be comparable to those found using other techniques; Manual Inflations of the lungs under anesthesia, and airway occlusion Technique (Tepper et al. [1984]).

The drawback of the weighted spirometer technique is it requires highly specialised spirometers. As a result, despite it's simplicity to use and interpret results, this technique is not commonly used to assess lung condition.

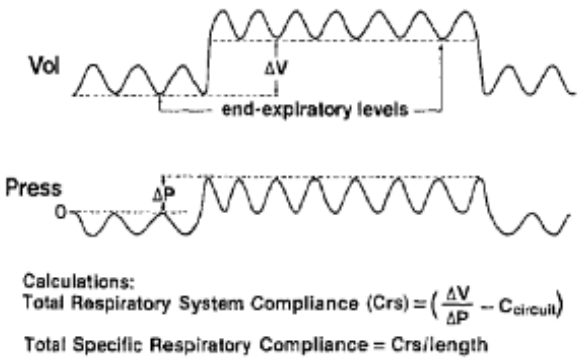

Figure 2.4 Calculation of the total respiratory system compliance. Image sourced from Tepper et al. [1984]

2.2.2 Plethysmography

Modern plethysmography started with DuBois et al. [1956]. Plethysmography provides information on lung residual volume (RV), total lung capacity (TLC), airway resistance and intrathoracic gas volume (ITGV). This information is not provided by spirometry, which is the gold standard in lung function testing.

Moreover, plethysmography records data while the patient is breathing normally, requiring no forced maneuvres. Due to the differences between plethysmography and spirometry, a typical plethysmography measurement cycle includes spirometry.

A constant volume, whole body plethysmograph is a glass-walled box with a volume of 700-1000L. An example of a modern plethysmography box is shown in Figure 2.5. The box is sealed during measurements. A controlled leak in the seal is used to stabilize the box's internal pressure, to account for slow pressure changes (eg. pressure changes caused by the temperature in the box increasing). Two pressure sensors are used in plethysmography. One measures the pressure in the box relative to atmospheric pressure, the second measures pressure at the subject's mouth relative to atmospheric pressure. A shutter mechanism is placed after the mouth pressure sensor. This shutter is able to completely block air flow during what is known as a shutter manoeuvre (Criée et al. [2011]).

Plethysmography relies on measuring changes in box pressure in conjunction with changes in mouth pressure or flow rate. Boyle's Law, described in Section 1.2 by Equation 1.2, is the underlying principle in plethysmography. This law states relative changes in the volume within a fixed compartment are equal in magnitude and opposite in sign to the relative pressure changes within the same compartment.

Figure 2.5 A modern plethysmography box. The box is completely sealed from the outside when the door is closed. Image sourced from GANSHORN (http://www.ganshorn.de)

This law allows the changes in absolute lung volume to be inferred from pressure changes in plethysmography.

During inspiration, inspiratory muscles increase the lung volume. However, airflow into the lung is not instantaneous because a pressure gradient is required before the air will flow. As a result, airflow lags behind lung volume. The small lag observed between airflow and lung volume is called the "shift volume". According to Boyle's law, the shift volume will induce an equal and opposite pressure shift, creating airflow. Because the plethysmograph box is sealed, the shift volume of the lung will be equal and opposite to the shift volume of the box. As a result, shift volume of the lung can be calculated from pressure changes in the box.

Because alveolar pressure measurements are not directly measurable, shift volume can be used as a surrogate for alveolar pressure (Criée et al. [2011]). A specific airway resistance (sRaw) can be calculated by comparing traces of shift volume vs flow, similar to how airway resistance is typically calculated (see Section 2.3). The magnitude of sRaw depends on both lung volume and airway resistance, because a higher lung volume will have a smaller volume shift for the same alveolar pressure change.

To measure airway resistance (Raw) directly, a relationship between shift volume and alveolar pressure must be found. This relationship can be determined by

breathing against a closed shutter in a plethysmograph (Stocks et al. [2001]). A disadvantage of using Raw to monitor the effect of intervention, is its low sensitivity. It requires relatively large changes (35 - 60%) to detect a significant response (Kaminsky [2012]), which significantly reduces its ability to monitor or guide care.

2.2.3 FOT

The forced oscillation technique (FOT) is a means of measuring respiratory system resistance and reactance (Kaczka and Dellacá [2011]). This method superimposes high frequency oscillations on inspired air. Measurements are taken across a range of frequencies to assess respiratory system resistance at different branch levels of the airways (Brashier and Salvi [2015], Navajas and Farré [2001]). The resistance measured by FOT has contributions from both the lung and chest wall. The main benefit of this technique is complex manoeuvres are not required, allowing monitoring of lung mechanics in patients who are uncooperative or unable to participate in standard spirometry, such as young children (Delacourt et al. [2000]). Drawbacks of this method are it interrupts breathing and requires extensive equipment not typical in home care.

2.2.4 Gas dilution

Respiratory diseases reduce the efficiency of gas transfer in the pulmonary capillaries. A reduction in gas exchange can be due to either a decrease in surface area of lung tissue or reduced airflow, or a combination of both. Gas diffusion testing uses a tracer gas to measure the level of gas exchange in the lungs (Ranu et al. [2011], Ruppel and Enright [2012]). A notable feature of COPD is air trapping. It is where a large amount of air is retained after exhalation, leading to hyperinflation and CO2 buildup in the lungs. Spirometry detects air trapping by measuring decreased FVC and FEV1. Air trapping is confirmed with further tests, most typically invasive CT scans (Mavili et al. [2010]).

In order to determine the total volumes of gas in the lungs at TLC, TGV or RV, indirect methods must be used since it is impossible to completely exhale all the gas from the lungs. Gas dilution involves the dilution of a known concentration and volume of inert gas by the gas in the lungs of the subjects and is critically dependent on complete mixing of the marker gas and lung gas. In subjects with poor gas mixing due to disease, this technique is very inaccurate and generally

underestimates the true FRC.

Currently, FRC is measured by two gas-based techniques: the rebreathing of an inert gas such as helium in a closed circuit, or the wash in or out of an inert marker gas, which can be the nitrogen normally present in the lung. Both techniques have been used for several decades and are known to have several shortcomings. Specifically, they are complex, hard to operate, and unreliable for the measurement of FRC in patients with poor gas mixing due to disease (Adam et al. [2018]).

2.2.5 Summary of lung function tests

The main properties lung function tests aim to measure are the ability of the lung to drive air, the volume of air in the lung, and how efficiently the lung is able to diffuse gas between the blood and atmosphere. Many lung function tests exist to accurately measure these properties. However, many of these tests are too expensive, invasive, or complex to be suitable for routine outpatient care.

Due to its simplicity, spirometry being the most widely used test. Although spirometry results are able to guide therapy, information about the underlying lung mechanics of tidal breathing is not readily available without additional testing. These underlying mechanics change as disease progresses, providing a potentially more accurate assessment of lung condition in response to therapy and care. Hence, there is a need to link easily obtained spirometry data with clinically and physiologically relevant, identifiable models of lung mechanics.

2.3 LUNG MECHANICS

The work done by the respiratory muscles during breathing depends on both how stretchy the lung is (elastance) and the resistance to airflow in the airways (resistance) (Chiew et al. [2011], Otis [1954]). In healthy lungs, both lung elastance and airway resistance are low, but disease can alter either one or both these mechanics (Ward [2005]). An increase in either mechanic will increase the work of breathing.

Lung elastance is a measure of the lungs ability to stretch, where a highly elastic lung will resist stretching and have high recoil when inflated. Mathematically, elastance is defined as the pressure in the lung per unit volume.

$$Elastance = \frac{Lung\ pressure}{Volume} \tag{2.2}$$

A lung with high elastance will be stiff, and can be thought of as a thick balloon. Highly elastic lungs are often seen in fibrosis, with extra work needed during inspiration to bring in a normal volume of air.

In contrast, a lung with low elastic recoil is pliable and will not easily return to its resting position. This lung can be thought of as a thin plastic grocery bag. Lungs with low elastic recoil are seen in emphysema, where extra work is required to get air out of the lungs. In addition, patients with low elastic recoil in the lungs often have difficulties inhaling air as well. This difficulty with inspiration is due to the fact low lung elastance results in many collapsed alveoli, which require a high pressure to re-open (Schirrmann et al. [2010]).

The respiratory system is made up of a system of branching airways, with the airways dividing 23 times between the trachea and alveolar sacs. Models of airway resistance show that the resistance varies for each generation, depending on the length and diameter of the airways (Damanhuri et al. [2014]). However, an average airway resistance, assuming the lung contains only a single airway, can be calculated from flow and oesophageal pressure measurements:

$$Resistance = \frac{Pressure\ drop}{Flowrate} \tag{2.3}$$

Airway resistance will increase if the diameter of airways is reduced. Airways diseases include asthma, COPD, bronchitis, and abnormal build-up of fluid in the lung.

Figure 2.6 shows the airway resistances for a healthy patient and patients in intensive care. It highlights just how much resistance can be increased by lung disease. The increase in resistance caused by narrow or blocked airways can be described by Poiseuille's law for resistance:

$$Resistance = \frac{8\mu l}{\pi r^4} \tag{2.4}$$

When lung mechanics are measured over a series of subsequent breaths, a small amount of natural breath-to-breath variation will be observed (Kim et al. [2015]). Over a longer period of time, this variation can be averaged out. As a result monitoring lung mechanics over time can indicate trends in lung condition, as lung mechanics change in response to disease or treatment.

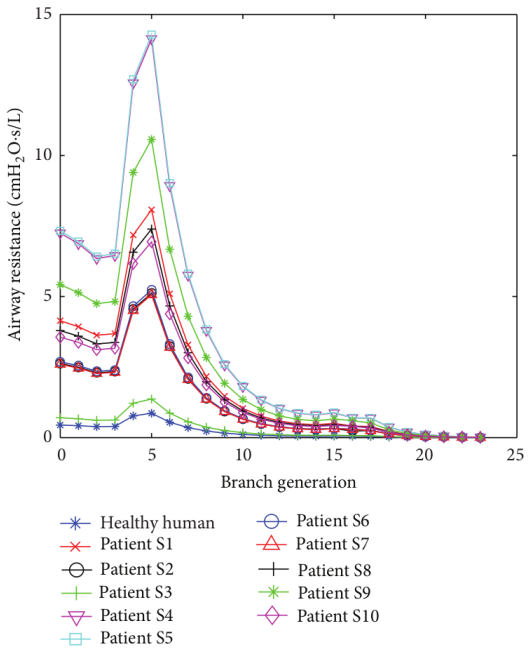

Figure 2.6 Airway resistance at each lung generation for a variety of patients (Damanhuri et al. [2014]).

Static vs time-varying lung mechanics

Lung mechanics can be measured as either static or dynamic. Static lung mechanics are able to be measured at a plateau or occlusion during respiration at no-flow conditions, when no air flows into or out of the lung. Static lung mechanics give an average value for lung mechanics for that particular instance in the breathing cycle.

Lungs are not homogeneous. Regions of the lung can be affected by disease or trauma altering the local mechanics, while other regions remain healthy (Barrow and Pandit [2017]). Average lung mechanics are not able to describe this heterogeneity well enough to identify affected regions. Lung mechanics also change during a breathing cycle as the lung tissue expands and contracts with inspired volume (Chiew et al. [2015a], Redmond et al. [2017]). Time-varying lung mechanics are calculated with measurements of tidal flow and volume at a given intrathoracic pressure.

The driving pressure generated by respiratory muscles can also be modeled as a time varying elastance (Chiew et al. [2015a]). Measurements of this mechanic can be used to identify the magnitude of breathing effort during respiration, and the total work of breathing. This approach can yield an estimate of patient condition, and sedation levels.

2.4 MODELING LUNG MECHANICS

2.4.1 Single compartment lung model

The respiratory system has been modeled in many ways, ranging from a simple single compartment model to complex airway branching models (Ben-Tal [2006]). The single compartment lung model was developed in 1953 (Mead and Whittenberger [1953]). It is a very simple model, describing the respiratory system as a resistive component representing the airways, combined with an elastic component representing the lung.

Patient-specific model-based lung mechanics can be identified from patient data using the linear single compartment lung model defined (Bates [2009]):

$$P_{aw}(t) = R_{rs}Q(t) + E_{rs}V(t) + P_0 \tag{2.5}$$

where P_{aw} is the inspiratory airway pressure, t is time, E_{rs} is the respiratory system elastance, R_{rs} is the combined resistance of the conducting airway and endotracheal tube, V is volume, Q is flow, and P_0 is the offset or positive end expiratory pressure, PEEP (Bates [2009]).

This model describes airway pressure as the sum of two pressures in the respiratory system. $R_{rs}Q(t)$ defines the pressure dissipated due to airflow through the airways and endotracheal tube, and $E_{rs}V(t)$ defines the pressure created by the lung's elastic recoil. This model assumes air flow measured at the airway opening is equal to airflow at all points in the respiratory system.

Figure 2.7 shows the lung as described by this model, with elastance separated into three separate components. For any breathing cycle, time varying or constant values for inspiratory E_{rs} and R_{rs} can be identified using a linear least squares fit to measured P_{aw}, V and Q during inspiration (Chiew et al. [2011]).

This model has been shown to effectively estimate lung mechanics for fully sedated, mechanically ventilated (MV) patients (Chiew et al. [2015b], Morton et al. [2018b], Redmond et al. [2016]), but it does not produce reasonable parameter estimates for MV patients with lower sedation levels who are actively participating in breathing (Chiew et al. [2011]). During mechanical ventilation, P_{aw} is a known pressure supplied by the ventilator. However, when patients actively breathe on top of ventilator support, an additional unknown magnitude of pressure from the

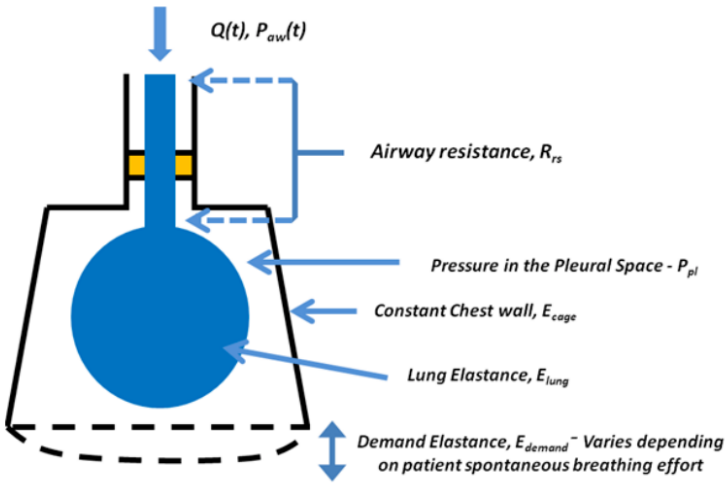

Figure 2.7 Single compartment lung model extended by Chiew et al to describe different elastance components (Chiew et al. [2014]).

respiratory muscles is superimposed on measured P_{aw}. This issue is also found when using the model on NICU cohorts (Kim et al. [2017, 2018]).

Determining passive lung mechanics during spontaneous breathing typically requires additional equipment or invasive manoeuvres (Benditt [2005], Khirani et al. [2010]). Measuring oesophageal pressure is one method used to determine mechanics during spontaneous breathing (Talmor et al. [2008]). Other methods were described in Section 2.2.

2.4.1.1 Time-varying elastance

Previous UC research has extended the standard single compartment model to develop a time-varying respiratory elastance model (Chiew et al. [2015a]) and a basis-function based model (Morton et al. [2018a]). The model has been used in several studies and has been shown to capture and provide an understanding of lung mechanics in both sedated and spontaneously breathing mechanically ventilated patients (Chiew [2013], Chiew et al. [2011], Szlavecz et al. [2014], van Drunen et al. [2014]). The model has also been extended to predict future lung condition for adult ICU patients (Morton et al. [2018a, b])

To extend the single compartment lung model, patient-specific lung elastance can be described as a time varying lung elastance, E_{drs} (Chiew et al. [2011]). Time-varying elastance adapts the conventional single-compartment lung model in Equation 2.5 to provide specific detail and understanding of the lung physiology and mechanics in SB patients. When patients are actively participating in breath-

ing, Equation 2.5 can be extended to include a pleural or driving pressure:

$$P_{aw}(t) - P_{pl}(t) = R_{rs}Q(t) + E_{rs}V(t) + P_0 \tag{2.6}$$

Where pleural pressure P_{pl}, is the multiplication of elastance required to generate the driving pressure, E_{pl}, and lung volume $V(t)$. The driving pressure gives information about P_{pl}, which can be measured with the use of an oesophageal pressure catheter. Unfortunately, accuracy is limited because these catheters can be difficult to place correctly (Benditt [2005]).

P_{pl} is divided between two pressure components in the time-varying elastance model: 1) P_{chest} is the patient-specific pressure in the chest wall, dependent on patient position and weight; and 2) P_{demand} is the variable pressure changes dependent on patient breathing effort. This approach yields:

$$P_{pl}(t) = P_{chest}(t) + P_{demand}(t) \tag{2.7}$$

These pressure components are attributed to the air volume entering the lung, meaning each pressure can be represented as a combination of an elastic component and air volume. To maintain structural identifiability of Equation 2.6, the elastance terms are combined into one time-varying elastance, E_{drs}. In any breathing cycle, E_{drs} captures the combined effect of the driving elastance and lung elastance. It is assessed as the change in pressure for a given tidal volume of flow.

$$E_{drs}(t) = E_{chest} + E_{demand} + E_{lung} \tag{2.8}$$

$$P_{aw}(t) = R_{rs}Q(t) + E_{drs}(t)V(t) + P_0 \tag{2.9}$$

When a patient is fully sedated and dependent on a ventilator to breathe, it can be assumed there is no active breathing effort. Dynamic elastance can be calculated in this case to show the changing lung elastance over a breath. Lung elastance falls if new alveoli are recruited faster than pressure is able to build-up in the lung. If pressure is increased and elastance increases, it indicates the increase in pressure was unable to recruit a significant number of new alveoli, and instead the additional pressure is beginning to stretch already recruited lung (Chiew et al. [2015b], Vieira et al. [1998]).

The measured airway pressure and flow of the ventilator can then be used to calculate a constant value of respiratory elastance, E_{rs}, and resistance, R_{rs} for each breathing cycle using multiple linear regression (Lucangelo et al. [2007], van Drunen et al. [2014]). Using the time-invariant R_{rs} value the time-varying respiratory elastance within inspiration of each breathing cycle is calculated as:

$$E_{drs}(t) = \frac{(P_{aw}(t) - P_0) - R_{rs}Q(t)}{V(t)} \tag{2.10}$$

For each breathing cycle, the value of E_{drs} can be normalised to the total inspiration time, and the area under the E_{drs} curve used to calculate stiffness. This normalisation allows lung mechanics to be compared within a given ventilation mode regardless of respiratory rate, or across different ventilation modes where respiratory rates may vary. The area of E_{drs}, $AUCE_{drs}$, is obtained by integrating E_{drs} over time during the patient's breathing cycle.

$AUCE_{drs}$ is clinically relevant as it is proportional to the patient-specific work of breathing (WOB). Thus, it can be used as an indicator for the severity of respiratory failure (Chiew et al. [2014, 2015a]). It is known WOB is proportional to lung elastance, meaning a highly elastic lung requires a high WOB to inflate to a given volume of air. WOB is defined:

$$WOB = P_{aw}V(t) \tag{2.11}$$

Substituting Equation 2.5 for P_{aw} with an assumed PEEP of 0 cmH_2O into Equation 2.11 results in WOB in terms of elastance and resistance.

$$WOB = (E_{lung}V(t) + RQ(t))V(t) \tag{2.12}$$

The work of breathing defined in Equation 2.12 can be divided into two parts. The first is the work of breathing to overcome elastic forces in the lung, $WOB_E = E_{lung}V(t)^2$, and the second is the work of breathing to overcome airway resistance, $WOB_R = RQ(t)V(t)$. Substitution of E_{drs} for E_{lung} allows the dynamic WOB over a breath to be derived:

$$E_{drs} = WOB_E(t)/V(t)^2 \tag{2.13}$$

$AUCE_{drs}$ is the integral of Equation 2.13.

2.4.2 Summary of lung mechanics modeling

Many models have been developed to represent the respiratory system, but most are too complex for monitoring respiratory mechanics in real-time or are unsuitable for spontaneously breathing patients (Baoshun and Bates [2010], de Ryk et al. [2007], Kitaoka et al. [2007], Reddy et al. [2011], Schirrmann et al. [2010], Tawhai and Bates [2011], Tawhai et al. [2004]). Hence, this thesis focuses solely on the single-compartment lung model. This model is simple to understand and apply in practice, especially for sedated patients.

The single compartment lung model is much more difficult to use for fully spontaneously breathing patients, where direct measurement of driving pressure is unavailable. Previous work has laid the foundation for using this model to measure lung mechanics in outpatient care (Chiew et al. [2015a], Morton et al. [2018b], Szlavecz et al. [2014], van Drunen et al. [2014]), and this thesis aims to extend this knowledge.

Chapter 3

THESIS OVERVIEW

There is a lack of ability to easily measure lung mechanics in outpatient care. These underlying mechanics change as disease progresses, thus providing a true, potentially more accurate assessment of lung condition in response to therapy and care provided. The most commonly performed pulmonary function test is spirometry, which is currently the gold standard for assessing lung function in outpatient care, but unable to measure lung mechanics. Spirometry is widely available in practice due to it's low cost, and relative ease of use. However, it is limited by its focus on peak breathing effort, which can exclude some patients from participating, and reduces test repeatability.

The aim of this thesis was to develop a new lung function test to address two identified areas of improvement, lung mechanics measurement and test accessibility. A new lung function test was developed to measure lung mechanics during tidal breathing with spirometry. This test is based on the occlusion technique used in plethysmography, and uses the dynamic elastance single compartment lung model to calculate lung mechanics.

The following chapters describe the development of the new test, and lessons learnt during this process:

Chapter 4 analyses the validity of using the single compartment lung model to measure lung mechanics during passive expiration. During spontaneous tidal breathing, expiration is primarily a passive process.

Chapter 5 describes a failed test to measure lung mechanics during spontaneous tidal breathing expiration. This test uses an automated shutter to manipulate expiratory airflow. Lessons learnt from this test influenced the development of the final lung function test.

Chapter 6 describes the novel lung function test developed to measure lung mechanics during tidal breathing, and the test validation.

Chapter 7 analyses how well the new test is able to represent viscoelastic and small airways lung mechanics.

Chapter 8 analyses the effect of cheek support on lung mechanics measurement. In breath-occluding lung function tests, cheeks are supported to prevent the cheeks from expanding outwards. However, no rule-of-thumb to account for missing cheek support exists.

Chapter 9 describes the proof-of-concept spirometer designed for use with the new test and accompanying software. This is available as open source. The overall goal was to ensure both engineers and clinical audiences are informed of novel results in a format and viewpoint suitable to their interest.

Chapter 4

PASSIVE EXPIRATION

The aim of the study described in this chapter was to assess whether lung mechanics could be measured from expiration of mechanically ventilated patients. Typically, lung mechanics are calculated from inspiration for patients in intensive care. If lung mechanics are able to be identified from passive expiration in fully sedated, mechanically ventilated patients, lung mechanics may then be able to be identified from tidal expiration in spontaneously breathing patients.

Data from mechanically ventilated patients is a good test case because driving pressure measurements are readily available from the ventilator. In spontaneously breathing patients, this pressure is generated by respiratory muscles and the lung's elastic recoil, and is not easily measured in real-time. However, expiration during tidal breathing is hypothesised to be a primarily passive process (Grinnan and Truwit [2005]), giving similarities to the entirely passive expiration of sedated patients.

4.1 METHODOLOGY

4.1.1 Model identification

The single compartment lung model described in Section 2.4 is:

$$P_{aw}(t) = R_{rs}Q(t) + E_{rs}V(t) + P_0 \tag{4.1}$$

Solving the ODE formed by this lung model gives:

$$Q(t) = Q_0 e^{-E_{rs}t/R_{rs}} \tag{4.2}$$

where Q is the airflow measured, E_{rs} is the respiratory system elastance, and R_{rs} is the respiratory system resistance.

The derivation of Equation 4.2 is shown in Appendex A.1. Equation 4.2 shows the natural decay rate of airflow from the lungs depends on the lung's mechanics. It follows that measurements of exponential decay rate should give information about the relationship between E_{rs} and R_{rs}.

Expiration in mechanical ventilation for fully sedated patients is an entirely passive process. As a result, expiratory airflow of these patients can only be due to the lung's natural recoil. Thus, expiratory airflow in mechanical ventilation decays exponentially. This effect is shown in Figure 4.1, which is clinical data of a single breath of a mechanically ventilated patient in volume control mode. Previous work has shown this method can be used to monitor lung elastance trends in mechanically ventilated patients (van Drunen et al. [2013]).

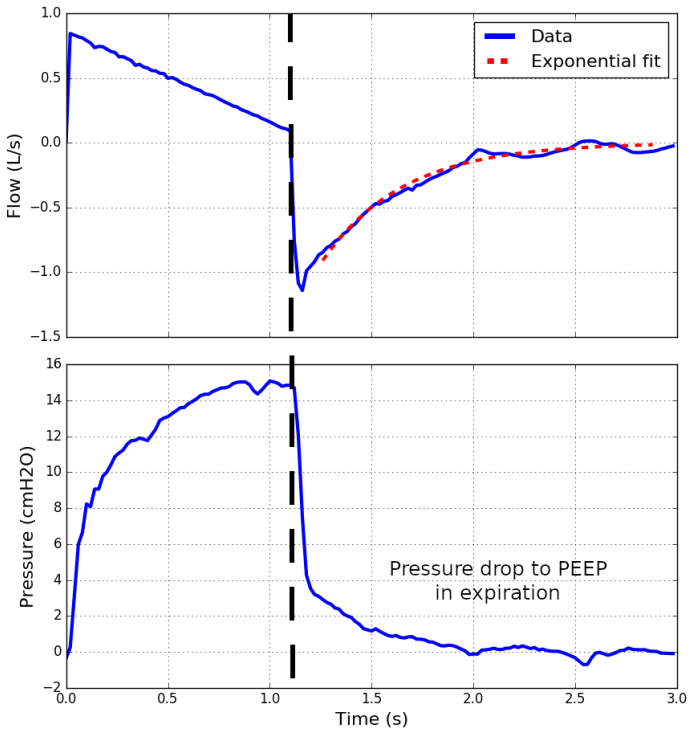

Figure 4.1 Top: Flow profile of a breathing cycle with an exponential model fit to expiration. Bottom: Pressure profile of a breathing cycle with pressure measurements relative to PEEP.

4.1.2 Problem with model identification

It has previously been shown the single compartment model becomes structurally non-identifiable when analysing passive expiratory data (Möller et al. [2009], van

Drunen et al. [2013]). This unidentifiability stems from E_{rs} and R_{rs} being lumped together in the exponential decay term, so the relative effects of resistance and elastance cannot be separated from measuring decay rate alone. This inseparability of parameters in passive expiration can also be seen by substituting the expected airflow of passive expiration, Equation 4.2, into Equation 4.1:

$$P_{aw}(t) = R_{rs}Q_0e^{-E_{rs}t/R_{rs}} + E_{rs}V_0e^{-E_{rs}t/R_{rs}} + P_0 \tag{4.3}$$

Because both E_{rs} and R_{rs} induce exponentially decaying flow with the same decay rate in passive expiration, it is impossible to determine how much each mechanic contributes to the total measured airflow.

4.1.3 Using passive expiration to estimate lung mechanics for spontaneously breathing MV patients

The following is a proposed method to modify expiratory pressure data to allow a direct least-squares estimation of expiratory respiratory mechanics from just the expiration data alone. This method adjusts the pressure and volume waveforms to estimate E_{rs}. Once an estimate is obtained, R_{rs} may be separated from the decay rate.

Patients with respiratory failure requiring breathing support are mechanically ventilated. Clinicians must provide patient- and disease-specific mechanical ventilation (MV) therapy to prevent alveoli collapse and improve gas exchange (Amato et al. [1998], McCann et al. [2001]). A key component of MV therapy is selecting the ideal postive end expiratory pressure (PEEP) setting. A high PEEP may cause over distension, damaging healthy lung tissue, but applying too little PEEP will allow alveoli to collapse, reducing gas exchange (Richard et al. [2001]). Thus, a significant amount of research focuses on identifying the optimum PEEP for each patient (Chiew et al. [2011], Das et al. [2013], Sundaresan and Chase [2012]), with all these issues summarised in Major et al. [2016] and Sundaresan and Chase [2012].

Clinically useful information for selecting PEEP settings are provided by model-based lung mechanics monitoring (Bates [2009], Sundaresan et al. [2009]). In critical care, any method of measuring lung mechanics must be appropriate for both fully and partially sedated patients, and provide lung mechanics metrics in real-time. However, at present, many models do not meet these criteria. They

are typically too computationally complex for real-time respiratory mechanics monitoring, or may require procedures or measurements unavailable in a typical clinical setting (Baoshun and Bates [2010], Chase et al. [2018], de Ryk et al. [2007], Kitaoka et al. [2007], Reddy et al. [2011], Schirrmann et al. [2010], Tawhai and Bates [2011], Tawhai et al. [2004]).

Simple lung models, such as the single compartment lung model, are unable to produce accurate measurements for spontaneously breathing (SB) patients. Patient breathing efforts, such as reverse-triggering in response to ventilator driven inhalation, can significantly alter measured ventilator pressure or flow. These changes cannot be fully described by the model without additional invasive measures of alveolar pressure (Baoshun and Bates [2010], Brochard et al. [2012], Chiew et al. [2015a], de Ryk et al. [2007], Khirani et al. [2010], Kitaoka et al. [2007], Reddy et al. [2011], Schirrmann et al. [2010], Tawhai and Bates [2011], Tawhai et al. [2004]). Hence, spontaneously breathing patients may be given suboptimal PEEP settings when lung mechanics measurements are lost due to breathing efforts. Figure 4.2 shows how the single compartment fits to a breath with (unmodelled) patient SB effort at the end of inspiration.

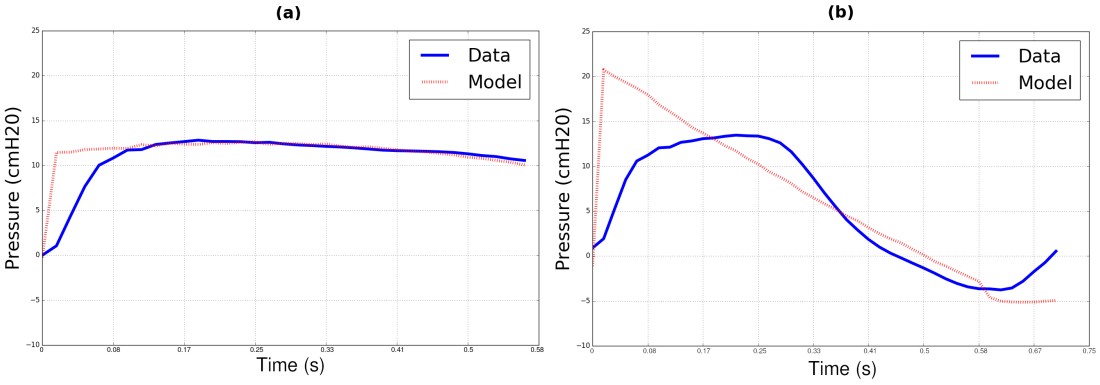

Figure 4.2 Model fitting to a sample breath during inspiration. (a) Breath without SB effort. (b) Breath with SB effort at the end of inspiration

This chapter describes a study using the single compartment lung model method to assess lung mechanics of spontaneously breathing patients retrospectively. Muscular breathing effort is assumed to be minimal during passive expiration, and independent of any inspiratory SB efforts, such as reverse-triggering (Al-Rawas et al. [2013], Grinnan and Truwit [2005]). Therefore, linking respiratory mechanics captured during expiration in SB patients back to inspiration could extend the ability of respiratory mechanics to titrate MV care. In this study, the relationship between inspiratory and expiratory mechanics was assessed, to

identify and validate any non-patient specific trends.

The driving pressure supplied by the mechanical ventilator during expiration may be viewed as a large negative pressure applied at the start of expiration. This negative driving pressure causes air to flow out of the lung, decreasing volume from its initial end-inspiratory value. To analyse the ventilator waveforms from this point of view, expiratory pressure and volume can be shifted to have initial values of zero. This data shift allows easy estimation of lung elastance from the new end-expiratory pressure and volume measures, by forcing the elastance estimate to be equal to final pressure divided by final volume.

Figure 4.3a shows expiratory lung and resistive pressures identified with a least squares fit to expiratory airflow, unaltered expiratory pressure and unaltered expiratory volume data. The estimated respiratory mechanics are not physiologically possible. The lung pressure is clearly incorrect, as P_{lung} should start at the same pressure as maintained by the ventilator at the end of inspiration, P_i. Figure 4.3b shows pressure estimates for the same breath after shifting pressure and volume to have initial values of zero. P_{lung} now decays exponentially from the pressure measured at the start of expiration. Further support for this method of calculating expiratory lung mechanics is provided by the positive, physiologically reasonable estimates of respiratory mechanics. Hence, all expiratory respiratory mechanics presented in this study were estimated using shifted pressure and volume data.

SB efforts occurring at the end of inspiration will alter the end-inspiratory pressure. The method used in this study to calculate expiratory respiratory mechanics is highly dependent on this value, hence any error in P_i reduces estimation accuracy. To identify breaths likely to have unreliable estimates, a simple reconstruction method developed by Damanhuri et al. (Damanhuri et al. [2016]) was used to quantify the magnitude of SB effort.

In this study, breaths with end-inspiratory SB efforts are reconstructed using a simple pressure reconstruction method (Damanhuri et al. [2016]). This method determines the gradient of the airway pressure drop at the end of inspiration and extrapolates a line of this gradient back until the maximum pressure in the breath is met. If the end-inspiratory gradient is significantly, in this study 20%, smaller than the start-inspiratory gradient, the start-inspiratory gradient is used instead. The reconstructed pressure creates a proxy for the correct, unaffected pressure waveform. Thus, the change in area after reconstruction gives an indication of

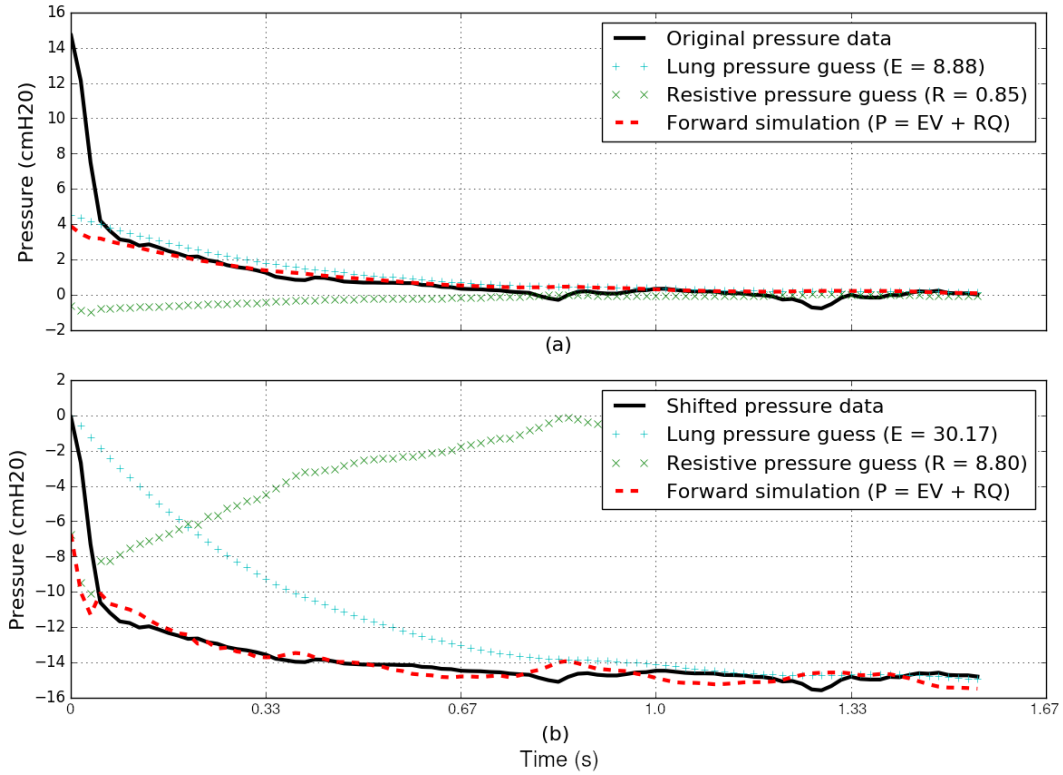

Figure 4.3 Pressure profile and forward simulation of driving, lung, and resistive pressure for expiration. The forward simulation is the sum of the simulated lung pressure due to lung elastance acting on inspired volume, and the resistive pressure drop due to airflow through the airways. Respiratory mechanics used in simulations obtained from two approaches (a) Direct linear single compartment model fit to unchanged ventilator data. (b) Linear single compartment model fit to data, with pressure and volume data adjusted to have initial values of 0.

the magnitude of SB effort present in the breath.

The reconstructed end-inspiratory pressure was only used when the change in area of the pressure waveform after peak pressure was more than 12.5% of the same area post-reconstruction. This threshold was the level at which researchers trained to identify dissynchrony in waveforms were no longer able to confirm a reduction in pressure was due to breathing effort. Figures 4.4a and 4.4b show examples of estimation of end-inspiratory pressure using the pressure reconstruction method. Note the breath in Figure 4.4a was not affected by end-inspiratory breathing effort, and consequently did not require reconstruction.

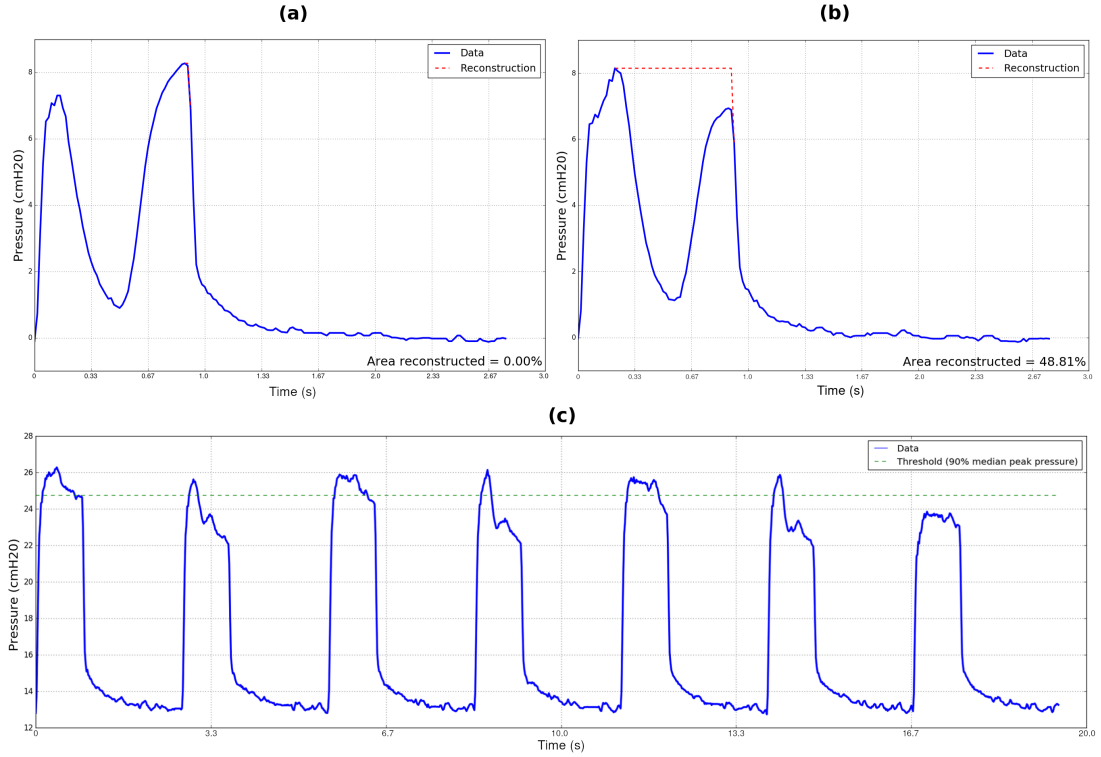

Figure 4.4 A simple reconstruction of inspiratory pressure to estimate end-inspiratory pressure value for breaths containing: (a) no end-inspiratory SB effort and (b) end-inspiratory SB effort. Panel (c): Use of a threshold peak pressure value at 90% median peak pressure of 7 breaths to identify breaths likely to contain long SB efforts.

SB efforts can last the entire duration of inspiration, effectively reducing measured peak pressure. To identify such a reduction in peak-pressure, the median peak pressure of the breath being analysed and the previous 6 breaths was determined. Expiratory elastance was not calculated if the peak pressure of the breath being analysed was below 90% of this value. For example, the final breath in Figure 4.4c would be excluded from analysis of expiratory elastance using this method.

4.1.4 Data

This study analysed retrospective datasets from 8 patients, where Patients 1A-D were fully sedated and Patients 2A-2D transitioned from partial to full sedation. Data from Patients 1A-D was used to generate a relationship between inspiratory and expiratory lung mechanics in ideal conditions. Data from Patients 2A-2D allowed validation of the identified relationship for predicting lung mechanics during SB and quantifying the impact of this approach.

All patients were ventilated with a volume controlled ramp flow profile on synchronous intermittent mandatory ventilation (SIMV) mode. The ventilators used were PB-840 ventilators (Coviden-Puritan Bennet, Boulder, CO). Patient ventilation details are presented in Table 4.1. Approval for this study and the use of the clinical data collected, were provided by the NZ Upper South Island Regional Ethics Committee.

Table 4.1 Patient information, including ventilation details

Patient	Primary diagnosis	Volume (ml)	Breathing rate (/min)	PEEP (cmH_2O)
1A	Peritonitis	510	20	16 - 25
		520	20	14 - 22
		315	20	18 - 26
		320	20	19 - 27
1B	Pneumonia	465	18	11 - 19
		465	18	12 - 20
1C	Pneumonia	385	20	12 - 32
1D	Ischaemic gut	470	18	20 - 36
		460	18	20 - 36
		420	20	24
		420	20	22 - 30
		420	20	22 - 30
2A	Peritonitis	365	18	15
2B	Peritonitis	370	19	17
2C	Cardiac surgery	480	14	11
2D	Pneumonia	540	18	13

Patients 1A-1D were fully sedated, with all breaths free from SB effort. This data was used to identify any relationships between inspiratory and expiratory respiratory mechanics. The data contains 1013 breaths with 12 recruitment manoeuvres (RM). Recruitment manoeuvres provide a greater spread of elastance values for each dataset due to the changing PEEP levels.

Each dataset from patients 2A-2D contained 60 breaths, 30 breaths each from

before and shortly after sedation administration. All patients exhibited varying levels of SB effort pre-sedation, and were then sedated without any changes to ventilation settings. Sedation was given for clinical reasons and was not planned intervention of the study. Figure 4.5 shows the first 10 breaths, pre- and post-sedation, where sedation eliminated SB efforts, as expected.

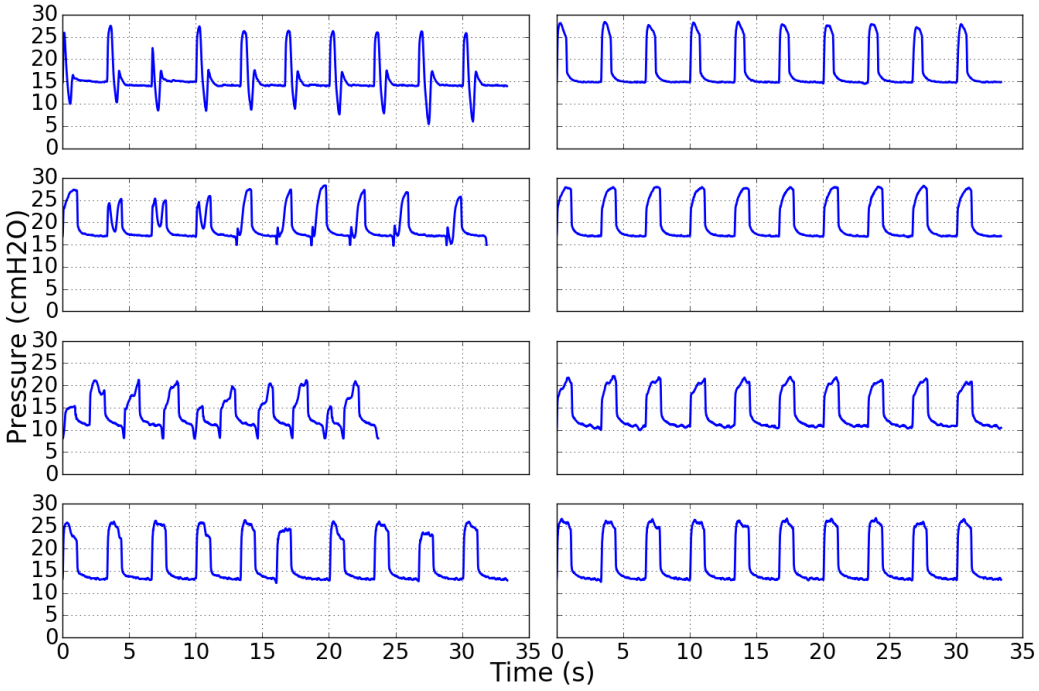

Figure 4.5 Pressure waveform of first 10 breaths pre- and post-sedation for datasets 2A (Top) through to 2D (Bottom).

4.1.5 Validation

Inspiratory and expiratory respiratory mechanics of each breath were calculated for patients 1A to 1D. If a cohort-wide trend was identified, a 95% confidence interval and 95% prediction interval were calculated using bootstrapping of 1000 random subsets of breaths generated with replacement.

To assess whether trends between inspiratory and expiratory mechanics provided clinically useful information, this study looked at whether expiratory mechanics could be used to estimate inspiratory mechanics in SB patients 2A to 2D. For these patients, expiratory mechanics estimates are expected to be reliable because expiration is hypothesised to be a primarily or completely passive process (Al-Rawas et al. [2013], Grinnan and Truwit [2005]).

Data from patients 2A to 2D has examples of both SB and full sedation. Within

the roughly 10 minute period recorded, it is assumed respiratory mechanics would show only minimal variation (Kim et al. [2015]). Hence, the median mechanics and Median Absolute Deviation (MAD) of these mechanical properties were calculated to indicate the accuracy of inspiratory mechanics estimates.

4.1.6 Breath Stacking

Stacking breaths to reconstruct pressure assumes only parts of each breath are affected by SB effort, leaving regions where the pressure is "correct". By combining multiple breaths, a larger region of the unaffected pressure waveform can be determined (Redmond et al. [2014]). Hence, by combining a breath-stacking method with expiratory lung mechanics analysis, we may expect to see more accurate estimates of lung mechanics at the cost of less breath-to-breath mechanics resolution.

To estimate expiratory elastance with breath stacking, a new pressure waveform was created from the maximum inspiratory pressure of the breath being analysed and 3 previous breaths. The end-inspiratory pressure of the stacked waveform was used to shift the mean expiratory pressure of the 4 breaths to estimate expiratory elastance. Estimates of inspiratory elastance were found using the PREDATOR breath stacking method (Major et al. [2016], Redmond et al. [2014]). The variability and median inspiratory elastance with breath stacking were calculated for patients 2A to 2D.

4.2 RESULTS

Figure 4.6 compares expiratory and inspiratory elastance for patients 1A to 1D. A linear relationship was identified between inspiratory and expiratory elastance. This linear relationship was very strong (R^2=0.94) and cohort-wide. The identified confidence intervals are very narrow, with 95% confidence the gradient falls within in the range 1.04 to 1.07. The offset shows a larger range, from 1.04 to 2.05, where 95% of the data was shown to be within $\pm$2.38 cmH_2O/L of the identified mean.

No cohort-wide trend could be identified for respiratory resistance. Respiratory resistance for all breaths for patients 1A to 1D and a 1:1 trend line are shown in Figure 4.7. Expiratory resistance appears generally higher and patient specific in Figure 4.7.

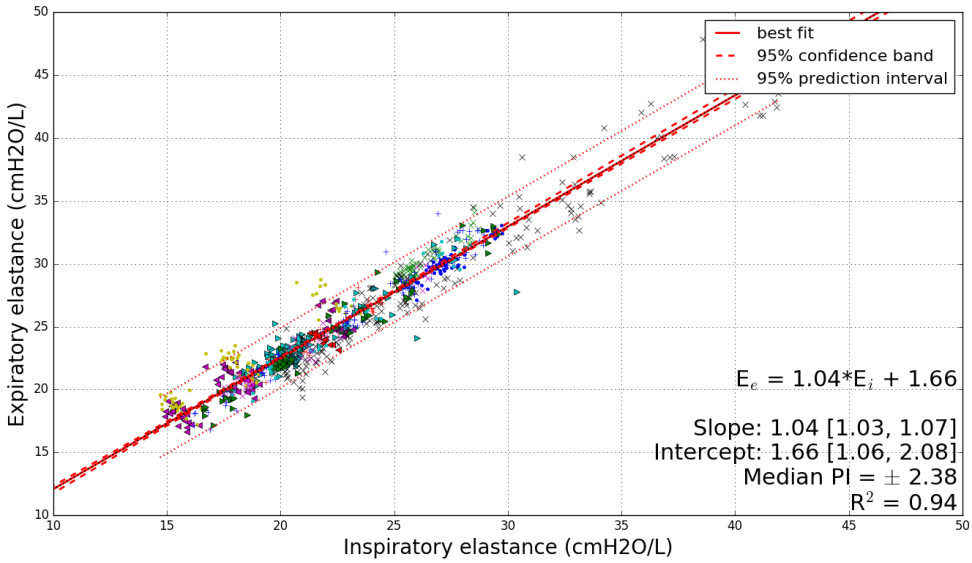

Figure 4.6 The linear regression of inspiratory and expiratory elastance (cmH_2O/L) for patients 1A to 1D. Also shown are 95% confidence interval and 95% prediction interval. A different marker is used for each of the 12 datasets. The regression was calculated from expiratory elastance to inspiratory elastance, as is reflected by the equation presenting the line-of-best-fit. The inverse of this equation, $Ei = Ee/1.04 - 1.60$, was used to calculate inspiratory elastance from expiratory data.

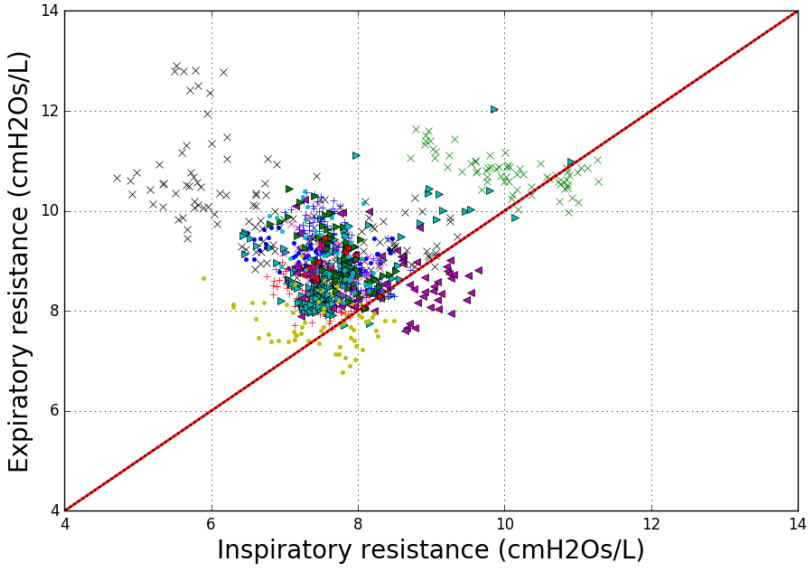

Figure 4.7 Inspiratory and expiratory resistance ($cmH_2O/L/s$) for patients 1A to 1D. Also shown is a 1:1 line. A different marker is used for each of the 12 datasets.

4.2.1 Using elastance trend to estimate elastance under SB

In this section, elastance estimated only from inspiratory data is referred to as "true inspiratory elastance", and elastance estimated using the trendline in Figure 4.6 is referred to as "estimated inspiratory elastance". Figure 4.8 shows a sample forward simulation for a typical breath from each patient.

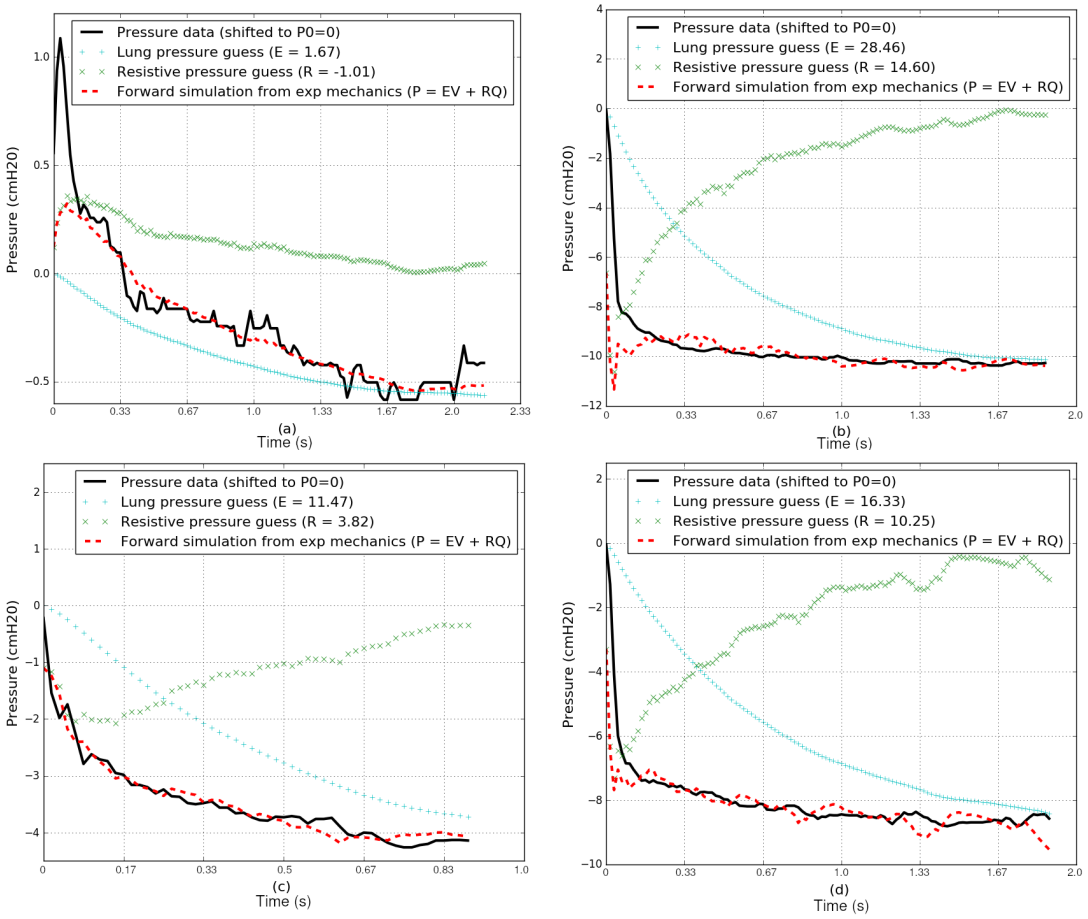

Figure 4.8 Pressure profile and forward simulation of driving, lung, and resistive pressure for expiration for patients 2A to 2D, respectively. Note the poor fit for patient 2A where the true end-expiratory pressure is obfuscated by breathing effort.

Figure 4.9 shows the post-sedation cumulative distribution of true and estimated inspiratory elastance values. The mechanics identified for sedated patients represents the minimum level or breath-to-breath variation. As variation increases, the slope of the distribution becomes less vertical. Hence, for an ideal case, the pre-sedation variation would exactly overlap post-sedation measurements.

The results are shown in Table 4.2. Expiratory mechanics were not able to

be calculated for Patient 2A because all breaths were significantly affected by end-inspiratory SB effort. In contrast, elastance predictions for Patient 2D were almost ideal. Post-sedation MAD for all patients was low, with similar values for true and estimated elastance. Median estimated elastance was larger than median true elastance for every patient, where the maximum difference was identified for Patient 2A at 2.99 cmH_2O/L.

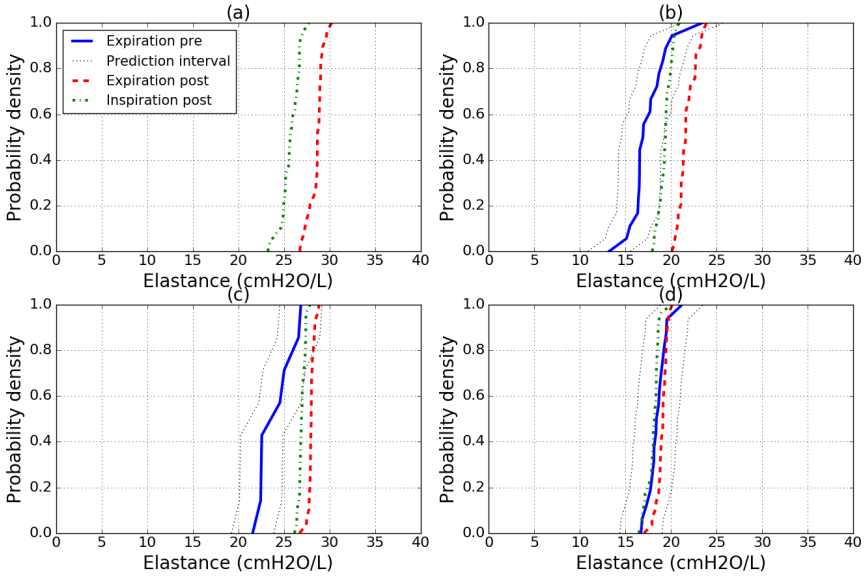

Figure 4.9 The cumulative distributions of elastance (cmH_2O/L) for patients 2A to 2D: Estimated pre-sedation (solid) with prediction interval (dotted), estimated post-sedation (dashed), and true post-sedation (dash-dot). For prefect estimation, pre-sedation estimate would exactly match true post-sedation elastance.

Table 4.2 Results for SB patients 2A to 2D. Median [interquartile range] and median absolute distribution (MAD) identified for true (left) and estimated (right) inspiratory elastance (cmH_2O/L).

		Inspiration (true)		Inspiration (estimated)	
		Median [IQR]	MAD	Median [IQR]	MAD
1	pre	-20.51 [-27.98:-18.70]	2.91	NA [NA:NA]	NA
	post	25.69 [25.11:26.52]	0.72	28.68 [28.33:29.01]	0.35
2	pre	10.46 [2.25:26.48]	9.74	23.57 [22.49:25.42]	1.29
	post	26.92 [26.76:27.26]	0.24	27.99 [27.88:28.12]	0.12
3	pre	15.66 [12.99:17.65]	2.60	16.91 [16.45:18.55]	0.86
	post	19.38 [18.87:19.83]	0.51	21.59 [21.09:22.49]	0.51
4	pre	16.75 [13.84:17.32]	0.99	18.38 [17.92:19.05]	0.66
	post	18.17 [17.83:18.42]	0.30	19.10 [18.75:19.42]	0.33

4.2.2 Effect of breath stacking on estimated elastance

Figure 4.10 shows the same results as Figure 4.9 using breath stacking reconstruction, which are summarised in Table 4.3. Pre-sedation expiratory elastance values were not able to be calculated for Dataset A with breath stacking, due to every breath containing a reduced end-inspiratory pressure. It is interesting to note, the variability and median of calculated expiratory elastances were comparable to the values obtained without breath stacking, shown in Table 4.2. Meaning combining multiple breaths to produce an average waveform did not produce noticibly more accurate measurements of the underlying lung mechanics. In fact, Dataset D saw significantly worse inspiratory elastance estimates after inclusion of breath stacking due to consistent pressure perturbations close to the start of inspiration leaving a small number of data points for breath reconstruction and model identification with PREDATOR.

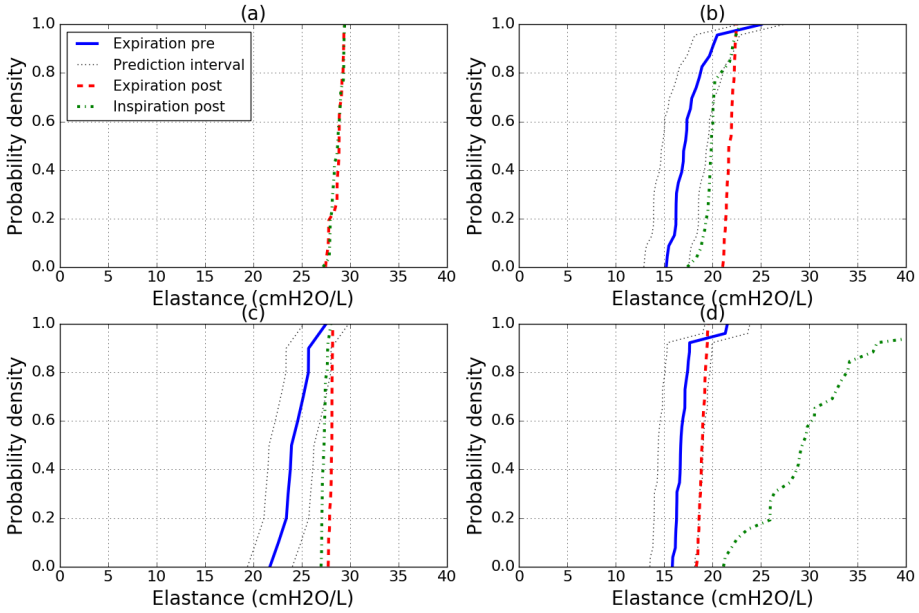

Figure 4.10 Cumulative distributions of elastance (cmH_2O/L) found using breath stacking methods. Expiratory elastance in pre-sedation (solid) with prediction interval (dotted) and post-sedation (dashed), and inspiratory elastance (cmH_2O/L) post-sedation (dash-dot) are shown.

4.3 DISCUSSION

For Patients 1A to 1D, a strong, linear, patient independent trend was observed between inspiratory and expiratory elastance. Inspiratory elastance was found to be lower than expiratory elastance. This outcome matches the findings of previous studies (Officer et al. [1998], Ulmer and Schäfer [2004]). However, no cohort-wide

Table 4.3 Median [interquartile range] and median absolute distribution of Elastance (cmH_2O/L) identified pre- and post-sedation for each patient using the PREDATOR method.

		Inspiration (true)		Inspiration (estimated)	
		Median [IQR]	MAD	Median [IQR]	MAD
1	pre	54.54 [51.46:60.61]	5.42	NA [NA:NA]	NA
	post	28.72 [28.15:29.18]	0.59	28.87 [28.52:29.16]	0.31
2	pre	29.13 [28.15:30.20]	1.11	23.96 [23.52:25.44]	1.21
	post	27.27 [27.12:27.43]	0.15	28.13 [27.94:28.15]	0.06
3	pre	18.82 [18.01:21.79]	2.31	17.10 [16.22:18.38]	0.90
	post	20.01 [19.65:20.20]	0.29	21.68 [21.42:22.14]	0.36
4	pre	33.26 [28.23:38.24]	5.20	16.70 [16.29:17.21]	0.43
	post	28.48 [22.24:32.55]	4.64	18.91 [18.65:19.20]	0.28

trend was found for resistance between inspiration and expiration. In general, expiratory resistance was higher than inspiratory resistance. This relationship was expected, as airways are compressed by expiratory effort and expanded by inspiratory effort. Overall, the relationships found between inspiratory and expiratory mechanics provide validation for the methods and underlying model used in this study.

4.3.1 Estimating inspiratory elastance with SB effort

The overall analysis is set to determine whether expiratory mechanics could be used to estimate inspiratory mechanics in SB patients. The comparison to sedated patients after a transition from partial to full sedation allows a clear test case of how inspiratory and expiratory mechanics are related without interference from the asynchrony seen in SB. This transition eliminates asynchrony as the patient is fully paralysed by sedation and the ventilator takes over the complete work of breathing. The transition to increased sedation was implemented for clinical reasons and was not an intervention made for this study. More importantly, for this research, the model is well validated in both SB and fully sedated patients in prior work (Chiew et al. [2011, 2015a]), so there is no error introduced by assessing or comparing mechanics across this clinical transition.

Despite all patients being sedated and ventilated in volume control mode, different severity and rates of SB efforts were observed. These datasets represent a wide range of SB effort, from mild to very severe, where mild means infrequent and/or small changes in pressure waveform and severe means the pressure waveform was almost completely destroyed by breathing effort, a worst case scenario. Patients in intensive care are generally over-sedated, rather than under-sedated (Kress

et al. [2000]). Outside of weaning a patient from ventilator support, SB effort is thus less common.

Patient 2A represents the worst case result for measuring expiratory lung mechanics. Every breath pre-sedation showed a very high level of SB effort in the approximately 1.5 minutes recorded, preventing any reliable lung mechanics measurements. However, lung mechanics are not expected to change significantly over such relatively small time periods. In practice, a good elastance estimate does not need to be calculated for every breath, or perhaps for several minutes. However the frequency of measurements needed is not assessed by this study.

Expiratory elastance measurement were generally stable, showing moderate breath-to-breath variation. The change in median estimated elastance from pre- to post sedation is small, with a maximum change of 4.7 cmH2O/L for Patient 2C. The estimated elastance pre-sedation showed significantly less variation than true inspiratory elastance measurements for all patients. However, the variability of estimated elastance is larger than may be acceptable clinically. Moreover, the results show this method is robust in the absence of SB effort, producing similar variation and median values as inspiratory data post-sedation.

In contrast to other methods, using expiratory data does not alter the pressure waveform in an attempt to remove the effect of SB efforts (Redmond et al. [2016], Schranz et al. [2012], Vicario et al. [2015]). Altering pressure data can only give a proxy for the true waveform. The final result would also be strongly affected by the assumed lung behaviour. Identifying lung mechanics directly from expiratory pressure is expected to give a better reflection of lung condition.

4.3.2 Effect of breath stacking on estimated elastance

When using breath stacking instead of breath reconstruction, expiratory elastance estimates showed l similar variation to the directly estimated expiratory elastances in Table 4.2. Lower variation using breath stacking was expected due to the pooling of multiple breaths, reducing the effect of natural breath-to-breath variation. This result highlights a key weakness of breath stacking: Lung mechanics estimates are only as good as the data, and pressure cannot be reconstructed in a region consistently affected by SB effort. Notably, every breath pre-sedation in Dataset A contained end-inspiratory SB efforts. Because no reasonable estimates of end-inspiratory pressure could be obtained for this dataset, there were no estimates for expiratory elastance. Consistent pressure perturbations close to the start

of inspiration in Dataset D left few datapoints for model identification using PREDATOR. This issue increased the variation of inspiratory elastance estimates, beyond what might be physiologically true.

Datasets B and C saw small reductions in variation of pre-sedation expiratory elastance. Although the variability remained larger than may be acceptable clinically, this outcome highlights the potential benefit of using expiratory elastance in conjunction with other reconstruction techniques. The estimation of expiratory elastance in SB patients may benefit from inclusion of a reconstruction method able to accurately predict the end-inspiratory pressure in SB patients. In addition, patient SB effort is not limited to inspiration and can occur at any point in a breathing cycle. Although SB effort was not observed during expiration in this study, a reconstruction technique, such as breath-stacking, may improve expiratory elastance estimated in breaths with expiratory SB effort.

4.3.3 Limitations

All patients in this proof of concept study were ventilated in volume control mode. Hence, the relationships identified by this study may not apply beyond this ventilation mode. Additionally, the relationship may not extrapolate beyond the relatively wide elastance range (Chiew et al. [2015a]) of 15-45 cmH_2O/L observed in this data.

At low inspiratory elastance values, close to 0 cmH_2O/L, the possible expiratory elastance values given by the CI ranges from -1.63 to 3.98 cmH_2O/L. Although negative elastance has been measured in SB patients, this negative value may not be physiologically reasonable in fully sedated patients (Chiew et al. [2015a]). A larger study is required to verify whether the linear relationship is valid over a wider range of elastance values and larger cohort.

4.4 SUMMARY

A method capable of measuring expiratory respiratory mechanics was presented in this proof of concept study. The method provided reasonable estimates of expiratory respiratory mechanics of SB patients, when no large end-inspiratory SB efforts were present. This method is capable of real-time, breath-to-breath mechanics estimation without additional invasive manoeuvres or measures. This study shows that when conventional methods fail, expiratory data may provide clinicians with

the lung mechanics measurements needed to guide MV therapy.

Chapter 5

SPONTANEOUS LUNG MECHANICS MEASUREMENT FROM DECAY RATE

The previous chapter showed expiration can be modeled by the single compartment lung model. However, the lung mechanics cannot be simply separated from the decay rate of airflow if expiration is purely passive. Another lung mechanics measurement is required to separate lung mechanics.

This chapter presents a novel, model-based method of measuring tidal breathing lung mechanics from the decay rate of flow, measured during spirometry. The model used is a dynamic elastance single compartment lung model. The exponentially decaying flow was created by occluding expiratory breaths using a plethysmograph with built-in shutter. Lung elastance was also measured, allowing the decay rate to be separated.

Note that this specific method of measuring flow decay rate was not able to reliably measure lung mechanics, and the reasons are discussed in this chapter.

5.1 METHODS

5.1.1 Linear single compartment lung model for spontaneous breathing

Spirometry is the most frequently performed lung function test. It is a simple and low cost test of lung health which analyses airflow and lung volume during specific breathing manoeuvres (Coates et al. [2014], Miller et al. [2005], Owens et al. [1991]). Spirometry results are able to guide therapy, by indicating the type and severity of any lung condition present. However, lung mechanics are not measured by typical spirometry testing.

Spirometry focuses on the results of the forced expiration manoeuvre. Patients are asked to inhale as deeply as possible, then exhale as forcefully as possible until forced vital capacity (FVC) is reached. This maximum effort breathing can be difficult to achieve for small children and other patients with limited levels of cooperation or lung function (Miller et al. [2005], Ruppel and Enright [2012]). Additionally, large muscular expiratory effort can increase airway resistance as airways are constricted, and even cause gas trapping if small airways collapse. Hence, there is need for lung function testing during normal tidal breathing, to link clinically and physiologically relevant lung mechanics models with tidal breathing spirometry measurements.

Lung mechanics are affected by lung disease, and monitoring how they change over time may provide a more accurate assessment of lung condition in response to therapy. The lung mechanics model used in this study is the dynamic elastance, single compartment lung model, as described in Section 2.4.1.1. Respiratory muscles produce the driving pressure needed to oppose passive respiratory elastic forces, such as lung and chest recoil, and maintain airflow through respiratory airways. The model is defined:

$$E_{dy}(t)V(t) = E_{rs}V(t) + R_{rs}Q(t) \tag{5.1}$$

Where E_{dy} is the dynamic elastance representing muscular breathing effort to create driving pressure, E_{rs} is the sum of all passive respiratory system elastances, R_{rs} is the combination of respiratory airway resistance and external resistances, V is volume, Q is flow, and t is time,

Direct measurement of respiratory driving pressure, $E_{dy}(t)V(t)$, is not possible without highly invasive measures, such as an oesophageal balloon catheter. Without direct measurement of driving pressure, lung mechanics cannot be simply identified. As an example, variations in individual lung mechanics can cause identical airflow in different subjects to be be created by vastly different driving pressures.

A described in Chapter 5, exponentially decaying flow will be created in response to a large, sudden change in driving pressure. This property can be shown by combining E_{dy} and E_{rs} into a total driving elastance term, E_d. The result is a simple lung model describing the balance of elastic and resistive forces in the

lung:

$$E_d(t)V(t) = R_{rs}Q(t) \tag{5.2}$$

In the same method as Appendix A.1, the resulting response of this system to a sudden change in driving pressure is analytically defined:

$$Q(t) = Q_0 e^{\frac{-tE_d(t)}{R_{rs}}} \tag{5.3}$$

Equation 5.3 shows the decay rate of airflow in response to a change in driving pressure depends on a combination of the spontaneous breathing lung mechanics terms, $E_d(t)$ and R_{rs}.

5.1.2 Mechanics identification

A shutter built into a plethysmograph was used to induce exponentially decaying flow. The shutter occluded expiration for 200 ms, which is longer than the 100 ms minimum needed for pressure to equalise across the respiratory system (Panagou et al. [2004]). When the shutter was released, pressure at the mouth would drop from driving pressure to atmospheric pressure, creating the exponentially decaying flow described by Equation 5.3.

The lung's response to shuttering can be simulated with an electrical circuit, with the shutter modeled as a voltage controlled switch, as shown in Figure 5.1. Figure 5.2, shows the simulated pressure and airflow measurements. The airflow measured after the shutter is re-opened is a superposition of tidal flow due to respiratory muscles and exponentially decaying flow caused by the shutter reopening.

The exponentially decaying airflow can be separated from the measured flow using adaptive filtering. The breath-to-breath variation of tidal breathing is low, with breaths typically having similar magnitude, duration, and flow profile. Hence, the expected tidal airflow can be estimated by averaging all breaths before the shuttered breath. In this study, a minimum of 5 tidal breaths were recorded before each shuttered breath. The airflow created in response to the shutter re-opening is calculated by subtracting the average tidal airflow from airflow measured during shuttering.

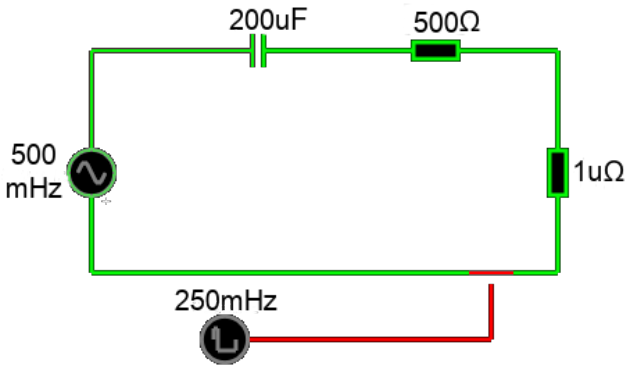

Figure 5.1 Electrical model of respiratory system. Shutter at mouth is modeled with with voltage controlled switch. Component values were chosen to approximately match human respiratory mechanics (C = 200 uF, Raw = 500 Ohm, frequency = 0.5 Hz, shutter duration = 200 ms).

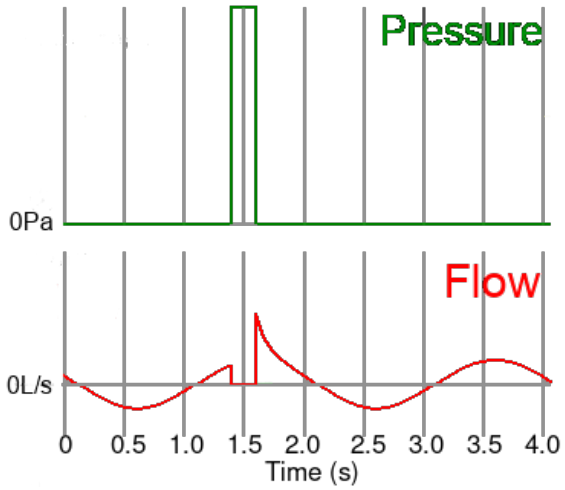

Figure 5.2 Response of electrical lung model. Top: Signal to simulate shuttering. Bottom: Modeled flow in spirometer. The response to shutter re-opening is the superposition of sinusoidal flow due to respiratory muscles, and an exponential decay induced by the large change in pressure.

Extra resistance was added to the spirometer mouthpiece to simulate upper airway obstruction. The resistances added were 0 (baseline), 0.4, 0.8, and 1.2 cmH_2Os/L, respectively. A simple way to separate the lung mechanics from the decay rate may be to add a known resistance and analyse how the decay rate changes.

In this study, elastance was directly measured through a different method. This added method allows the decay rate to be separated. If the resistance values produced by this technique are valid (meaning resistance measured is physiological and increases by the correct amount as external resistance is added), then using external resistances to permit parameter separation would also hold.

An assumption of the single compartment lung model is passive lung mechanics do

not change during the breath. If muscular breathing effort also remains constant after the shutter is re-opened, the decay rate of flow caused by the shutter, E_d/R_{rs}, can be calculated with a linear fit to the trace of airflow vs volume (QV loop). However, the elastance and resistance cannot be separated by measuring passive decay rate alone, as explained in Chapter 4. An additional measure of either R_{rs} or E_d is required to separate the combined mechanics of the decay rate. (Docherty et al. [2011], Howe et al. [2020], Möller et al. [2009]).

Elastance is defined as the pressure in the lung per unit volume. Pressure measured while airflow is occluded will approximate the respiratory driving pressure. Hence, if muscular effort remains constant, the elastance after the shutter re-opens can be calculated from the pressure and volume measured momentarily before the shutter re-opens (P_0 and V_0, respectively):

$$P_0 = E_d(t)V_0 \tag{5.4}$$

The value of R_{rs} was able to be separated from the decay rate after this elastance was calculated, as per Equation 5.3.

Due to minimum flow limits built into the shuttering software employed, lung mechanics were measured while panting. For each test, the shutter was activated 5 times with a minimum of 5 normal breaths recorded before shuttering. The test was repeated twice at each of the 4 added resistance levels.

5.1.3 Data

Seventeen healthy subjects were enrolled in this study (8 Female, 9 Male, Age 27±4.5, BMI 25±4, 3 Smokers). Data was recorded using a Ganshorn PowerCube Body plethysmograph with LFX 1.8 Respiratory Diagnostic Software. The Shutter was controlled with LFX software's ROCC mode, in manual trigger mode with a shutter close duration of 200-250 ms (typically 200 ms). Table 5.1 shows specific details for each subject.

5.2 RESULTS

5.2.1 Response to shuttering

Airflow measured during shuttering matches the simulated airflow waveform shown in Figure 5.2. Figure 5.3 shows typical pressure and flow waveforms measured

Table 5.1 Subject data. Smokers were included in this study.

Subject	Sex	Age	Height (cm)	Weight (kg)	Smoker
1	M	30	190	100	n
2	M	38	175	100	n
3	M	32	187	87	n
4	M	29	183	95	n
5	F	24	173	80	y
6	M	29	183	78	n
7	M	23	185	73	y
8	M	23	184	71	n
9	M	27	178	90	n
10	F	29	168	62	n
11	F	22	167	53	n
12	F	29	161	53	y
13	F	23	164	64	n
14	F	25	172	70	n
15	M	31	181	114	n
16	F	21	164	72	n
17	F	21	160	56	n

at baseline and at added resistance for comparison. The overall shapes are as expected.

The average tidal airflow is shown by the purple line in Figure 5.3. This average tidal flow was used to calculate airflow caused by the shutter, which is shown by the dashed line in Figure 5.3. The QV loop presented in Figure 5.4 is for the airflow attributed to the shutter. Airflow attributed to the shutter was expected to have decayed away after point B in Figure 5.4. However, the shutter-induced airflow was still greater than zero. This non-zero airflow was due to the tidal flowrate remaining elevated above the expected average tidal airflow rate for the entire duration after shuttering.

The response of a short linear region, typically 20-50 mL of tidal volume, followed by a long typically linear region with much lower or zero slope can be observed for all subjects at baseline added resistance. Non-linear and non-zero regions in the QV loop represent time-varying mechanics not present in the average tidal breathing waveform.

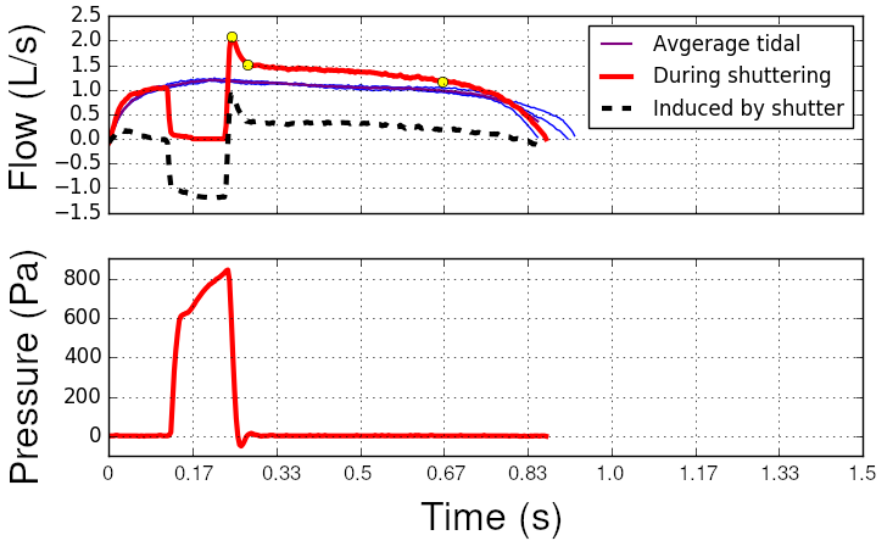

Figure 5.3 Flow and pressure traces measured during shuttering. Top: Average tidal flow is shown in purple, measured flow is red, and the difference representing flow caused by shuttering is the dotted line. Bottom: Pressure increases to approximate driving pressure while shutter is closed.

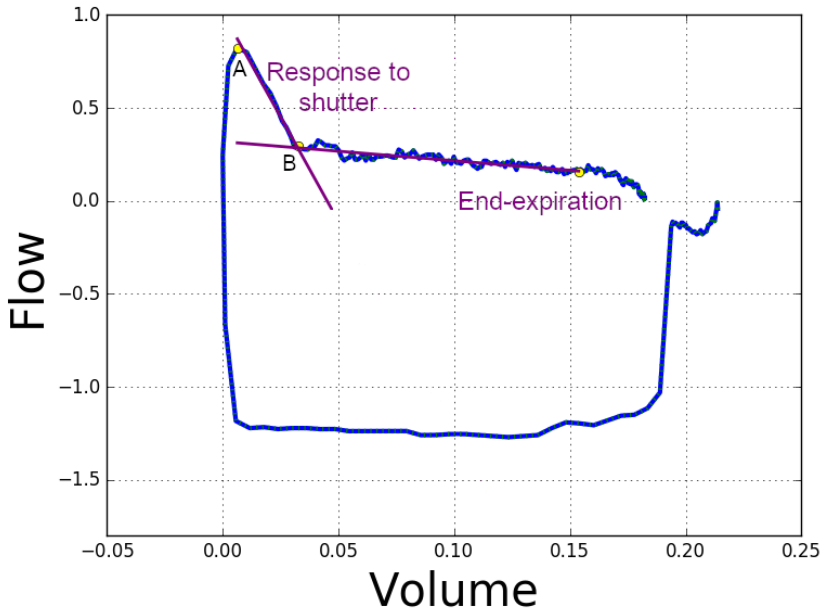

Figure 5.4 QV loop of flow induced by shutter makes identification of shuttering easy. A linear region between points A and B defined by the lung's response to shutter reopening, and a longer region at end-expiration are shown. Note: Linearity in a QV loop suggests lung mechanics remain constant. The total volume induced by the shutter has been translated in this figure to have a minimum value of zero.

5.2.2 Decay rates

The decay rate of shutter-induced flow was calculated from the QV loop, as shown in Figure 5.4. The exponentially decaying range was defined as from peak flow within 100 ms after shutter re-opening, to the first flow inflection point. The peak and inflection points are shown in Figure 5.4 as points A and B, respectively. A linear least-squares fit was made to this data range. When collating all shuttered breaths, outliers were defined as data greater than 1.5 standard deviations above the 75^{th} or below the 25^{th} percentile. In addition, the decay rate was not calculated if the decaying range identified contained less than 3 datapoints. No other methods were used to exclude data from analysis.

Table 5.2 presents the decay rates measured for all subjects for all external resistance levels. Decay rates measured range from 0.1 to 48 (1/sec). Flow decay rate is inversely proportional to resistance. So as resistance is added to the system, measured decay rate is expected to decrease. However, this trend was only observed for 7/17 subjects (Subjects 1, 3, 5, 11, 14, 16, 17), and only for the first three resistance levels (0, 0.4, 0.8 cmH_2Os/L).

Additionally, because the amount of resistance added for each test was 0.4 cmH_2Os/L, the decay rate was also expected to decrease less at higher resistance. Figure 5.5 shows the trends observed for all subjects. Overall, no clear trend can be identified, with the average decay rate at each resistance level remaining unchanged.

Values for R_{rs} separated from airflow decay rate using elastance measurements are presented in Table 5.3. At all added resistance levels, measured R_{rs} was very small. The exception is Subject 9, with entirely negative R_{rs}, and measured R_{rs} of -12.45 cmH_2Os/L for the baseline measurement. The largest resistance of 2.84 cmH_2Os/L was measured for Subject 12. Generally, R_{rs} was less than the resistance of the added venturi alone. Figure 5.6 shows how R_{rs} changes with added resistance. R_{rs} does not increase proportional to added resistance, as had been expected.

5.3 DISCUSSION

The region of exponential decay was easily located for all subjects, except Subject 9. The shutter duration used in this study (200 ms) was twice as long as the minimum required. This shutter length was hard-coded into the shutter control software, and could not be changed. The drawback of a longer shutter duration is it gives

Table 5.2 Mean decay rate and standard deviation measured for all subjects at all resistance levels. Decay rates are defined as negative, due driving pressure creating negative flow.

Subject	Decay rate (1/s, mean [std]) at added resistance (cmH_2Os/L)			
	None	0.4	0.8	1.2
1	-15.52 [2.99]	-12.75 [3.17]	-15.50 [4.83]	-17.51 [7.19]
2	-33.17 [9.25]	-48.21 [20.57]	-43.05 [23.85]	-34.53 [17.81]
3	-33.75 [8.04]	-23.92 [5.24]	-14.25 [7.71]	-12.77 [5.37]
4	-22.13 [3.41]	-22.93 [2.69]	-21.66 [9.19]	-19.48 [5.58]
5	-14.43 [6.16]	-9.18 [4.50]	-11.35 [5.94]	-9.19 [6.59]
6	-19.30 [3.37]	-16.30 [4.80]	-23.66 [8.47]	-13.72 [9.48]
7	-24.70 [6.56]	-20.86 [7.52]	-28.59 [10.13]	-25.26 [7.07]
8	-13.92 [3.08]	-21.50 [16.65]	-19.08 [3.78]	-19.72 [12.66]
9	-0.13 [4.35]	-2.74 [4.71]	-20.95 [19.28]	-20.89 [26.62]
10	-16.86 [5.02]	-22.60 [6.51]	-27.53 [6.48]	-19.23 [7.09]
11	-26.33 [6.46]	-21.32 [5.21]	-20.06 [3.52]	-16.18 [13.86]
12	-7.85 [2.25]	-11.96 [3.50]	-12.59 [6.51]	-12.98 [9.34]
13	-15.64 [4.10]	-9.09 [1.93]	-11.49 [4.35]	-9.41 [4.42]
14	-30.66 [4.53]	-28.86 [3.67]	-21.72 [3.77]	-18.06 [5.40]
15	-30.58 [9.52]	-25.34 [3.73]	-22.78 [2.55]	-31.29 [14.30]
16	-17.94 [3.13]	-17.17 [3.51]	-15.05 [4.57]	-13.56 [6.06]
17	-21.11 [6.23]	-18.46 [8.75]	-14.74 [8.32]	-18.45 [17.68]

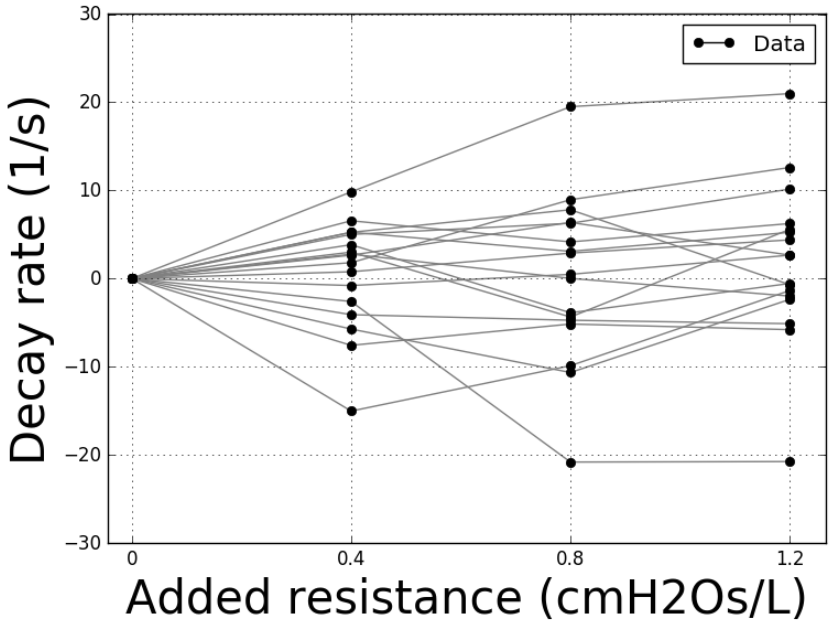

Figure 5.5 Decay rate trend for each subject. Decay rates are translated to 0/s at baseline. The decay rate did not consistently decrease as expected as resistance was added. Roughly half of the subjects saw increased decay rate at 1.2 cmH_2O added resistance, while the other half saw decreased decay rate.

Table 5.3 Resistance (mean [STD dev]) identified from decay rate at each added resistance level. Elastance used to separate decay rate is shown in the following chapter in Table 6.2, where it is discussed in detail.

Subject	R_{rs} (mean [std]) cmH_2Os/L			
	None	0.4	0.8	1.2
1	0.36 [0.10]	0.52 [0.17]	0.42 [0.11]	0.43 [0.20]
2	0.16 [0.06]	0.12 [0.08]	0.15 [0.12]	0.22 [0.12]
3	0.19 [0.04]	0.28 [0.05]	0.64 [0.32]	0.66 [0.47]
4	0.35 [0.06]	0.36 [0.05]	0.52 [0.34]	0.47 [0.14]
5	0.70 [0.47]	1.40 [0.72]	1.20 [0.61]	2.72 [2.97]
6	0.34 [0.08]	0.41 [0.11]	0.27 [0.10]	0.65 [0.37]
7	0.18 [0.07]	0.24 [0.10]	0.16 [0.05]	0.22 [0.08]
8	0.45 [0.16]	0.20 [0.45]	0.33 [0.08]	0.41 [0.24]
9	-12.45 [32.65]	-2.81 [10.44]	1.48 [1.20]	-1.19 [2.82]
10	0.55 [0.23]	0.42 [0.12]	0.27 [0.07]	0.52 [0.20]
11	0.64 [0.32]	0.90 [0.26]	0.84 [0.21]	1.92 [1.61]
12	1.25 [0.43]	0.98 [0.50]	1.16 [0.60]	2.84 [4.54]
13	1.22 [0.37]	2.19 [0.86]	2.30 [1.08]	2.31 [1.52]
14	0.49 [0.09]	0.55 [0.06]	0.76 [0.13]	0.95 [0.26]
15	0.28 [0.09]	0.36 [0.08]	0.56 [0.12]	0.47 [0.12]
16	1.01 [0.25]	1.05 [0.20]	1.43 [0.73]	1.58 [0.76]
17	0.47 [0.16]	0.72 [0.41]	1.26 [1.12]	0.93 [0.45]

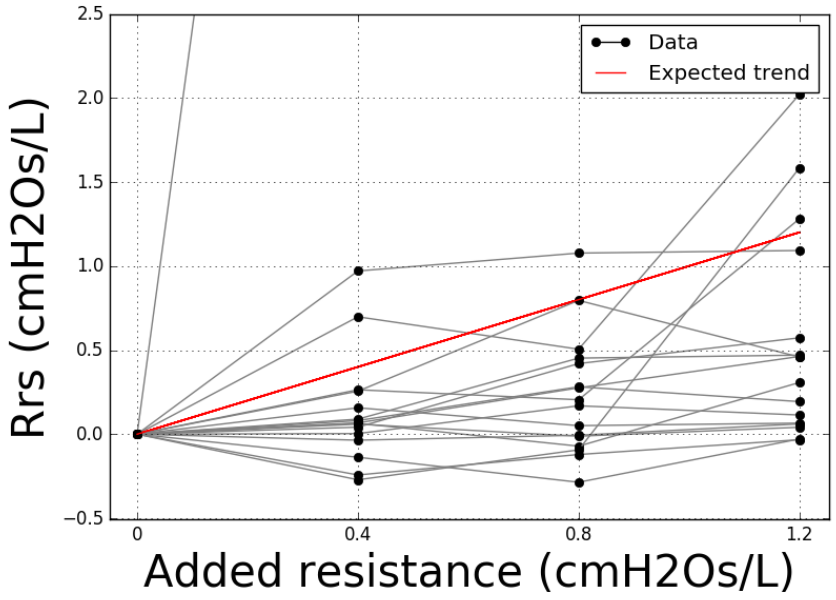

Figure 5.6 R_{rs} trend with added resistance observed for all subjects. R_{rs} is translated to 0 cmH_2Os/L at baseline. No clear trend is seen for increasing added resistance. R_{rs} measured at each added resistance level was expected to rise by the same amount added.

more time for subjects to react to the shutter. Subject 9 appeared to react to

shuttering by significantly reducing respiratory effort after approximately 100 ms of shutter closure, or an air-leak was created around the mouthpiece. This flow reduction resulted in incorrect measurements of decay rate and, consequently, for the resistance calculated from the decay rate.

An assumption of data analysis was the airflow induced by shuttering would be superimposed on average tidal breathing. Due to the reduction in airflow for Subject 9, the effective airflow induced by the shutter is negative, as seen in Figure 5.7. As a result, the correct region could not be identified.

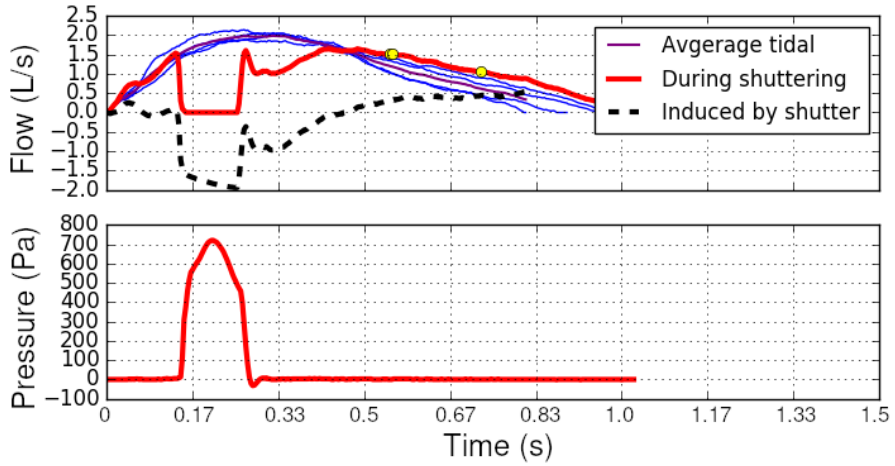

Figure 5.7 Flow measurements for Subject 9 were lower than expected after shutter release. Airflow measured after shuttering was less than average tidal airflow (purple line) and pressure reduced during shutter closure, indicating a muscular reflex in response to the shutter.

In general, the measured decay rates had fairly large intra-subject variation with the standard deviation often as high as 30% of the mean value. Notably, Subjects 2 and 3 showed extremely large variation in measured decay rate. These subjects had a variety of different looking post-shutter waveforms, but no significant reduction in driving pressure. However, the changes in airflow shape indicate possible muscular reaction to shuttering, inducing the observed variability. Hence, even though the decaying flow is correctly identified, the decay rate calculated may be incorrect because it is not possible to separate the effects of the shutter from unexpected muscular reaction.

The degree of muscular reaction to shuttering is expected to decrease with a shorter occlusion duration. Thus, higher breath-to-breath consistency should be able to be achieved by decreasing the duration closer to 100 ms. In addition, subjects in this study were required to consciously breathe deeper than usual due to minimum flow rate limitations. If this limit were reduced or removed, breath-to-breath variation may reduce, because each breath could be driven subconsciously.

An additional cause of variation was the resistance added to the spirometer mouthpiece via venturis specifically designed for this study. The venturi was inserted between the mouthpiece and flow sensor. This positioning added noise to the flow measurements due to turbulent airflow from the venturi. An example is shown in Figure 5.8. This noise increased with increasing resistance, and was large enough for some subjects to obscure the underlying waveform, preventing any valid measurements of decay rate.

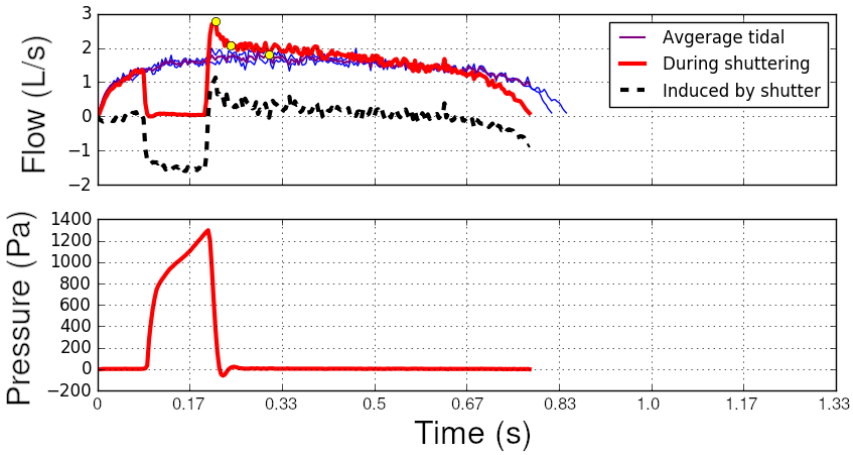

Figure 5.8 Large amounts of noise were added to the flow signal when a venturi was added in series before the flow sensor. Three venturis were used in this study, with constrictions of diameter diameters of 9.5 mm, 10.5 mm and 12.5 mm.

Resistance value, R_{rs} extracted from the decay rate was much smaller than expected. The typical range of airway resistance for healthy subjects is around 1.5-2.5 cmH_2Os/L (Guo et al. [2005], Ward [2005]). However, R_{rs} was less than 1.3 cmH_2Os/L for all subjects at baseline added resistance, shown in Table 5.3. Often, R_{rs} calculated was less than added external resistance alone. Calculated values of elastance all did fall within the expected physiological range for healthy subjects, of 2-10 cmH_2Os/L (Cherniak and Brown [1965], Desai and Moustarah [2019], Galetke et al. [2007]). These results are presented in Chapter 6, where another method was used to calculate airway resistance alongside lung elastance.

Thus, R_{rs} was not significantly or consistently affected by added external resistance, as shown by Figure 5.6. This result shows the decay rate parameters cannot be separated by adding a known external resistance, as was initially thought and indicated mathematically. The phenomenon causing the low R_{rs} values is airflow originating in areas in the centre of airways with low skin friction effects. Because airflow induced by the shutter decays quickly, typically only 20-50 ml of air is

involved. The small volume does not allow enough time for air to flow from higher friction areas, resulting in a poor airway resistance estimate.

The results of this study show that, monitoring decay rate of flow in response to shuttering or other pressure impulses only gives information on lung elastance trends. However, these trends may be hidden by changes in measured R_{rs}. The variability of R_{rs} was found to be fairly low, however this study did not analyse how R_{rs} varies over a long period of time. Monitoring decay rate over a period of time could be clinically useful when assessing the progression of restrictive lung disease types. However, the method proposed in this paper uses a shutter, which allows for direct lung mechanics measurements, as is explained in the following chapter.

5.4 SUMMARY

Monitoring lung mechanics by analysing the respiratory system's response to mechanical shuttering is not recommended. The resistance component of the decay rate only represents a minimal resistance area in the upper airways, not the entire respiratory system. This prevents the separation of lung mechanics using added external resistances. Monitoring the decay rate overtime would only give information about lung elastance trends overtime, but not direct values to assess severity.

Chapter 6

HOW TO MEASURE MECHANICS OF SPONTANEOUS BREATHING

Underlying, tidal-based lung mechanics of spontaneous breathing cannot be directly measured from airflow measurements alone, as has been discussed in the previous two chapters. However, by taking advantage of lung properties described by the single compartment lung model, a spirometer with a built-in shutter to occlude breathing can be used to measure lung mechanics. The lung mechanics measured are a dynamic elastance, which represents a combination of the lung's elastic recoil and muscular expiratory effort, and occlusion resistance, which is a tried-and-tested measure of airway condition.

The lung function test presented in this chapter assesses the lung mechanics of tidal breathing during expiration. These mechanics represent lung condition at average breathing effort. Emphasis was placed on tidal breathing, because average expiratory effort may prove a better marker of lung condition for daily-life, especially for those with respiratory disease, and be more readily and consistently measurable on a regular basis, than peak expiratory effort.

6.1 METHODS

6.1.1 Mechanics identification

Lung mechanics were calculated using the dynamic elastance, single compartment lung model, modified for fully spontaneous breathing, as described in Equation 5.2. A property identifiable using the single compartment lung model occurs when there is no airflow during SB, at which point any pressure measured at the mouth must be due to elastic lung mechanics. If the airways are held open to the atmosphere, lung recoil and muscular effort will balance at atmospheric pressure.

However, if breathing is occluded, the pressure measured at the mouth will be equal to the combination of driving pressure and lung recoil.

This situation creates an opportunity. A shutter built into a plethysmograph was used to occluded expiration for 200 ms, which is longer than the 100 ms minimum needed for pressure to equalise across the respiratory system (Panagou et al. [2004]). When the shutter was released, pressure at the mouth dropped from driving pressure to atmospheric pressure.

Elastance is defined as the pressure in the lung per unit volume. Hence, if muscular effort remains constant for the entire duration of expiration after the shutter is re-opened, end-expiratory elastance can be calculated from the pressure and volume measured momentarily before the shutter re-opens (P_0 and V_0, respectively):

$$P_0 = E_d(t)V_0 \tag{6.1}$$

Occlusion resistance (ROCC) can also be calculated following standard protocol (Eric Yat-Tung Chan [2007], Panagou et al. [2004]). The gradient of pressure from 30-75 ms after the shutter was closed was extrapolated backwards to 30 ms before closure. The difference between this extrapolated pressure and the true pressure measurement at that time was divided by the airflow recorded at that time to produce an estimate for total airway resistance before occlusion, as defined:

$$ROCC = \frac{\Delta P}{Q} \tag{6.2}$$

The pressure and flow points used are shown in Figure 6.1.

Extra resistance was added to the spirometer mouthpiece to simulate upper airway obstruction. The test was repeated twice at each resistance level. The resistances added were 0 (baseline), 0.4, 0.8, and 1.2 cmH_2Os/L, respectively. The large resistance of 1.2 cmH_2Os/L was chosen as an upper limit because this resistance value is only slightly below the expected median resistance of healthy lungs at around 1.6 cmH_2Os/L (Panagou et al. [2004]Ward [2005]Damanhuri et al. [2014]). As a result, with this resistance and the resistance of the device added to the respiratory system, the resistance to breathing felt by a healthy subject would be approximately three times normal. Consequently, breathing would be noticeably more difficult than normal. The two lower resistance values were selected to give a linear increase in resistance from baseline to the upper resistance level.

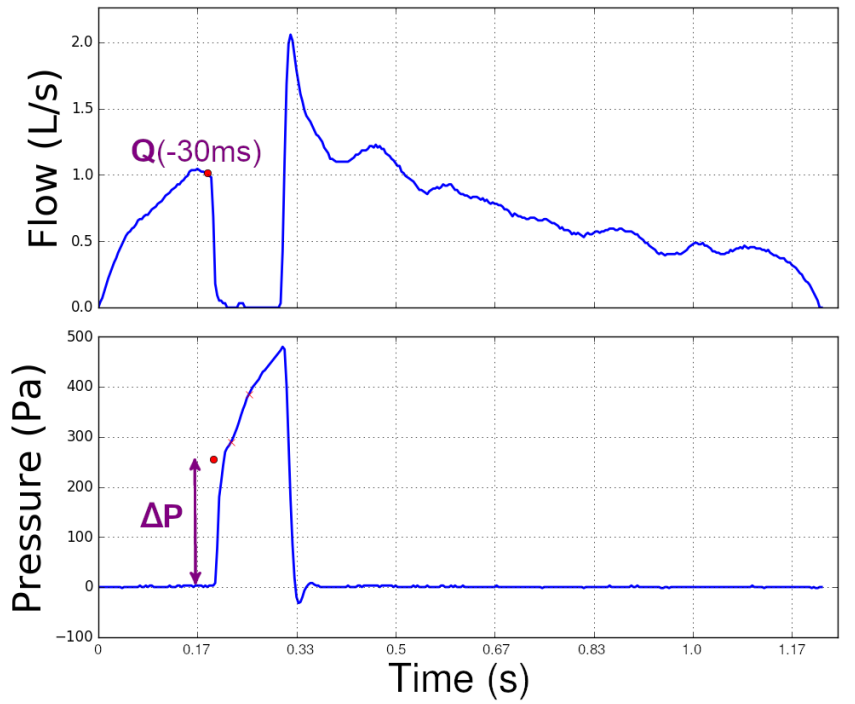

Figure 6.1 Values of flow and pressure used for the calculation of occlusion resistance. The airflow value used is located 30 ms before shutter closure. The pressure used is the difference between pressure extrapolated from 30-75 ms after shutter closure back to 30 ms before closure and the true pressure measurement at that time.

Due to minimum flow limits built into the shuttering software employed, lung mechanics were measured while lightly panting. This panting required slightly more breathing effort than tidal breathing, but significantly less than peak expiratory effort. For each test, the shutter was activated 5 times with a minimum of 5 normal breaths recorded before shuttering.

6.1.2 Data

The same subject data as Chapter 5 was used in this study. Subject data is restated in Table 6.1

This data was recorded using a Ganshorn PowerCube Body plethysmograph with LFX 1.8 Respiratory Diagnostic Software. The Shutter was controlled with LFX software's ROCC mode, in manual trigger mode with a shutter close duration of 200-250 ms (typically 200 ms).

Table 6.1 Subject data. Smokers were included in this study.

Subject	Sex	Age	Height (cm)	Weight (kg)	Smoker
1	M	30	190	100	n
2	M	38	175	100	n
3	M	32	187	87	n
4	M	29	183	95	n
5	F	24	173	80	y
6	M	29	183	78	n
7	M	23	185	73	y
8	M	23	184	71	n
9	M	27	178	90	n
10	F	29	168	62	n
11	F	22	167	53	n
12	F	29	161	53	y
13	F	23	164	64	n
14	F	25	172	70	n
15	M	31	181	114	n
16	F	21	164	72	n
17	F	21	160	56	n

6.1.3 Ethics

The University of Canterbury Human Ethics Committee granted approval for this study, and the collection and use of the clinical data analysed in this study.

6.2 RESULTS

6.2.1 Response to shuttering

Lung elastance calculated at shutter opening is presented in Table 6.2 and the effect of added external resistance on elastance is shown in Figure 6.2. Elastance values range from 3.9-22.1 cmH_2O/L, and generally showed small intra-subject variation for each resistance level with a typical standard deviation less than 1.0 cmH_2Os/L. No clear trend was observed between elastance and added resistance, with elastance remaining fairly consistent between resistance levels.

Expiratory elastance calculated by this test is presented as positive, due to the spirometer defining positive pressure as expiration. When pressure is typically measured for calculating lung mechanics, such as during mechanical ventilation, positive pressure is defined as inspiration. However, a goal of this research is to quantify expiratory effort, so the sign convention is sensible.

Table 6.2 Dynamic elastance (mean [STD dev]) identified for each subject for each resistance level. Elastance was measured at shutter re-opening.

Subject	Ed (mean [std]) cmH_2O/L			
	None	0.4	0.8	1.2
1	5.36 [0.45]	6.14 [0.47]	5.91 [0.14]	6.23 [0.42]
2	4.78 [0.73]	4.47 [0.48]	4.27 [0.39]	5.60 [0.56]
3	5.98 [0.44]	6.34 [0.30]	7.01 [1.74]	6.03 [0.63]
4	7.62 [0.61]	8.06 [0.60]	8.60 [0.77]	8.34 [0.46]
5	7.68 [1.14]	9.98 [1.43]	10.56 [1.18]	11.39 [1.73]
6	6.41 [0.60]	6.16 [0.27]	5.63 [0.19]	5.83 [0.36]
7	3.93 [0.35]	4.23 [0.54]	4.20 [0.45]	4.98 [0.54]
8	5.75 [0.86]	5.22 [1.01]	5.94 [0.65]	5.63 [0.86]
9	7.62 [2.54]	8.25 [1.89]	12.34 [2.81]	10.26 [1.43]
10	8.27 [1.20]	8.64 [0.64]	6.95 [1.18]	8.81 [1.04]
11	14.84 [3.94]	18.19 [3.10]	16.44 [2.97]	14.20 [1.15]
12	8.92 [1.32]	10.15 [1.32]	11.22 [1.77]	10.99 [0.74]
13	17.73 [1.35]	18.44 [2.75]	22.07 [2.77]	16.24 [3.51]
14	14.53 [1.18]	15.72 [0.61]	16.07 [0.87]	15.79 [1.14]
15	7.76 [0.97]	8.88 [1.22]	12.68 [2.50]	13.10 [0.80]
16	17.44 [2.12]	17.42 [1.78]	18.34 [2.95]	17.85 [3.10]
17	8.94 [0.94]	10.10 [1.50]	10.52 [1.17]	10.55 [1.09]

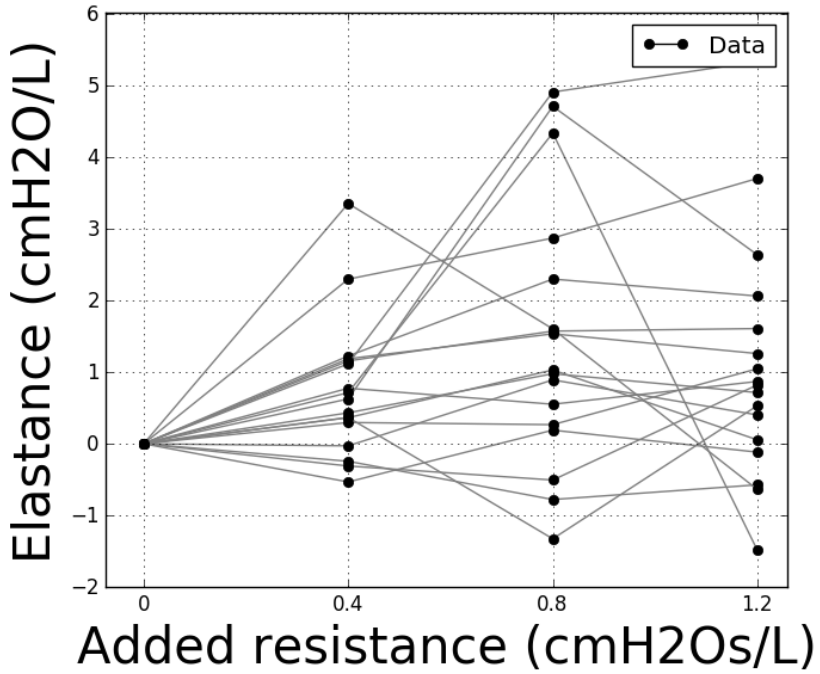

Figure 6.2 Elastance trend with added resistance observed for all subjects. Elastance is translated to 0 cmH_2O/L at baseline. No clear elastance trend is seen for increasing added resistance. However, elastance is likely to increase as external resistance increases.

Table 6.3 shows ROCC calculated for each subject, and the effect of external resistance on ROCC is shown in Figure 6.3. ROCC ranged from 3.0 to 8.0. Measured resistance is expected to increase proportional to the added resistance. Overall, ROCC results match this expectation. However, the deviation from expected ROCC could be quite large, at approximately ±1 cmH_2Os/L at all added resistance levels in this study.

Table 6.3 Occlusion resistance was calculated for each subject at each resistance level. ROCC is expected to increase by 0.4 cmH_2Os/L per external resistance level.

Subject	Rocc (mean [std]) cmH_2Os/L			
	None	0.4	0.8	1.2
1	3.33 [0.55]	3.05 [0.19]	3.51 [0.28]	4.45 [0.79]
2	3.45 [0.36]	3.60 [1.12]	4.47 [1.30]	4.73 [0.95]
3	3.38 [0.25]	3.94 [0.34]	4.31 [0.46]	4.70 [0.86]
4	3.70 [0.73]	3.82 [0.38]	4.01 [0.34]	4.64 [1.15]
5	4.56 [0.62]	4.89 [0.59]	5.23 [0.56]	5.56 [0.65]
6	5.83 [0.60]	6.42 [0.32]	6.41 [0.57]	6.70 [0.49]
7	3.41 [0.31]	3.97 [0.34]	4.09 [0.32]	4.53 [0.55]
8	5.37 [0.88]	5.21 [0.55]	5.66 [0.78]	6.05 [0.70]
9	3.64 [0.29]	3.84 [0.36]	4.23 [0.47]	4.78 [0.89]
10	3.58 [0.27]	4.02 [1.33]	4.34 [0.41]	4.16 [0.47]
11	4.54 [0.38]	4.80 [0.24]	5.40 [0.46]	5.62 [0.75]
12	3.97 [0.29]	5.20 [1.88]	4.87 [0.47]	4.84 [0.45]
13	6.47 [0.39]	6.84 [1.16]	7.85 [1.09]	7.96 [0.92]
14	4.17 [0.19]	5.27 [1.70]	5.29 [1.15]	4.93 [0.61]
15	3.58 [0.30]	3.75 [0.34]	4.71 [0.72]	4.90 [0.53]
16	4.32 [0.35]	5.05 [0.51]	5.45 [0.57]	5.72 [0.77]
17	4.43 [0.51]	5.08 [0.47]	5.96 [0.66]	5.53 [0.80]

6.3 DISCUSSION

6.3.1 Mechanics

The expected range of static elastance for healthy lungs is 2-10 cmH_2Os/L (Cherniak and Brown [1965], Desai and Moustarah [2019], Galetke et al. [2007]). Elastance measured in this study generally fit into this expected range, indicating the majority of airflow could be attributed to lung elastic recoil. As expected, there was no consistent trend between measured elastance and added resistance, because the elastic recoil of the lung is not expected to be affected by changes in external resistance. However, elastance tended to be slightly higher when external resistance was added, indicating increased breathing effort to overcome the extra

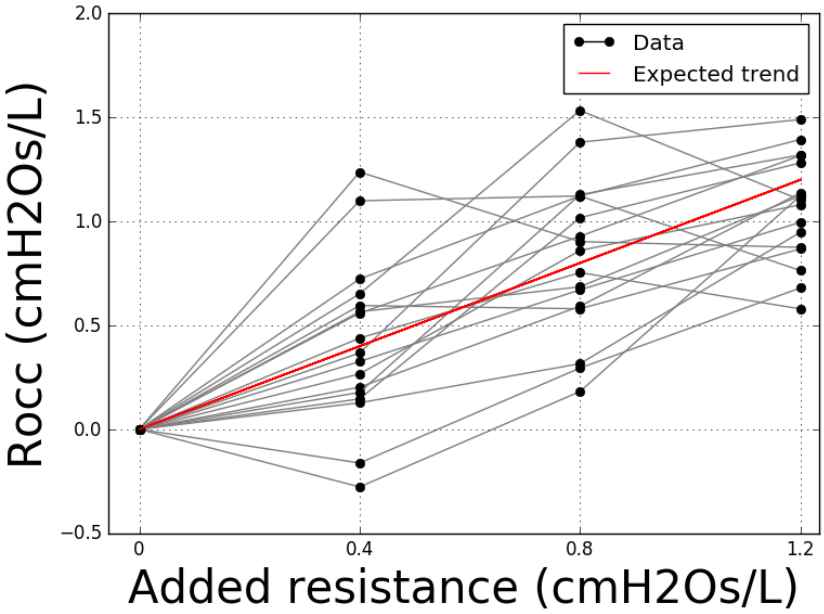

Figure 6.3 ROCC trend with added resistance observed for all subjects. ROCC is translated to 0 cmH_2Os/L at baseline. Generally, ROCC measured at each added resistance level generally increased by the same amount added.

resistance. These results suggest external resistance and the use of shuttering may not significantly affect measured elastance, so measured elastance reflects the true respiratory system elastance. It should also be noted that some breath-to-breath elastance change is expected (Kim et al. [2015]).

Elastance measured for Subjects 11, 13, 14, and 16 was higher than expected. For healthy, tidally breathing subjects, increased elastance in expiration indicates additional muscular expiratory effort on top of lung recoil. The additional elastance due to muscular effort cannot be separated from static elastance without further measures. Hence, expiratory breathing effort during meachanics measurement could indicate restrictive disease where none is present. However, the measurement of combined elastance of tidal breathing may provide clinically relevant information. A larger than expected elastance during quiet tidal breathing indicates an elevated work-of-breathing, which could negatively impact quality of life.

Rocc is an established method to measure airway resistance during tidal breathing. The combined resistance of plethysmograph and mouthpiece was 1.5 cmH_2Os/L. Subtracting this resistance from ROCC measured at 0 cmH_2Os/L added resistance, all subjects fell into the range 1.9-5.2 cmH_2Os/L, which is within but on the upper end of the expected range for healthy subjects (Panagou et al. [2004]Ward [2005]Damanhuri et al. [2014]). ROCC increased as external resistance was added.

However the increase in Rocc was not consistently the 0.4 cmH_2Os/L expected, showing a limitation of the single compartment model or the effect of subject adaption to increased resistance.

The results of this lung function test are expected to show reasonably accurate physiological response to upper airway obstruction (UAO). Resistance was added to the spirometer mouthpiece to mimic UAO. The result was increased measured ROCC and a slight increase in elastance for some subjects as work of breathing increased. These outcomes are as expected for UAO (Bijaoui et al. [2002], Di Mango et al. [2006]).

The venturi design used injected a large amount of noise into the airflow measurements. However, the elastance and ROCC measurements produced by this test notably focus on pressure measured during occlusion, which is not affected by the added resistance. Hence, the test is robust to noisy airflow measurements. An example of the noise injected is shown in Figure 6.4. (Note this figure also appears as Figure 5.8 in Chapter 5).

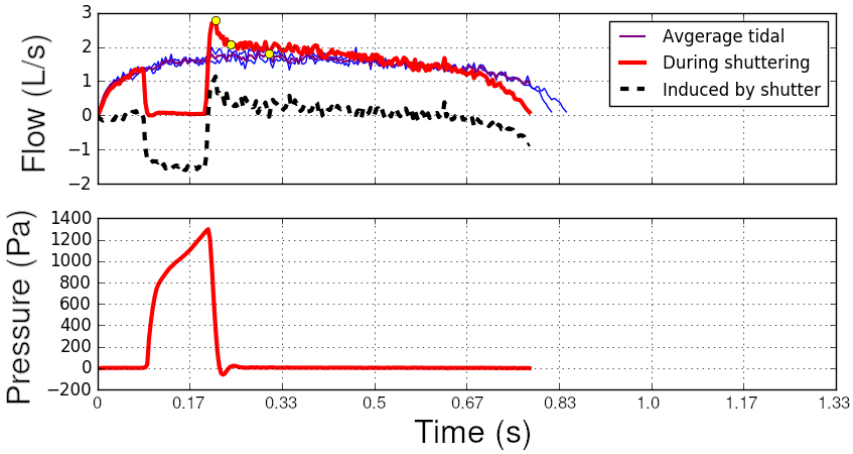

Figure 6.4 Large amounts of noise were added to the flow signal when a venturi was added in series before the flow sensor. Three venturis were used in this study, with constrictions of diameter diameters of 9.5 mm, 10.5 mm and 12.5 mm.

6.3.2 Extrapolating mechanics

In general, the average tidal QV loop for all subjects showed a long, linear end-expiratory relationship between flow and volume, as shown in Figure 6.5. This linear portion begins at peak airflow, and ends 100-200 ml before the lungs empty at end-expiration. A linear relationship between airflow and volume suggests lung mechanics are not changing during this time or are changing at the same rate, as shown by Equation 6.3.

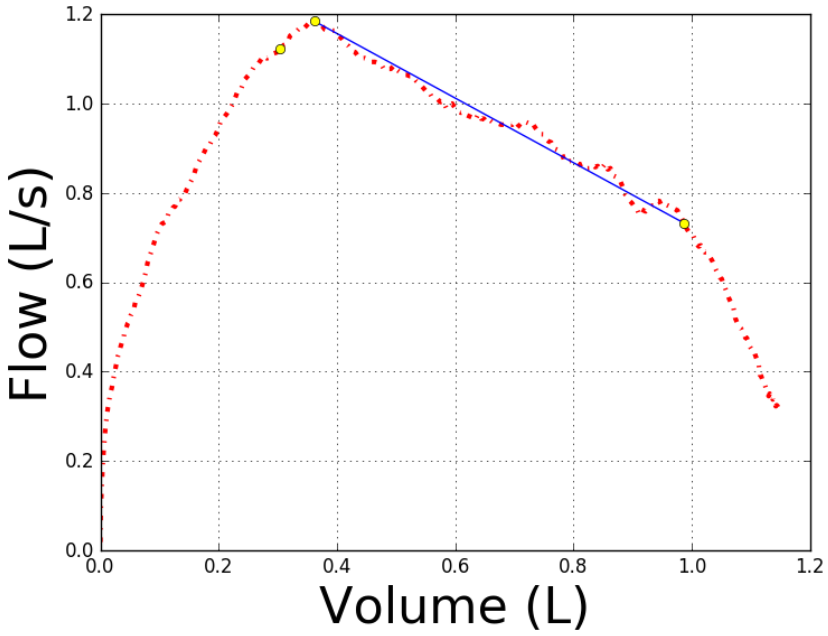

Figure 6.5 Expiration is not an entirely passive process, as seen by non-linearity between flow and volume. This QV loop is the top half of the typically analysed spirometry QV loop, as only expiration is assessed. However, the end-expiratory portion shows a generally linear trend, indicating lung mechanics do not vary significantly in this portion.

$$\frac{E_d}{R_{rs}} = \frac{Q(t)}{V(t)} \tag{6.3}$$

Lung mechanics are not expected to vary significantly in healthy lungs during tidal breathing (Kim et al. [2015]). Therefore, the linear QV relationship seen suggests healthy lung mechanics of end-expiration are relatively constant, with either no or constant muscular activity affecting elastance.

When instantaneous mechanics are measured during end-expiration, the mechanics can be expected to represent the entire end expiratory portion. As a result, lung mechanics measurements could be combined with airflow and volume measured to produce a driving pressure curve for every point in end-expiration.

6.3.3 Limitations

Without further measures, the contribution of static lung tissue elastance cannot be separated from the dynamic elastance created by muscular breathing effort. Subjects in this study showed a range of breathing effort. Increased breathing effort was shown to clearly obscure passive elastance in some cases. This adaption by subjects is effectively "unconscious" in response to added resistance. However,

subjects with respiratory illness, such as COPD, may have less end-expiratory breathing effort capability, as their capacity for breathing effort is reduced, and thus could reduce the effect of the "unconscious" response to increased resistance.

The shutter closure duration was quite long, at 200-250 ms. Reducing occlusion to 100 ms may lead to more consistent intra- and inter-subject results. In particular, because there is less time for subjects to react to shuttering, the adaptation to shuttering would be limited. Hence, there is a tradeoff between shutter duration, readily increased sampling rate, and sensor noise to assess mechanics in this way.

Although QV loops of tidal breathing suggest lung mechanics remain fairly constant at end-expiration, the shutter may cause changes in lung mechanics. The large pressure built-up in the respiratory system during occlusion may cause airways to increase in diameter, reducing their resistance to airflow. Additionally, lung viscoelasticity tends to increase the pressure during shutter closure. The viscoelastic pressure build-up may increase measured elastance calculated at shutter re-opening. This issue may be minimised by reducing the length of breath occlusion with a faster shutter, reducing the amount of pressure build-up in the lung.

Access to a plethysmograph, as used in this study, or a spirometer with built in shutter may be limited. To broaden access to this test, a simple, portable, hand held device could be used to measure these lung mechanics.

6.4 SUMMARY

This chapter describes a novel method to non-invasively measure lung mechanics of tidally breathing subjects. This test was able to identify reasonable dynamic lung elastance along with Rocc, providing new insight into expiratory breathing effort. However, future work is needed to validate this test with different disease states.

Clinically, this lung function test could impact current practise. It does not require high levels of cooperation from the subject, allowing a wider cohort of patients to be assessed. Additionally, this test could be widely accessible as it can be implemented with either a small standalone device, or standard lung function testing equipment.

Chapter 7

TWO-COMPARTMENT LUNG MECHANICS

So far, this thesis has examined lung mechanics measurement using the single compartment lung model. This model assumes lung mechanics are constant for the entire time period analysed. The dynamic elastance model developed by Chiew et al. [2015a] and dynamic resistance model developed by Redmond et al. [2017] extend the single compartment lung model to allow analysis of breathing effort, alveoli collapse and recruitment, and airway collapse and distension. Further extensions by Morton et al. [2018a, b] identify elastance and resistance basis functions over ranges to enable virtual patient prediction. However, all these models are limited by assuming only one lung compartment and one airway.

In the lung, structural differences in the airways can reduce airflow to some regions of the lung while other regions receive higher airflow (Bates [2009]). Additionally, tissue elasticity and imbalances between alveoli can cause air to flow from one part of the lung to another. More complicated lung models are needed to assess these lung heterogeneities. Three multi-compartment lung mechanics models are described in this chapter. They are the parallel two-compartment lung model, series two-compartment lung model, and the viscoelastic lung model, shown by Figures 7.1, 7.2, and 7.3, respectively.

In this chapter, a simple method is used to assess small compartment lung mechanics. These mechanics represent the condition of small airways and viscoelastic lung tissue. The relationship between these mechanics, and the elastance and resistance calculated by the single compartment lung model are compared. This comparison indicates whether the single compartment model captures information about small airways and lung tissue.

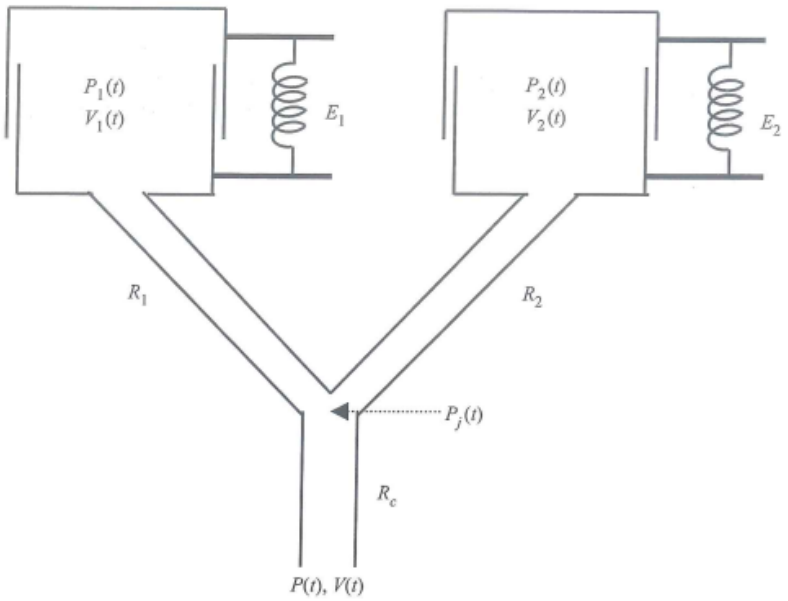

Figure 7.1 Two compartment, parallel lung mechanics model. Reproduced from Bates [2009]. Two elastic compartments with internal pressures P_1 and P_2 are connected by airways with resistance R_1 and R_2 to a larger airway with resistance R_t which leads to the mouth. This effectively models the lungs as having two discrete lung units with different elastic properties. If P_1 and P_2 are different, air may flow from one unit to the other.

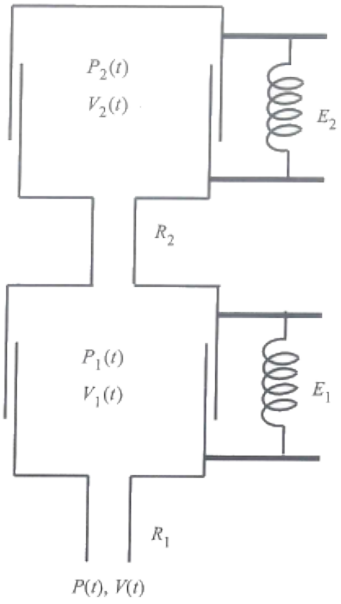

Figure 7.2 Two compartment, series lung mechanics model. Reproduced from Bates [2009]. This models the lung as a chain of two elastic compartments. The internal pressure of the end compartment is P_2, and it is connected to the second compartment by an airway of resistance R_2. The start compartment has internal pressure P_1 and is connected to the mouth with an airway of resistance R_1

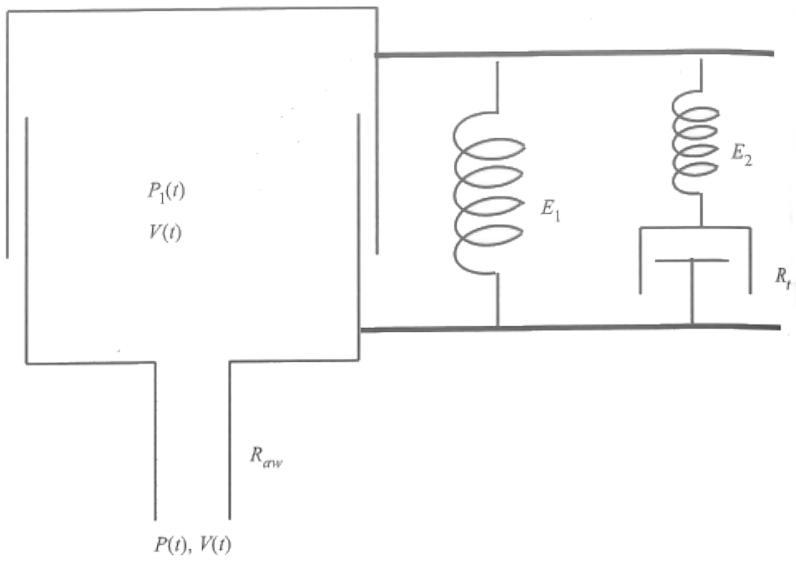

Figure 7.3 Viscoelastic lung mechanics model. Reproduced from Bates [2009]. The lung is modeled as a single, homogeneously ventilated compartment, with internal pressure P_1. This compartment is ventilated through an airway with resistance R_{aw}. Lung tissue elastance creating P_1 is represented by a Kelvin body, made up of components E_1, E_2, and R_t. The Kelvin body represents a fast elastic response to changing lung volume, by E_1, and a slower, damped elastic response by components E_2 and R_t.

7.1 METHODOLOGY

7.1.1 Identifying the best parameter to model

The derivations of the equations of motion for the three lung models introduced in this chapter are significantly more complicated than for the single compartment lung model. All three models describe alveolar pressure using a four parameter model, dependent on flow, rate of change of flow, rate of change of pressure, and volume. These derivations are explained in detail by Bates [2009]. The lung models can be simplified to the form:

$$P(t) = A\ddot{V}(t) + B\dot{V}(t) + CV(t) - D\dot{P}(t) \tag{7.1}$$

where t is time, V is volume, and P is driving pressure.

A shutter prevents airflow during breath-occluding lung function tests. While the shutter is closed, the pressure measured at the mouth is an approximation of the driving pressure. When airflow is interrupted during passive expiration, an immediate, relatively large pressure increase followed by a smaller gradual increase over time can be measured at the mouth. This effect is shown in Figure 7.4.

The large pressure increase can be attributed to pressure equalisation in the large proximal airways. The smaller gradual increase can be attributed to stress recovery, and gas redistribution within the lung (Bates et al. [1988]).

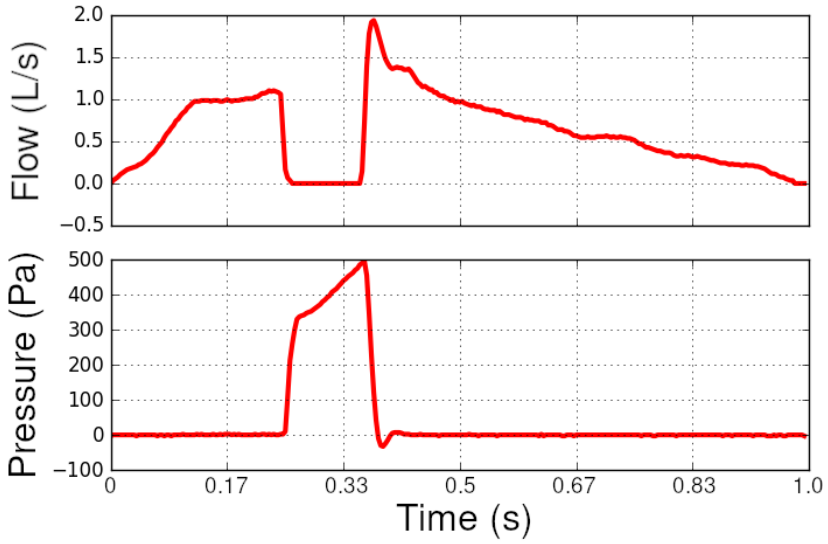

Figure 7.4 Top: Flow measured during shuttered tidal expiration. No airflow is measured when shutter occludes breath. Bottom: Pressure measured at mouthpiece during shuttered tidal expiration. Note the rapid pressure increase followed by a slower increase sustained for entire shutter duration.

The parameters A, B, C, and D in Equation 7.1 represent different combinations of underlying resistance and elastance for different two-compartment models. Due to this model ambiguity, with different properties of lung tissue and gas exchange able to be modeled by the same equation, it is not possible to say which property predominantly causes the slow increase in pressure during occlusion. Hence, there are potential identifiability issues (Docherty et al. [2011])

Total lung volume remains constant during shuttering. As a result, parameter C creates a constant effect on pressure during this time. Parameters A and B depend on the airflow between lung compartments, which cannot be measured by an interrupter technique, and parameter D depends on the rate of change of measured pressure.

To simplify analysis of the effect of cheek holding on stress recovery and air redistribution during breath occlusion, only parameter D was estimated. Parameter C is dependent on lung volume, which is constant during occlusion. Parameters A and B are assumed to be dominated by parameter D because all subjects in this study were healthy with minimal expected levels of air redistribution in the lung.

The resulting model to solve under these assumptions is defined:

$$P(t) = P_0 + D\dot{P}(t) \tag{7.2}$$

In parallel, series, and viscoelastic two compartment lung models, parameter D is described as the sum of all small compartment resistance divided by the sum of all small compartment elastance (Bates [2009]). The combination of lung mechanics represented by parameter D for the parallel, series, and viscoelastic lung models are respectively defined.

$$D = \frac{R_1 + R_2}{E_1 + E_2} \tag{7.3}$$

$$D = \frac{R_2}{E_1 + E_2} \tag{7.4}$$

$$D = \frac{R_t}{E_2} \tag{7.5}$$

Because the time during which breathing is occluded is kept to a minimum in this study, all small compartment lung mechanics are assumed to be constant for the entire duration of the occlusion. As a result, the average rate of change of pressure from 30 ms after shutter closure until 30 ms before peak pressure was used to calculate parameter D from Equation 7.2. The result is a combined measurement of the small airways resistance and viscoelastic lung tissue.

7.1.2 Mechanics identification

A shutter built into a plethysmograph was used in this study to induce a decay rate in flow during tidal expiration. The plethysmograph and accompanying software is the same as for the studies in Chapters 5, and 6. Subjects in this study were asked to pant into the plethysmograph's mouthpiece. The shutter closed after the point of peak expiratory flow for 200-250 ms, and was activated 5 times with a minimum of 5 normal breaths between each shutter activation. This test was repeated twice for each subject, with a several minute rest between each test.

For each shuttered breath, the lung mechanics calculated were occlusion resistance,

and end-occlusion elastance. Occlusion resistance was calculated as per standard method (Eric Yat-Tung Chan [2007], Panagou et al. [2004]). The gradient of pressure from 30-75 ms after shutter was closed was extrapolated backwards to 15 ms before closure. This value was divided by the airflow recorded at that time to produce an estimate for airway resistance. Elastance was calculated as the pressure measured 30 ms before the shutter reopened divided by the measured volume of air in the lung during shuttering.

7.1.3 Data

Fifteen healthy subjects were enrolled in this study (6 Female, 8 Male, Age 27±4, BMI 24.5±3.8, 3 Smokers). All data used in this study was recorded by a Ganshorn PowerCube Body plethysmograph using LFX 1.8 Respiratory Diagnostic Software. Shuttering was controlled using the LFX software's ROCC manual activation mode. Table 7.1 shows specific details for each subject.

Table 7.1 Subject data. Smokers were included in this study.

Subject	Sex	Age	Height (cm)	Weight (kg)	Smoker
1	M	30	190	100	n
2	M	38	175	100	n
3	M	32	187	87	n
4	M	29	183	95	n
5	F	24	173	80	y
6	M	29	183	78	n
7	M	23	185	73	y
8	M	23	184	71	n
9	M	27	178	90	n
10	F	29	168	62	n
11	F	22	167	53	n
12	F	29	161	53	y
13	F	23	164	64	n
14	F	25	172	70	n
15	M	31	181	114	n

7.1.4 Ethics

The University of Canterbury Human Ethics Committee granted approval for this study, and the collection and use of the clinical data analysed in this study.

7.2 RESULTS

The pressure gradient measured between 30 ms after shutter closure and 30 ms before peak pressure is referred to as the "relaxation gradient". The relaxation gradient is parameter D in Equation 7.2, and represents the combined small airways and viscoelastic lung tissue mechanics. The relaxation gradient was compared to volume and pressure measurements reflecting initial and final conditions of the lung during shuttering, and to the lung mechanics calculated.

These relationships were analysed using a linear regression between the measurements of interest. R^2 values were calculated on these regression lines separately for each subject, and for all subjects combined to give an overall trend. These trends indicate whether single-compartment lung mechanics are able to capture small lung compartment mechanics. The R^2 values and overall gradients of the regression lines are shown in Tables 7.2 and 7.3, respectively.

Table 7.2 R^2 value on regression line between relaxation gradient and measured data. Values were calculated separately for each subject, all subjects combined, and all subjects combined excluding subject 13.

Subject	Volume	Start pressure	End pressure	Elastance	Rocc
1	0.53	0.23	0.66	0.15	0.16
2	0.07	0.06	0.06	0.06	0.02
3	0.78	0.26	0.81	0.01	0.06
4	0.54	0.06	0.73	0.02	0.23
5	0.21	0.52	0.83	0.57	0.21
6	0.40	0.07	0.64	0.02	0.13
7	0.13	0.01	0.42	0.12	0.04
8	0.50	0.22	0.44	0.01	0.13
9	0.49	0.40	0.03	nan	0.10
10	0.06	0.08	0.23	0.48	0.07
11	0.27	0.02	0.35	0.01	0.10
12	0.04	0.02	0.12	0.00	0.00
13	0.22	0.11	0.68	0.35	0.01
14	0.00	0.01	0.46	0.10	0.00
15	0.32	0.47	0.74	0.27	0.02
overall	0.05	0.37	0.68	0.27	0.15
without S13	0.13	0.08	0.37	0.03	0.00

7.2.1 Volume

A linear regression of relaxation gradient and volume was calculated for each individual in this study. For 14/15 subjects, the relaxation gradient was positively

Table 7.3 Gradient of overall regression line between relaxation gradient and measured data. Regression calculated for all subjects combined, and all subjects combined excluding subject 13.

	Volume	Start pressure	End pressure	Elastance	Rocc
Overall	3.38	2.25	1.60	0.68	1.66
Without S13	3.68	0.99	1.36	0.18	-0.01

correlated with lung volume.

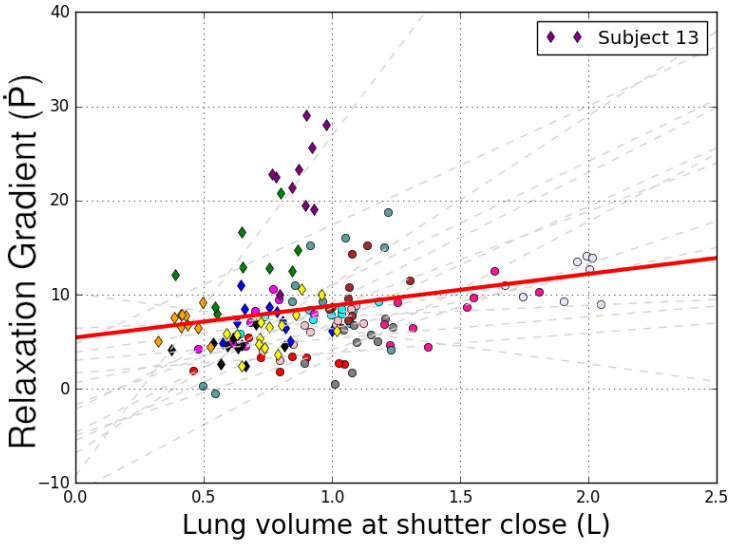

Figure 7.5 Regression lines calculated between relaxation gradient and lung volume at shutter closure for each subject are shown in grey. Positive overall regression is shown in red.

A positive overall regression for all 148 shuttered breaths was calculated, and is shown in red in Figure 7.5. The R^2 of this regression was very low at 0.05. However, excluding the outlier Subject 13 raised the R^2 value to 0.13 without significantly affecting the gradient of the regression line (see Table 7.3).

7.2.2 Pressure

Pressure was measured at both 30 ms after shutter closure and at 30 ms before peak pressure. Both of these pressures were positively correlated to relaxation gradient, as shown in Figures 7.6 and 7.7, respectively.

As shown in Tables 7.2 and 7.3, the regression calculated at shutter closure was highly dependent on Subject 13. The subject-specific R^2 value for pressure measured 30 ms after shutter closure decreased from 0.37 to 0.08 and the gradient reduced from 2.25 to 0.99 when Subject 13 was removed from the overall regression line. The changes for peak pressure were much smaller, with R^2 reducing from

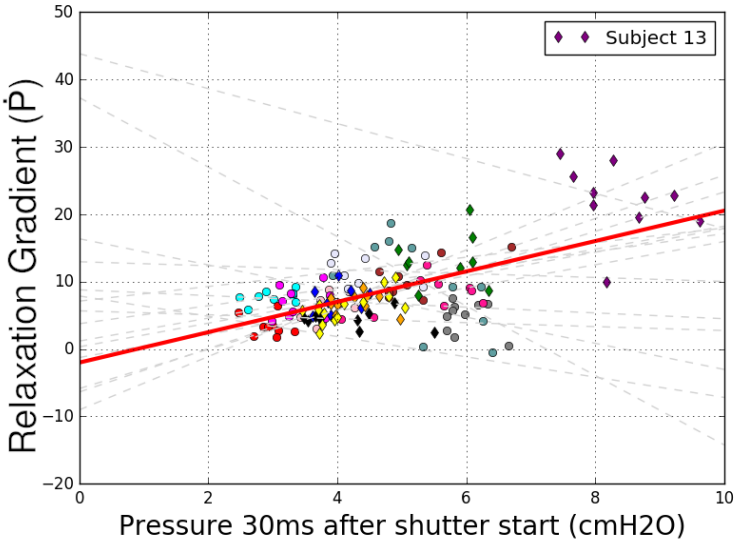

Figure 7.6 Regression lines calculated for each subject between relaxation gradient and pressure measured 30 ms after shutter closure are shown in grey. Positive overall regression is shown in red.

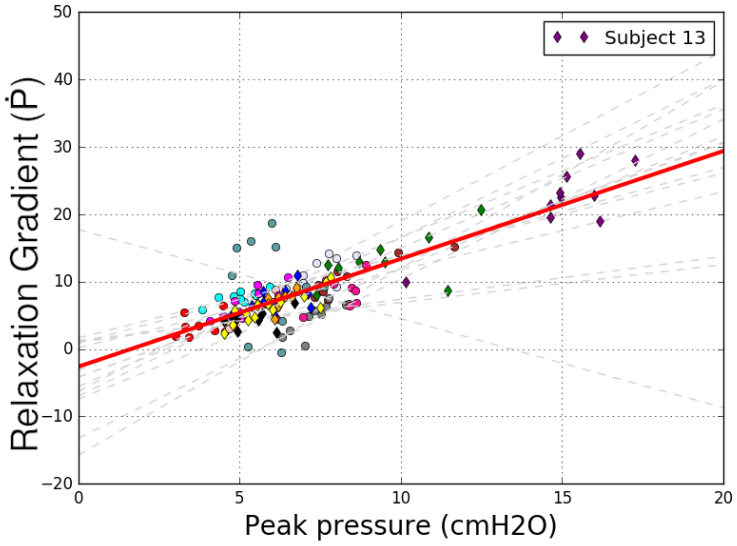

Figure 7.7 Regression lines calculated for each subject between relaxation gradient and pressure measured 30 ms before peak shuttered pressure are shown in grey. Positive overall regression is shown in red.

0.68 to 0.37 and the regression line's gradient reducing from 1.60 to 1.36.

7.2.3 Lung elastance

With Subject 13 included, elastance appeared to be weakly correlated with the relaxation gradient, as shown in Figure 7.8, with R^2 value of 0.27 and gradient 0.68. However, when Subject 13 was removed the R^2 value dropped to 0.03, and

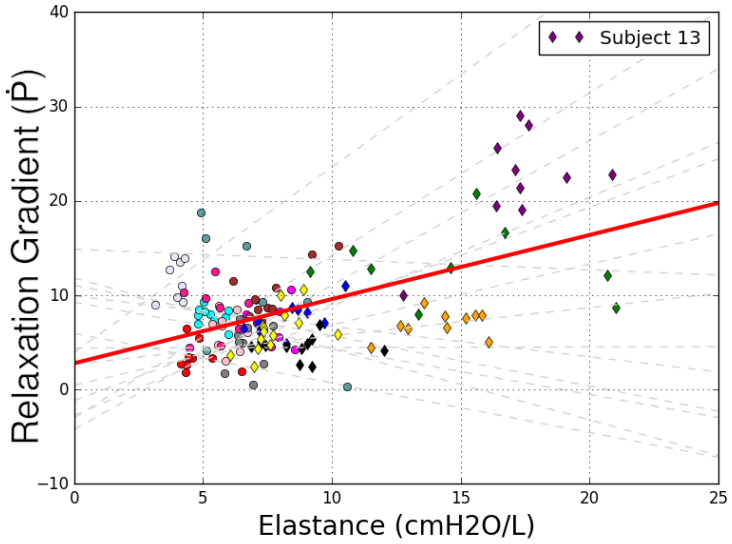

Figure 7.8 Regression between relaxation gradient and elastance calculated at shutter opening. Separate regression for each subject is shown in grey, and overall regression is shown in red.

gradient also reduced significantly to 0.18.

Subject 9 was not included in analysis, due to a reflexive response to shuttering preventing elastance measurement. This response is explained further in the discussion.

7.2.4 Airway resistance

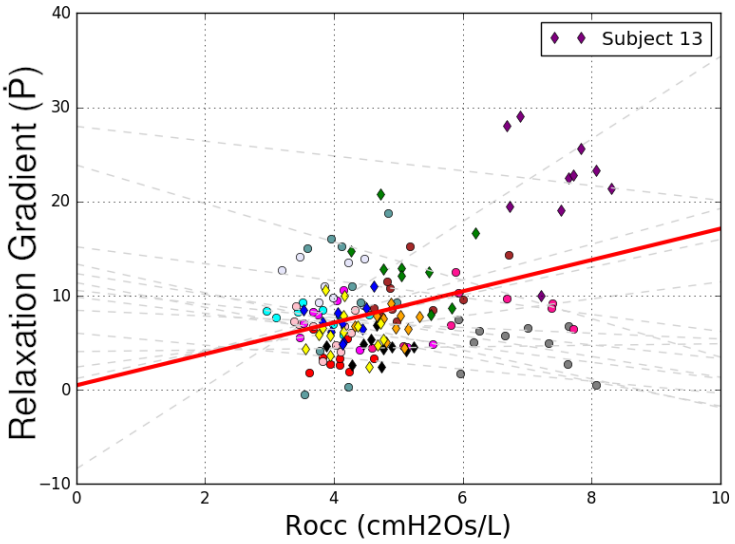

Figure 7.9 Regression between relaxation gradient and occlusion resistance calculated at shutter closing. Separate regression for each subject is shown in grey, and overall regression is shown in red.

Similar to elastance results, no clear relationship was identified between occlusion resistance (ROCC) and relaxation gradient. The regression line is shown in Figure 7.9. R^2 of the regression with Subject 13 excluded was 0.00, with gradient -0.01 as shown in Tables 7.2 and 7.3. The R^2 value and gradient changed significantly with Subject 13 added to the regression.

7.3 DISCUSSION

7.3.1 Subject 13

Data from Subject 13 significantly influenced the overall regressions calculated in this study. This influence was due to many of their metrics being significantly higher than all other subjects. They had the highest measured ROCC, relaxation gradient, pressure, and average elastance, with normal flow decay rate and lung volume at shutter closure. These changes were likely due to Subject 13 having teeth extracted several hours before their lung mechanics were measured, resulting in the increased mechanics observed.

The significant changes in metrics mean this subject is visible as a clear outlier in every regression figure in this study. No other subjects were found to significantly alter overall results when removed from the regression. Hence, results are presented with and without this subject.

7.3.2 Subject 9

Elastance could not be measured for Subject 9. The shutter duration used in this study (200 ms) was twice as long as the minimum required, and could not be changed for this study. The drawback of a longer shutter duration is it gives more time for subjects to react to the shutter. Subject 9 appeared to react to shuttering by significantly reducing respiratory effort after approximately 100 ms of shutter closure, or an air-leak was created around the mouthpiece, as seen in Figure 7.10. As a result, the airflow measured at shutter re-opening was less than expected for tidal breathing alone. Increased airflow is expected at shutter re-opening due to a superposition of airflow due to the shutter and tidal breathing. Hence, no elastance was calculated.

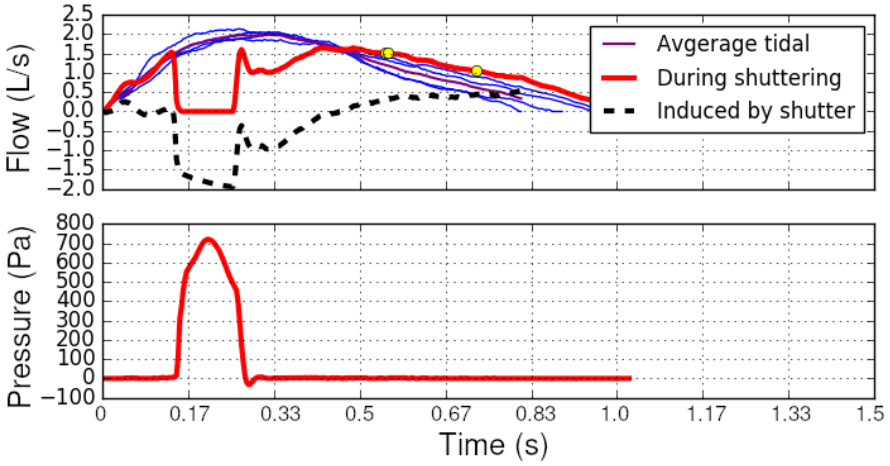

Figure 7.10 Flow measurements for Subject 9 were lower than expected after shutter release. Airflow measured after shuttering was less than average tidal airflow (purple line) and pressure reduced during shutter closure, indicating a muscular reflex in response to the shutter.

7.3.3 Initial conditions (Volume and pressure at shutter closure)

The results of this study suggest relaxation gradient is affected by lung volume at shutter closure. Linear regression to volume measurements were stable, even after the removal of the outlier data from Subject 13, as shown in Tables 7.2 and 7.3. Lung volume was the only metric to show an increased R^2 on the regression line when the outlier, Subject 13, was removed.

In this study, lower lung volumes were associated with lower rates of pressure increase at the mouth during occlusion. As lung volume reduces, airway resistance will increase as airway diameter reduces. The reduction in diameter slows the rate air can redistribute in the lung, and consequentially the rate of pressure increase at the mouth. Additionally, some portions of the lung may no longer be recruited, trapping air in the lungs. Trapped air would not contribute to the pressure increase seen at the mouth.

In contrast, the relaxation gradient does not appear to be correlated with the pressure measured at shutter close. This pressure is created by two main mechanics. The first is the natural recoil from the lung and chest wall. The second is the additional external pressure from muscular breathing effort.

The pressure generated by lung recoil increases proportional to the volume of air in the lung, $P = EV$. This relationship with volume, which does appear to affect the relaxation gradient, may explain the slight positive correlation seen between relaxation gradient and pressure.

Changes in muscular breathing effort during shuttering significantly affect the measured pressure, obscuring the contribution of air redistribution and viscoelasticity. Because subjects were asked to pant, there may be additional time-varying pressure due to breathing effort on top of the underlying relaxation gradient. A faster shutter could alleviate this effect.

7.3.4 Final conditions (Peak pressure)

Peak pressure has a stronger correlation with the relaxation gradient than any other metric. This correlation is due to the relaxation gradient defining the end-occlusion pressure, due to pressure at the mouth increasing according to the relaxation gradient during shuttering.

7.3.5 Lung mechanics

The elastance calculated from end shutter pressure, which typically equaled the peak pressure, was not closely correlated with relaxation gradient. This result shows the lung elastance calculated by the single compartment model does not account for small lung tissue mechanics well. Elastance is calculated as $P_d(t)/V(t)$. Because peak pressure is affected by the relaxation gradient, and the relaxation gradient is affected by the lung volume, when elastance is calculated, dividing by volume appears to remove the effect of the relaxation gradient on pressure.

The lack of correlation between relaxation gradient and elastance supports the hypothesis that the relaxation gradient of healthy lungs is not significantly affected by the range of driving pressures seen during normal tidal breathing (Freezer et al. [1993]). At larger lung volume and driving pressures, an increase in elastance would be seen, due to limitations of non-elastic lung tissue (Al-Rawas et al. [2013]).

No clear relationship was identified between occlusion resistance and relaxation gradient. This outcome was expected because occlusion resistance is calculated from the pressure change at shutter closure. This pressure change is attributed to the static lung resistance of the proximal airways. The effects of small airways and tissue deep in the lung take longer to be observed.

The results of this study indicate the lung mechanics measured with the interrupter technique do not represent mechanics of air redistribution and viscoelastic effects within the lung. As a result, mechanics measured from shuttering may not be

able to be used to accurately monitor or detect conditions affecting small airways or tissue deep in the lungs, such as ARDS.

However, the relaxation gradient is readily available for measurement in breath-occluding lung function tests. Monitoring this parameter alongside standard lung mechanics measurements from the single compartment lung model could give insight into the condition of the small airways and viscoelastic lung tissue. The specific small-tissue mechanics combined to create the relaxation gradient cannot be separated using the method described in this study. Hence only the trend of these mechanics can be monitored overtime, not the absolute changes in each specific mechanic. Clinically, monitoring the relaxation gradient could be a simple and useful tool for tracking disease progression in outpatient care over a period of time. It could show changes in lung condition which single compartment lung mechanics measurements could miss in diseases which are known to affect the small airways or lung tissue (such as COPD).

7.3.6 Limitations

This study analysed tidal breathing of healthy subjects. Hence, the results found may only be applicable to healthy lungs. Lung disease may affect the observed lung mechanics significantly, and the relationships analysed in this study. These results are also only applicable for low levels of lung volume and breathing effort, typically seen during normal tidal breathing. Mechanics measured during peak expiratory effort may be different, but also more variable in patients with lung disease.

Expiration during spontaneous tidal breathing is not entirely passive. Hence, decoupling the effect of breathing effort and air redistribution or viscoelasticity on the relaxation gradient is not possible without more invasive measurements. Such measurements are atypical, even for inpatients in hospital, but could be provided by Electrical impedance tomography (EIT) for example (Gong et al. [2015], Krueger-Ziolek et al. [2017], Zhao et al. [2014]).

7.4 SUMMARY

Lung elastance and airway resistance measured by the single compartment lung model during tidal expiration in healthy subjects were not found to be reflective of small airways resistance and lung viscoelasticity. As a result, using these lung

mechanics measures alone to monitor changes in lung condition over time may miss information about changes in condition of small airways and lung tissue.

Measuring the relaxation gradient during breath-occluding lung function tests is simple, and two-compartment lung models show it is highly dependent on small airway resistance and elasticity. Hence, monitoring this metric alongside other lung function testing may provide useful insight into lung condition.

Chapter 8

EFFECT OF CHEEK SUPPORT ON MECHANICS MEASUREMENTS

The mechanics from all previous chapters in this thesis were collected without cheek support. Lung function tests provide significant diagnostic potential, so it is vital results correctly and consistently represent respiratory system mechanics. This chapter will assess the effect of missing cheek support on measured lung mechanics in breath-occluding lung function tests.

Typically, patients are told to place their hands on their cheeks during lung function testing. Correct levels of cheek support are particularly important during lung function tests which occlude airflow, because the build-up of pressure in the mouth causes the cheeks to rapidly expand outwards. This expansion adds an additional elastic component to the respiratory system (Jaeger [1982]) and alters the measured pressure at the mouth. As a result, lung mechanics measured by breath-occluding lung function tests without cheek support will not represent the true state of the respiratory system.

Previous research quantified the effect of the cheeks on airway resistance measurements using the interrupter technique (Hadjikoumi et al. [2003], Jaeger [1982]). These studies found measured resistance increased when cheek support was added, and the variability of resistance measurements remained consistent regardless of the level of cheek support. However, the effect of cheek support on other lung mechanics, such as lung elastance, has not been studied as thoroughly. Lung elastance and airway resistance measurments can assess patient state in lung disease, such as COPD.

The data assessed in this chapter was obtained with the goal of developing a standard lung function test to more readily measure elastance and resistance. The test briefly occludes airflow at regular breath intervals to obtain lung mechanics,

with and without cheek support. If a reliable method to account for missing cheek support in this test can be established, breath-occluding lung function tests could be further simplified for easier and more regular use and monitoring in outpatient care.

8.1 METHODOLOGY

The aim of this study was to identify cohort-wide trends which could be used to correct for missing cheek support. Nine healthy subjects were recruited for this study. Resistance, elastance and viscoelastic lung mechanics of each subject were measured by briefly occluding expiration during tidal breathing, and the effect of cheek support on each mechanic was quantified.

8.1.1 Model and Experiments

Lung mechanics were calculated using the dynamic elastance, single compartment lung model (Bates [2009], Chiew et al. [2015a]), modified for fully spontaneous breathing, as described in Equation 8.1:

$$E_d(t)V(t) = R_{rs}Q(t) \tag{8.1}$$

where $E_d(t)$ and R_{rs} are the dynamic lung elastance and airway resistance, respectively. This model describes the respiratory system as a balance between respiratory muscles creating pressure to drive airflow, and the airway resistance and passive elastic respiratory forces opposing airflow. A detailed description of this model can be found in Chapter 5.

Expiration was occluded in this study by a shutter built into a plethysmograph. The plethysmograph used was the same as for Chapters 5, 6, and 7. The shutter occluded expiration for 200 ms, which is longer than the 100 ms minimum needed for pressure to equalize across the respiratory system (Panagou et al. [2004]). Due to built-in minimum flow limits in the shutter control software, lung mechanics were measured while panting. Panting is somewhat more effort than normal tidal breathing, but is not near peak breathing effort.

For each test, the shutter was activated a minimum of 5 times with a minimum of 5 normal breaths recorded before shuttering. To provide cheek support, subjects were asked to place their hands on their cheeks and thumbs under the mouth base

for the entire duration of the test. Two tests with cheek support and two tests without cheek support were recorded for each subject.

No air flows out of the lung when expiration is occluded. Hence, the pressure measured during occlusion is equal to the driving pressure, $E_d(t)V(t)$. In this study, E_d was calculated as pressure measured 30 ms before the shutter reopened divided by volume.

Occlusion resistance, ROCC, can be estimated from the pressure change at the instant airflow is occluded. This was measured using the standard method for calculating occlusion resistance (ROCC) (Eric Yat-Tung Chan [2007], Panagou et al. [2004]). The gradient of pressure from 30-75 ms after shutter was closed was extrapolated backwards to 15 ms before closure. This value was divided by the airflow recorded at 15 ms before closure to produce an estimate for airway resistance.

Two-compartment lung models account for the effect of tissue stress recovery and air redistribution within the lung. To simplify analysis of the effect of cheek holding on stress recovery and air redistribution during breath occlusion, one parameter was calculated to describe the combination of small airways and viscoelastic lung mechanics. A detailed description of this parameter can be found in Chapter 7.

The resulting model to solve under these assumptions is defined:

$$P(t) = P_0 + D\dot{P}(t) \tag{8.2}$$

Where, D is the parameter of interest. As a result, the average rate of change of pressure from 30 ms after shutter closure until 30 ms before the peak pressure was used to indicate the effect of cheek holding on viscoelastic lung mechanics.

8.1.2 Patients and Data

Nine subjects had their lung mechanics calculated with the shuttering technique after obtaining informed consent. Four tests were run for each Subject, two with cheeks held and two without cheeks held. The shutter was activated a minimum of 5 times each test. Table 8.1 shows specific details for the subjects.

All data used in this study was recorded by a Ganshorn PowerCube Body plethysmograph using LFX 1.8 Respiratory Diagnostic Software. Shuttering was con-

Table 8.1 Subject data.

Subject	Sex	Age	Height (cm)	Weight (kg)	Smoker
1	M	31	181	114	n
2	F	21	164	72	n
3	F	21	160	56	n
4	M	19	179	81	y
5	F	22	167	53	n
6	M	29	173	105	n
7	F	22	180	68	n
8	M	27	178	68	n
9	F	21	177	72	n

trolled using the LFX software's ROCC mode, configured for manually triggered shuttering with a shutter closure duration of 200-250 ms (typically 200 ms).

8.1.3 Ethics

The University of Canterbury Human Ethics Committee granted approval for this study, and the collection and use of the clinical data analysed in this study.

8.2 RESULTS

The percentage change in mean elastance and resistance (Equations 6.1 and 6.2 in Chapter 6, respectively) and viscoelastic lung mechanics (Equation 7.2 in Chapter 7) from unsupported to supported cheeks was calculated for each Subject. Full results of the change in mean measured lung mechanics are presented in Table 8.2. Outlier measurements were excluded when calculating the mean mechanics values. Outliers were identified as being 1.5x the IQR (interquartile range) above the upper quartile or below the lower quartile.

Table 8.3 shows the average maximum pressure and lung volume measured during occlusion for each subject, and the average change in pressure and volume observed when cheek support was added. Peak pressure typically occurs at the end of occlusion. Excluding Subjects 5 and 8, peak pressure remained constant or increased as cheek support was added. All subjects, except Subjects 5 and 8, also showed less than 10 % absolute change in lung volume when cheek support was added. Subjects 5 and 8 have high pressure, high volume breaths during the tests without cheek support. However, when cheek support was added, Subjects 5 and 8 have smaller and lower pressure breaths, causing the negative pressure change

Table 8.2 Percentage change in mean lung mechanics measurement from no cheek-holding to cheek-holding

Subject	Elastance (%)	ROCC (%)	Viscoelastic parameter (%)
1	27.0	7.6	49.3
2	1.6	17.6	4.6
3	5.4	6.1	44.6
4	66.8	4.4	68.2
5	29.7	17.1	-4.7
6	23.8	11.1	37.0
7	14.4	21.8	1.5
8	11.2	-4.5	36.0
9	23.0	7.4	9.0

observed.

Table 8.3 Average peak pressure (P) measured during occluded breaths, and lung volume during occlusion (V). The percent change in pressure when cheek support was added was also calculated.

Subject	Cheeks unsupported		Cheeks supported		Difference (%)	
	P (Pa)	V (L)	P (Pa)	V (L)	P (%)	V (%)
1	598	0.77	747	0.79	24.9	2.5
2	1253	0.74	1309	0.79	4.5	6.3
3	653	0.74	728	0.81	11.5	8.6
4	492	0.97	789	1.06	60.3	8.5
5	1960	1.09	1718	0.80	-12.3	-36.3
6	698	3.16	841	2.91	20.5	-8.6
7	683	0.93	844	0.99	23.6	6.1
8	603	1.14	541	0.93	-10.3	-22.6
9	484	0.78	589	0.80	21.7	2.5

Lung mechanics measurements with supported and unsupported cheeks are compared in boxplots in Figure 8.1-8.3. Results of tests without cheek support are identified as IDs 1-9, and tests with cheek support added are identified as IDs 1a-9a for Subjects 1-9, respectively.

Measured elastance for every shuttered breath is presented in Figure 8.1. Measured elastance remained constant or increased for every subject when cheeks were supported. The maximum increase in elastance was 66.8 % for Subject 4. In general, the variation of measured elastance for a subject was consistent, regardless of whether cheeks were supported or unsupported.

The amount of variation in measured elastance does not appear to correspond to how much mean elastance changes between supported and unsupported cheeks.

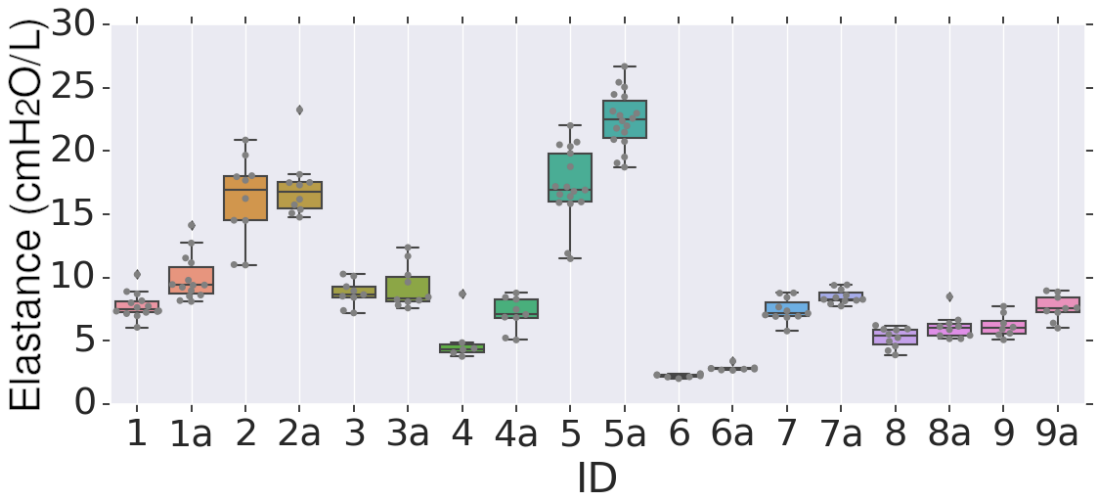

Figure 8.1 Comparison of elastance measurements without cheek support (ID 1-9) and with cheek support added (ID 1a-9a). Box-and-whisker graphs are displayed with measured data points overlaid. Outliers are the diamond shaped markers. The outlier measurements were identified as points 1.5x the IQR about the upper quartile, or below the lower quartile. Elastance was expected to increase with cheek support because the cheeks are prevented from expanding as pressure builds up in the mouth.

This lack of correlation is shown by Subjects 2 and 5 with similar variation and mean changes of 1.6 % and 29.7 %, respectively, and Subjects 3 and 4 with similar variation and mean changes of 5.4 % and 66.8 %, respectively.

Measured ROCC for every shuttered breath is presented in Figure 8.2. Mean ROCC increased with cheek support for every subject, except Subject 8 who showed a -4.5 % decrease. The change in mean ROCC when cheek support was added was on average much smaller than for either elastance or the viscoelastic parameter, with a maximum change of 21.8 % for Subject 7. The variation of measured ROCC for a subject was generally consistent regardless of whether cheeks were supported or unsupported. This result matches previous findings (Hadjikoumi et al. [2003]).

Figure 8.3 shows the measured viscoelastic parameter, D, for every shuttered breath. The measured viscoelastic lung mechanic was affected by the level of cheek support. The rate of increase in measured pressure during occlusion was much higher when cheeks were supported. The largest increase in mean measurement was 68.2 % for Subject 4. Unlike for elastance and ROCC, the variation in measurements of this mechanic was not consistent between measurements with cheeks supported and unsupported. Subjects 2, 4, and 5 are examples of large changes in variation between test conditions.

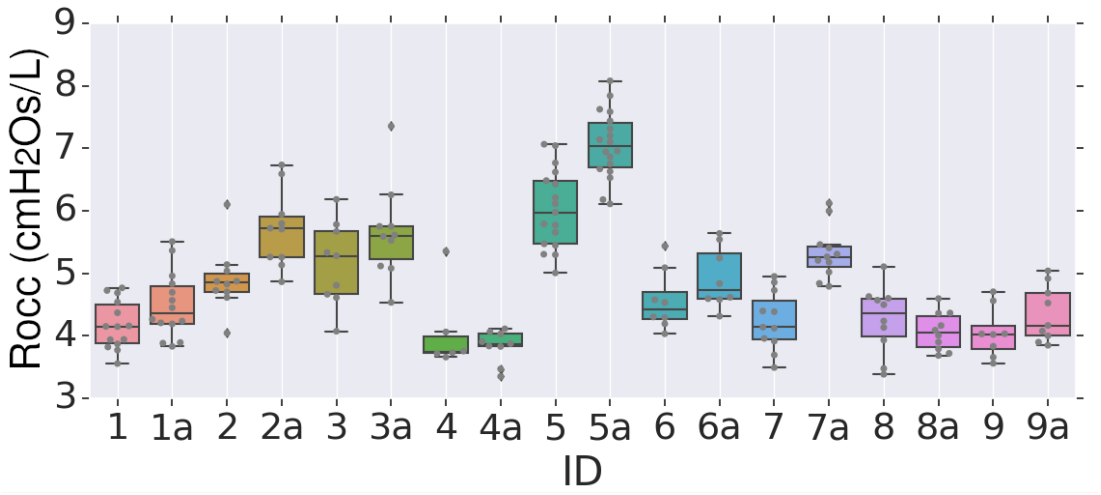

Figure 8.2 Comparison of ROCC measurements without cheek support (ID 1-9) and with cheek support (ID 1a-9a). Box-and-whisker graphs are displayed with measured data points overlaid. Outliers are the diamond shaped markers. The outlier measurements were identified as points 1.5x the IQR about the upper quartile, or below the lower quartile.

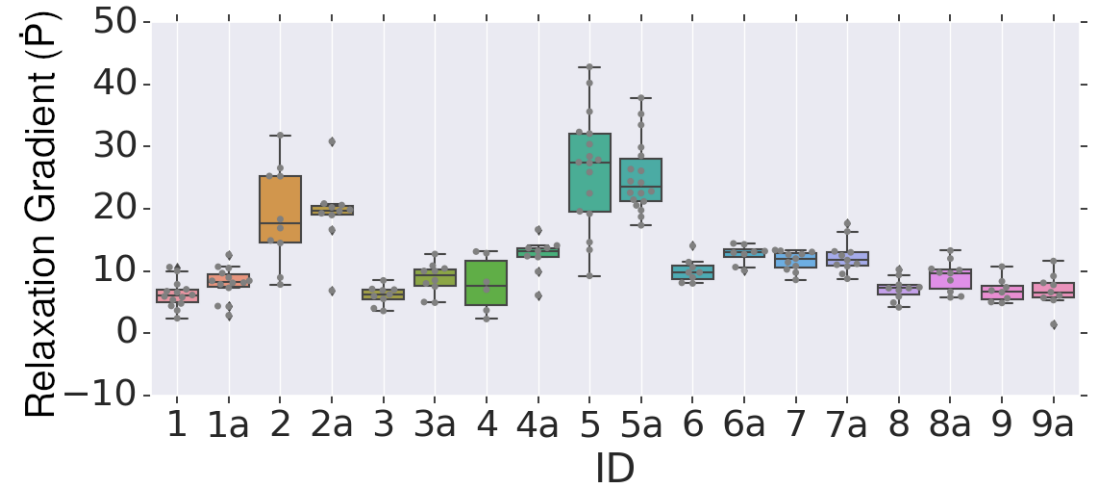

Figure 8.3 Comparison of measurements of the viscoelastic parameter without cheek support (ID 1-9) and with cheek support (ID 1a-9a). Box-and-whisker graphs are displayed with measured data points overlaid. Outliers are the diamond shaped markers. The outlier measurements were identified as points 1.5x the IQR about the upper quartile, or below the lower quartile.

The results were further analysed using kernel density estimation plots of the measured changes in mechanics, as shown on the diagonal of Figure 8.4. The density plot representing change in elastance (top left) has two distinct peaks. The small, right-most peak is caused by a single data point. Subject 4 showed a very large change in elastance, more than twice as large as any other subject. Due to the small number of subjects in this study, it is not clear whether this specific result is an outlier or the upper extreme of expected results. The density plots of change in ROCC (centre) and change in viscoelastic parameter (bottom right)

show a more even distribution of measurements around the mean value.

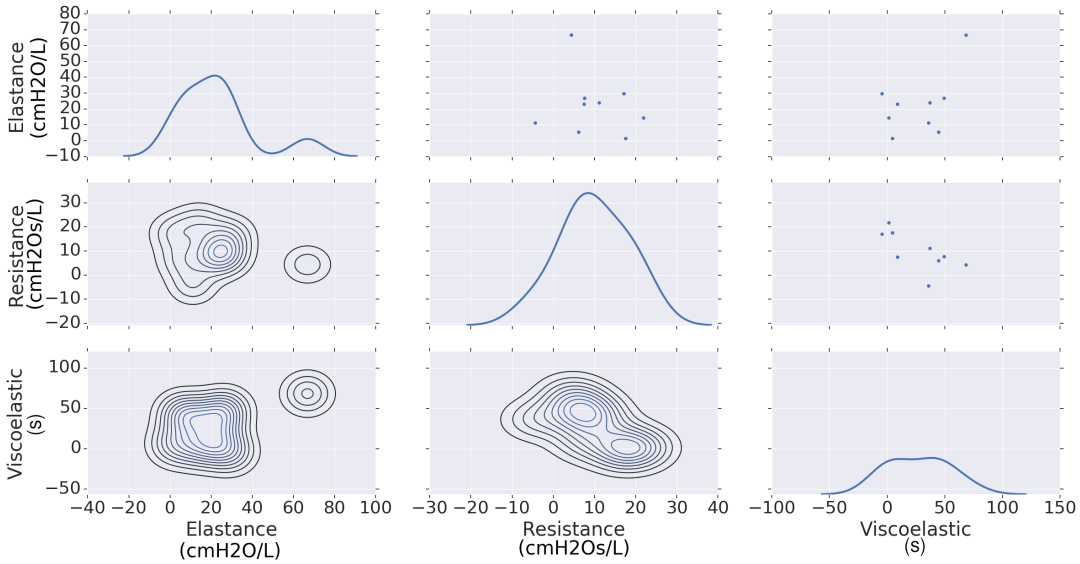

Figure 8.4 Relationships between different mechanics. The change in mean elastance, resistance and viscoelastic parameter for each subject are compared in scatter-plots in the upper triangel, and 2D-density plots in the lower triangle. These plots indicate possible correlations between changes in one mechanics with another. The diagonal plots show the kernal density estimation of the change in each mechanic (Elastance: top left, ROCC: centre, Viscoelastic parameter: bottom right).

The relationship between the mean change in different mechanics are shown in three scatter-plots on the upper triangle of Figure 8.4. To provide further information, the lower triangle presents the same relationships in a 2D density plot. This presentation of data shows how the datapoints are distributed across the range, and where they tend to cluster. From visual inspection, there appears to be a weak negative linear relationship between the change in ROCC and the change in viscoelastic parameter. So a subject showing a large change in ROCC when cheek support is added will tend to also show a small change in the viscoelastic parameter, and vice-versa. It is unclear from inspection whether there are any relationships between elastance and the other two mechanics, as Subject 4 sits far from the remaining cluster.

Table 8.4 shows the correlation coefficient (r) for the relationships between the mean change in each mechanic. Changes in elastance and ROCC do not appear to be related, with $|r|<0.2$. More tests would be needed to determine whether the change in elastance and viscoelastic parameter are related. When all subjects were analysed together, the results indicate a weak linear relationship between the change in elastance and the viscoelastic parameter, with $r=0.5$. However, when Subject 4 was excluded, r dropped to -0.04, indicating no relationship between

the mechanics. In contrast, there appears to be a relationship between the change in viscoelastic parameter and ROCC, with r=-0.69.

Table 8.4 Correlation coefficient (r) between changes in mean lung mechanics, where E is elastance, VP is the viscoelastic parameter, and R is ROCC.

Subjects included	E vs R	VP vs R	VP vs E
All subjects	-0.19	-0.69	0.50
Subject 4 excluded	0.06	-0.69	-0.04

8.3 DISCUSSION

All three mechanics measured in this study typically remained constant or increased in value when cheek support was added. The two decreases seen after cheek support was added were relatively small, at 4.5 % and 4.7 % decrease in mean measurement. For all three mechanics, the amount of change seen with cheek support was subject dependent. The change in elastance, ROCC, and the viscoelastic parameter ranged 1.6–66.8 %, -4.5–21.8 %, and -4.7–68.2 %, respectively.

The increase in elastance seen when cheek support was added was due to cheeks being prevented from expanding outwards when pressure built up in the mouth during occlusion. Cheek expansion is not instantaneous and while the cheeks expand, pressure in the mouth will be less than alveolar pressure, decreasing measured elastance during this time. This reduction in pressure when cheeks are unsupported can be seen in Table 8.3. Expiration was occluded for 200 ms in this trial, which does not appear to be long enough for full cheek expansion for most subjects. Only Subject 2 had less than 10% variation in peak pressure between tests with and without cheek support, indicating full cheek expansion.

Even though cheek holding may have been expected to only affect elastance, the results of this study show ROCC is also increased by adding cheek support. These results match previous findings, which showed increased ROCC when cheek support was added, while the variability of ROCC values remained constant (Hadjikoumi et al. [2003]). ROCC is calculated by measuring the amount of pressure change at the moment of occlusion. The pressure change is assumed to be entirely attributed to pressure losses due to airflow through the airways. When the cheeks are not supported, mouth pressure takes longer to build up to driving pressure due to cheek expansion. This difference reduces the pressure used when calculating ROCC, causing an underestimation of airway resistance when cheeks are not supported.

Similar to ROCC, cheek holding would not be expected to greatly affect viscoelastic lung mechanics. However, the mouth pressure measured while expiration is occluded will be a superposition of pressure due to cheek expansion, viscoelastic lung properties (such as tissue relaxation and air redistribution), and driving pressure. Quiet, tidal expiration is hypothesised to be a primarily passive process (Grinnan and Truwit [2005]). Hence, driving pressure is not expected to change during occlusion. As such, the decrease in measured viscoelastic parameter, D, without cheek support must be due to the time-varying decrease in pressure caused by cheek expansion.

The different times each parameter was measured, and how pressure was affected by cheek expansion at those times, explains the correlation between ROCC and the viscoelastic parameter observed in Figure 8.4 and Table 8.4. The lack of correlation between either of these two parameters and elastance is also explained by the timing of each measurement. Elastance is measured when the shutter is re-opened. Therefore, the change in elastance depends on whether the cheeks were able to fully expand during occlusion.

If the cheeks were able to fully expand, no change in elastance would be observed because mouth pressure would be equal to driving pressure regardless of the level of cheek support. ROCC is measured at the start of occlusion, meaning ROCC will always be reduced without cheek support due to decreased mouth pressure. Viscoelastic mechanics are measured during occlusion. The relatively short occlusion time of this study meant that the pressure drop caused by expanding cheeks would have heavily influenced this measurement.

Due to the inter-subject variation seen in this study, no cohort-wide trend to account for inadequate cheek support could be determined. As a result, true underlying lung mechanics could not be determined retrospectively if cheeks were unsupported during testing. Future work is needed to assess whether a model relating lung volume, mouth pressure and mechanics measurements could be developed for individual prediction.

More subjects and data would be required to develop such a model. The recommendation of this study is that cheeks should always be supported during breath-occluding lung function tests. All lung mechanics measurements were underestimated without cheek support, which would lead to incorrect analysis of lung health in a clinical environment.

8.4 SUMMARY

This study analysed the change lung mechanics caused by leaving cheeks unsupported during breath-occluding lung function tests. The mechanics assessed were ROCC, elastance and a parameter representing viscoelastic lung mechanics. All mechanics were found to be underestimated when cheeks were unsupported. This underestimation was due to reduced mouth pressure during cheek expansion when the breath was occluded.

The error in lung mechanics measurement caused by unsupported cheeks was subject dependent. As a result, there is no rule-of-thumb which could be applied to correct data for missing cheek support. In order to obtain correct lung mechanics measurements during breath-occluding lung tests, patients must have adequate cheek support. However, in future work, development of a model relating lung volume and breathing effort to mechanics may be able to provide individual prediction.

Chapter 9

SPIROMETER DESIGN

All test results for human subjects presented in previous chapters were obtained using a plethysmograph. A constant volume, whole body plethysmograph is a glass-walled box, with volume 700-1000L. Plethysmographs contain a spirometer with built-in shutter placed after the mouth pressure sensor. This shutter is able to completely block air flow during what is known as a shutter manoeuvre. This test is the "gold standard" for intrathoracic gas volume measurements and the measurement of specific airway resistance (Criée et al. [2011]).

However, regular use of plethysmographs for model development and validation was not possible. These devices are typically heavily used in clinical practise, leaving minimal remaining time for research projects. The size and limited access to plethysmographs also makes them impracticable for use in day-to-day care. To address the limited access to equipment, a simple spirometer was developed. The spirometer is capable of mouth pressure and airflow measurements at a high frequency and resolution, allowing for easy testing of changes to lung models or the novel lung function test. It is also a first prototype for a potential take-home device.

9.1 DESIGN OVERVIEW

The spirometer was designed to be compact, with dimensions 45 mm wide, 87.5 mm long without any tubing or mouthpieces attached to the front, and 75 mm tall to the highest point. A conducting airway 15 mm in diameter goes through the main body of the device, and up into a chamber on top of the device. A plug attached to a metal plunger has been placed inside the chamber. The plunger extends through a 15 mm diameter opening on the front of the chamber and inserts into a pull-type solenoid. When activated, the solenoid will pull the plunger towards

the front of the device. This motion causes the plug to occlude the 15 mm outlet hole, and as a result stop all airflow through the device. When voltage to the solenoid is dropped, a spring coiled around the plunger returns the plug to the fully open position. In the fully open position, the plug will be pressed against the back of the chamber, allowing a 3mm gap for air to flow through the outlet. The spirometer prototype is shown in Figure 9.1, and an overview of the parts making up the design is included in Appendex A.3.

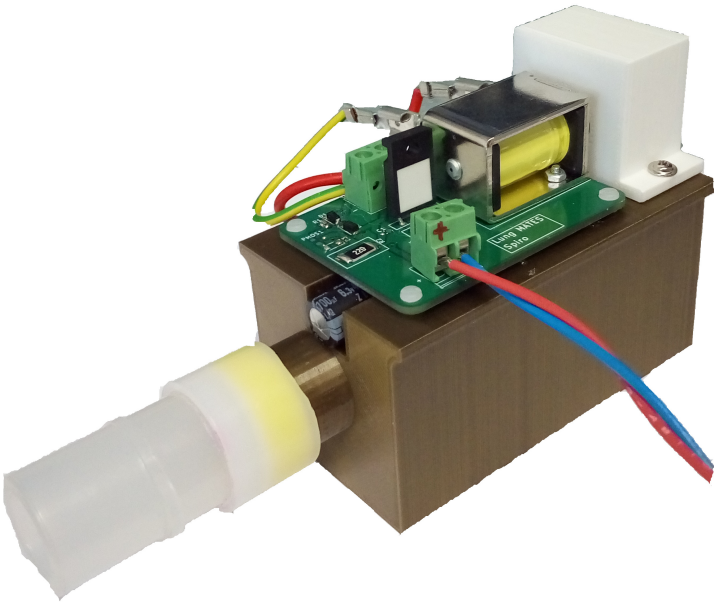

Figure 9.1 The spirometer prototype built for this thesis. The user breathes through a mouthpiece attached to the left-hand side of the device. Air flows into the device and up into the white chamber. A pull-type solenoid is positioned on the opening of the chamber. The solenoid draws in a plunger which occludes the opening. Note a flow sensor must be attached to the front of this device before use.

The spirometer designed in this thesis was used for development of the novel lung function test. Because it will not be used in a clinical environment, it was not required to meet typical standards for medical devices (ISO 13485, MedSafe's Web Assisted Notification of Devices (WAND) database, EU Notified Body, Health Canada or US FDA). The device was able to be developed to the level of a minimum viable spirometer, with the majority of computing performed off-board. A high-level overview of the full system is presented in Figure 9.2.

The airflow through the physical system is shown at the top of Figure 9.2. During expiration, airflow is generated by a person breathing into the spirometer. Air initially flows through a flow sensor, then past a shutter which is able to completely occlude airflow, and finally the air flows out of the device into the surrounding environment. Three pressure taps are taken from the system. The first tap is at

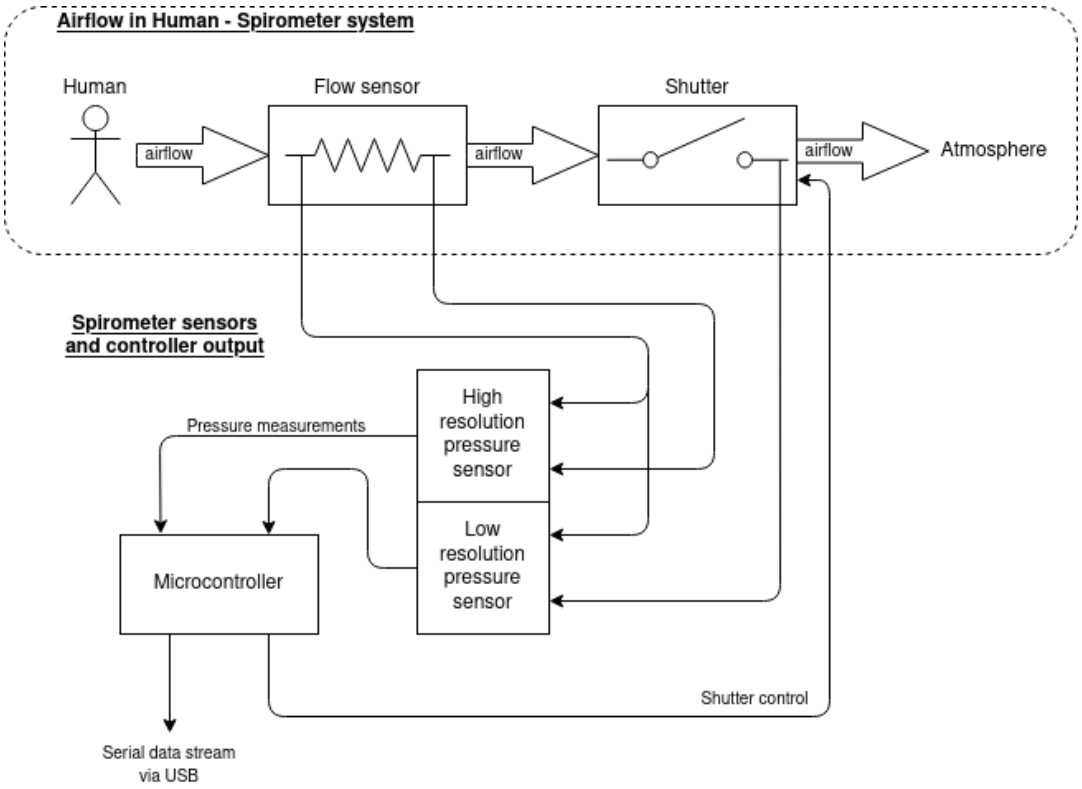

Figure 9.2 Overview of the spirometer system. The top of this figure shows the physical spirometer and how airflows through the system. Three pressure taps are taken in this system, one before the flow sensor, one after the flow sensor, and one at the very end of the system. The three pressure measurements are divided between two pressure sensors. The high resolution pressure sensor measures the differential pressure across the flow sensor. The low resolution pressure sensor measures pressure at the subjects mouth relative to atmospheric pressure. The pressure sensors deliver this information to the microcontroller. This data is output to a serial stream by the microcontroller, and is used to control the shutter.

the front of the flow sensor (the line closest to the human in Figure 9.2). Pressure measured at this first tap is equal to the pressure in the mouth. The second pressure tap is taken immediately after the flow sensor. The final pressure tap measures the atmospheric pressure, as a reference.

The pressure taps are connected to two pressure sensors. A low resolution pressure sensor (LRPS) and a high resolution pressure sensor (HRPS) are used in this design. Both sensors are bi-directional, differential pressure sensors. The HRPS is connected to the first and second pressure taps. It measures the pressure drop across the flow sensor. The pressure difference measured by the HRPS is equal to the pressure drop across the flow sensor. Knowing the internal resistance of the

flow sensor, the airflow rate can then be calculated using Poiseuille's Law:

$$Q = \frac{\Delta P}{R} \tag{9.1}$$

where Q is the flowrate, ΔP is the pressure difference measured, and R is the resistance of the flowmeter.

The LRPS is connected to the first and final pressure taps. This sensor combination gives an accurate measurement of the pressure in the mouth relative to atmospheric pressure. This pressure is also equal to the total pressure drop across the entire spirometer system, allowing the resistance of the spirometer to be measured.

The measurements from each of the pressure sensors are read by the microcontroller as an analogue voltage. The microcontroller converts these voltages to pressure, and uses the HRPS measurement to calculate the flow rate. The mouth pressure, flow rate, pressure drop across the sensor, and a timestamp are then written to the serial port at a rate of 300 Hz. The serial stream can be read and saved by an external computer connected to the spirometer via USB. The electrical schematic for the spirometer control board is in Appendix A.2.

The microcontroller is also able to send signals to the shutter to control when airflow through the spirometer is occluded. The shutter will close if one output pin of the microcontroller is set high. This pin is connected to a MOSFET, which will switch on higher voltage electronics. The electronics powering the solenoid are designed to close the shutter as quickly as possible, and allows for rapid reuse of the shutter so airflow can be occluded for very short time intervals multiple times per breath. The electrical schematic for the shutter control circuit is in Appendix A.2.

To minimise the size, weight and risk of injury from electronic componentry of the spirometer, the control board and solenoid control were placed on separate boards. As much componentry as possible was placed on a "control" board. These components included the sensors, microcontroller and majority of the higher power electronics. The schematics making up the control board are shown in Appendix A.2. The only electronics on the part of the device handled by the subject are the solenoid and some associated electronics, as shown in Appendix A.2.1. The two circuit boards are connected by a long (1.5 m) power-supply cable and the pressure tap tubing.

Note this design is a first prototype. A full solution could include rechargeable power sources and wireless communication with no significant added design complexity. These changes are not necessary for this research, but would remove fixed lines for ease of use.

9.2 DESIGN REQUIREMENTS

The spirometer designed for this project aimed to meet criteria outlined by the ATS/ERS taskforce (Miller et al. [2005]). The relevant requirements outlined by the taskforce include:

1. Accumulate volume for $\geq$15 s
2. Measure volumes $\geq$8 L with minimum accuracy $\pm$3% or $\pm$0.05 L
3. Measure flowrates in the range 0-14 L/s
4. Have a total resistance of $<$1.5 cmH_2O at a flowrate of 14 L/s
5. Compatible with anti-bacterial filter on input

   In addition to the specifications laid out by the ATS/ERS taskforce, the system aimed to have the following characteristics:

6. Completely occlude airflow for a minimum of 75 ms and up to at least 200 ms
7. Repeatedly-occlude airflow during a single breath
8. Export data via serial usb connection
9. Provide real-time measurements of airflow and mouth pressure

These 9 requirements are identified as "Requirements 9.2.1 – 9.2.9", respectively, when referred to in the following sections of this chapter.

9.3 COMPONENT SELECTION

9.3.1 Flow sensor

The flow sensor used for tidal breathing measurements was the Hamilton Medical Flow Sensor, PN 27331, shown in Figure 9.3. This sensor has several drawbacks for use in spirometry, with a low upper flow rate of 3 L/s and a reasonably large

resistance to airflow. However, it was acceptable for validating the spirometer design and novel lung function test to a reasonable degree of accuracy. Future designs will need to improve on this sensor selection for higher flowrate breathing manoeuvres to be measured by the device. When combined with a high resolution pressure sensor (SSCSNBN001NDAA5), the flow resolution was 0.01 L/s.

Figure 9.3 Hamilton Medical Flow Sensor used with the spirometer. Sensor can be linked in series with other components such as mouthpieces and extra resistances, but has an upper flow range of 180 L/min: It will be used for low flow rate measurements.

During peak effort expiration, flow rates can be as high as 13.3 L/s. The limited range of the Hamilton Medical sensor meant that the flow data recorded during forced expiratory breathing manoeuvres would be clipped and very noisy at higher flowrates. As a result, accurate measurement of typical spirometry measures (eg FEV1) could not be obtained with this sensor. However, this limit is acceptable for assessing the normal or quiet breathing considered in this research.

9.3.2 Pressure sensors

Two pressure sensors are used in this spirometer design. A high resolution, low maximum pressure sensor is used to calculate flowrate during tidal breathing. A single low resolution, high pressure sensor is used to record mouth pressure during tidal breathing and high pressure breathing manoeuvres, such as forced expiration

or breath occlusions. The sensors used are shown in Figure 9.4

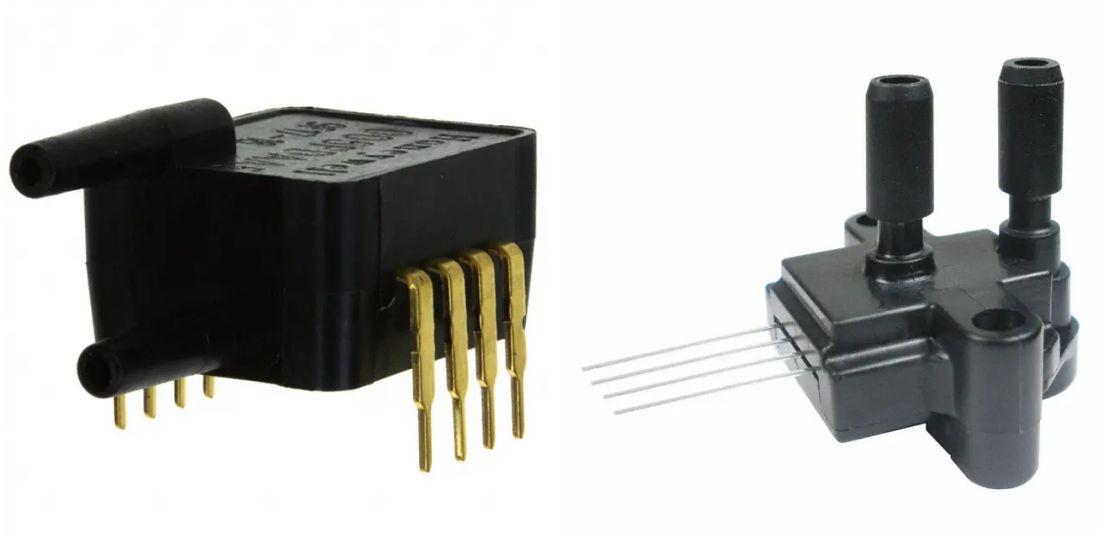

(a) ASDXRRX001PDAA5 (b) SSCSNBN001NDAA5

Figure 9.4 Pressure sensors used in the spirometer. a) The low resolution sensor used to measure absolute pressure at the mouth. b) The high resolution sensor used to measure flowrate.

All sensors used in this design are able to record differential pressure bidirectionally. The specifications of the sensors are given in the following:

9.3.2.1 High resolution

The high resolution sensor used was a bi-directional differential pressure sensor by Honeywell Sensing and Productivity Solutions (SSCSNBN001NDAA5). The sensor has the following characteristics:

- Maximum pressure of ±1 inH_2O (±248.84 Pa)
- 3% FSS total error band
- 0.5 V–4.5 V analog voltage output

9.3.2.2 Low resolution

The low resolution sensor used was a bi-directional differential pressure sensor by Honeywell Sensing and Productivity Solutions (ASDXRRX001PDAA5). The sensor has the following characteristics:

- Maximum pressure of ±1 PSI (±6894.76 Pa)
- 2% FSS total error band

- 0.5 V–4.5 V analog voltage output

The resistance of the flow sensor was measured at 1.1 cmH_2Os/L. This small resistance would lead to a pressure drop of 3.3 cmH_2O at the maximum flow rate of the flow sensor, 3 L/s. The High resolution pressure sensor was used to record this differential pressure. The maximum pressure measured by the pressure sensor is 2.5 cmH_2O, causing the pressure measurement to be clipped as the flowrate approached the upper limit.

The maximum pressure generated by the lung is very subject dependent, causing a wide range of spirometry results depending on age, sex, ethnicity, and health (Pellegrino et al. [2005]). To account for the large range of possible peak pressures, a sensor with a large upper limit of 68.9 cmH_2O was chosen. This pressure is more than twice the pressure typically used for PEEP in mechanical ventilation (Chiew et al. [2011], Kannangara et al. [2016]), and is much larger than the maximum pressures of tidal breathing measured in previous chapters. Hence, it is unlikely the mouth pressure generated by a breath occluding lung function will reach the upper pressure limit and cause damage to the sensor. The trade-off of using a higher pressure sensor is a reduction of resolution. The resolution of this high pressure sensor is quite large, at 0.33 cmH_2O. In future designs, a high pressure sensor with a lower maximum pressure limit may be acceptable to increase the resolution.

9.3.3 Soleniod

An inexpensive pull-type solenoid (DSOL-0630-05E) was used in the spirometer design. This solenoid weighs 80 g and has a maximum stroke length of 12.7 mm. The solenoid and its associated force-distance curves are shown in Figure 9.5.

The plunger was allowed to extend 3 mm, to allow air to flow past the plunger. At this distance, the minimum pulling force was around 2.2 N (8 oz-force.). The pulling force increases as the plunger is drawn in. To occlude flow, the solenoid must pull the plunger against the pressure generated by breathing. As the size of the hole the solenoid is occluding increases, the force the solenoid must overcome will also increase. The maximum permittable hole size for this solenoid can be calculated with the following equation:

$$P = \frac{F}{A} \tag{9.2}$$

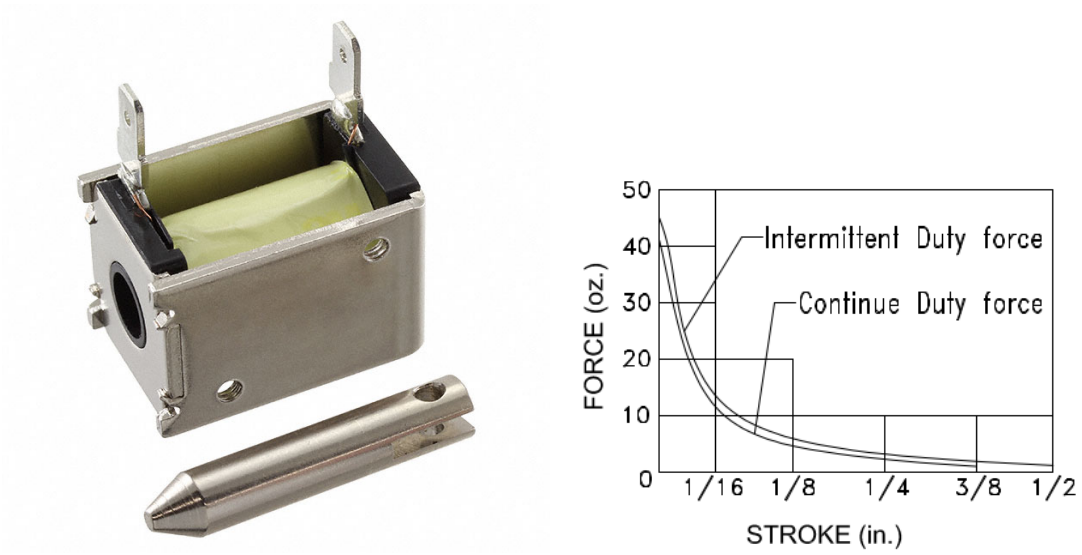

Figure 9.5 The solenoid used in the spirometer design. A plug was attached to the end of the plunger head to block all airflow when the solenoid was activated. A spring was added to return the plunger to an open position when voltage was removed from the solenoid. The maximum distance travelled by the solenoid was 3 mm, giving a force of around 2.2 N (8 force-oz.)

where P is pressure, F is force and A is the surface area of the hole.

The maximum pressure measured by the high pressure sensor is 7 kPa. This value is far greater than the pressures generated by tidal breathing subjects in previous chapters. Using 7 kPa as the upper pressure limit, and a puling force of 2.2 N, the maximum hole size which could be plugged by this solenoid is 20 mm in diameter. The actual hole size used in the spirometer design was well below the maximum hole size limit, at 15 mm diameter.

9.4 REQUIREMENT VALIDATION

9.4.1 Data collection

The spirometer designed for this thesis had no on-board data storage. The function of the spirometer was to read sensor voltages and convert these readings to the relevant flow rate and mouth pressure measurements. This data was then immediately transferred over serial connection to a computer. The data processing architecture of minimal on-board processing and storage was chosen to simplify the spirometer design, allowing rapid prototyping of the device. After validation of the novel test and device is complete, further refinement on the overall design would allow for on-board data storage and other features extending ease of use.

The sampling rate of the device is 300 Hz. The data recorded by this prototype spirometer includes:

- Mouth pressure
- Flowrate
- Pressure drop across flow sensor
- Timestamp

All data is stored in floating point representation. A floating point number takes 4 bytes of memory in C (the programming language used for the microcontroller). Hence, 16 bytes are needed to store all four parameters recorded by the spirometer. To meet Requirement 9.2.1, data must be recorded for 15 s. At a measurement frequency of 300 Hz, 15 s of data will require 72 KB of storage. This storage size is easily achieved by a desktop computer, and could be easily achieved with an onboard SD card in future designs (microSD cards are available with 32 GB memory).

The microcontroller used in the design was an ATMEGA32U4. This microcontroller is compatible with Arduino, and able to be programmed over USB after initialisation via ISPC header. The decision to use an Arduino aimed to minimise the amount of time required to set-up and programme the board. It also simplifies future development and software updates, due to the Arduino's open-source nature.

Data written over serial was to be recorded by a computer connected to the spirometer via USB, meeting Requirement 9.2.8. The spirometer contains no on-board data logging, or screen to display data real-time. As such the design does not meet Requirement 9.2.9. However, the lack of real-time measurement display was acceptable for the use of the prototype spirometer in testing and developing a novel lung function test.

9.4.2 Volume

The flow sensor was calibrated with a 1 L calibration syringe (Hans Rudolph). The calibration set-up is shown in Figure 9.6. The flow sensor (blue in the Figure) was attached to the calibration syringe (brown in the Figure) via rigid plastic tubes. No airleaks were observed when the outlet of the flow sensor was occluded while pressure was applied to the syringe.

Figure 9.6 Hans Rudolph 1L calibration syringe (brown), used to calibrate flow measurement and quantify volume error, attached to a hamilton medical flow sensor (blue).

After calibration, the maximum error in volume seen in three pumps of the 1 L syringe was 67 ml (6.7%). The traces of these calibration pumps are shown in Figure 9.7. Volume error was calculated by calculating the difference between the peak and minimum points in the volume curve. The downstroke of the first pump, and up-stroke of the last pump were ignored due to noise from handling of the device. This noise caused an elevated starting volume for the first stroke and elevated final volume for the last stroke.

The 7% error in volume measurement at 1 L means the design does not meet Requirement 9.2.2. The amount of measurement error in this device would mean it is not suitable for clinical use. However, the amount of error was deemed acceptable for proof-of-concept validation of the novel lung function test. Future designs should use a more sensitive flow sensor to meet Requirement 9.2.2.

9.4.3 Flowrate

The flow sensor used for this thesis is rated for flow rates up to 180 L/min (3 L/s), which means the spirometer does not meet design Requirement 1.1.3. However, the test designed in this thesis aims to measure lung mechanics during tidal breathing, which typically has flow rates well below 3 L/s, at around 0.5 L/s (Ward [2005]). As such, the sensor chosen was suitable for the development and validation of the novel lung function test, without meeting the flowrate criteria outlined by the ATS/ERS taskforce.

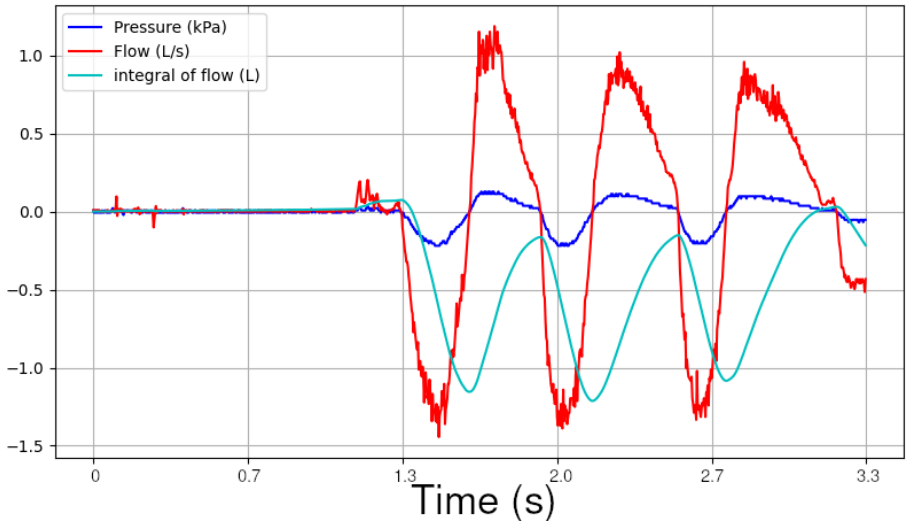

Figure 9.7 Pressure, flow and volume recorded when a 1 L calibration syringe was connected to the flow sensor. The syringe was fully depressed and extended 3 times to roduce these curves. The maximum measurement error in volume was 67 mL, ignoring the first depression and final extension.

9.4.4 Resistance

Resistance of the device was calculated by dividing the measured pressure by measured flow. The total resistance of the device was measured as 3.1 cmH_2Os/L. The resistance of the flow sensor was calculated using the pressure drop across the flow meter. The flow meter resistance is 1.1 cmH_2Os/L.

A device resistance of 3.1 cmH_2Os/L is twice as high as is recommended by the ATS/ERS taskforce. As such, Requirement 9.2.4 was not met by this spirometer design. Two design changes are needed to meet this requirement. First, a lower resistance flow meter should be used. The flow meter used in this design is intended for use in mechanical ventilators, and as a result can have much higher resistances due to the higher pressure capability of a mechanical ventilator. Second, a push-type solenoid with a larger travel range could be used. This larger travel range would remove the need for a 90° bend in the breathing circuit and allow for a larger airway between the plug and the spirometer opening, all of which would reduce overall device resistance.

9.4.5 Physical design

The spirometer was designed to have two boards to minimise the weight and size of the hand-held device, and reduce the risk of injury to the user from the power

electronics. To protect users from possible illness if the device is shared, the front of the device was designed to be compatible with widely available, clinically used, low resistance bacterial filters for spirometers. This design decision is consistent with Requirement 9.2.5.

9.4.6 Shutter speed

Requirement 9.2.6 specifies the minimum duration the shutter must be able to occlude airflow for. The shutter must be able to open and close at a sufficiently fast rate the subject breathing into the device is unable to reflexively react to the shutter. The shutter duration typically used in breath occluding lung function tests is 100 ms (Panagou et al. [2004]). A shuttering duration of 100 ms is long enough for pressure to equalise in the airways and lung, while also being faster than human reaction speed.

To occlude breathing, a solenoid plugs the spirometers airflow outlet. The time taken for the solenoid to fully retract the plug can be determined by monitoring the current across the solenoid. When a rod fully withdraws into the solenoid, a drop in current will be observed. This brief drop is due to back EMF being created in the solenoid coils by the plunger movement (Balakrishnan and Navaneeth [2015]). The expected current trace in an ideal solenoid is shown in Figure 9.8. The drop in current (I_{valley}) is clearly visible in this figure.

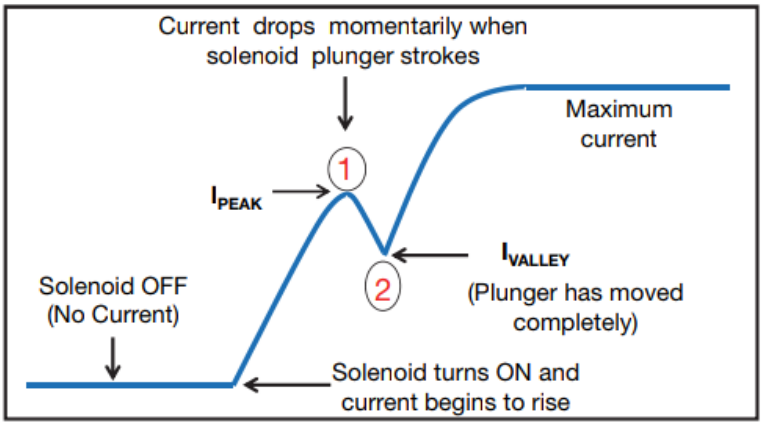

Figure 9.8 Current trace in ideal solenoid for full retraction of plunger. Sourced from Balakrishnan and Navaneeth [2015]

Voltage is proportional to current across a solenoid. Hence, voltage traces recorded on an oscilloscope were used to identify the time for the solenoid plunger to fully retract. Recorded traces of solenoid voltage can be seen in Figure 9.9. This figure presents two traces, the first (blue) shows the solenoid being powered with no

plunger inserted into the solenoid, the second (red) shows the solenoid with the plunger installed. The moment the solenoid is fully closed can be clearly identified by the voltage spike in the voltage trace with the plug installed (red).

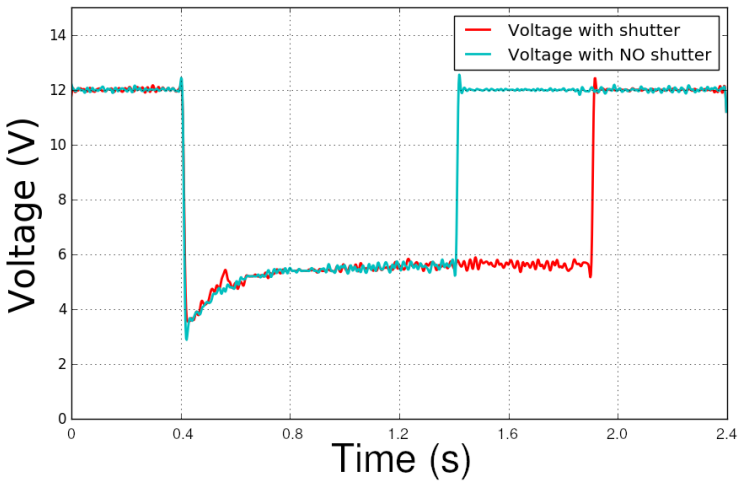

Figure 9.9 The voltage measured across the spirometer with and without the shutter inserted. Note the voltage spike when the shutter is fully retracted.

When power is removed from the solenoid, a spring returns the plug to the fully opened position. The time taken for the spring to reopen the shutter was calculated numerically. The spring constant was calculated by adding weights to the spring, both in compression and in tension, and measuring the displacement. The linear regression of this test is shown in Figure 9.10.

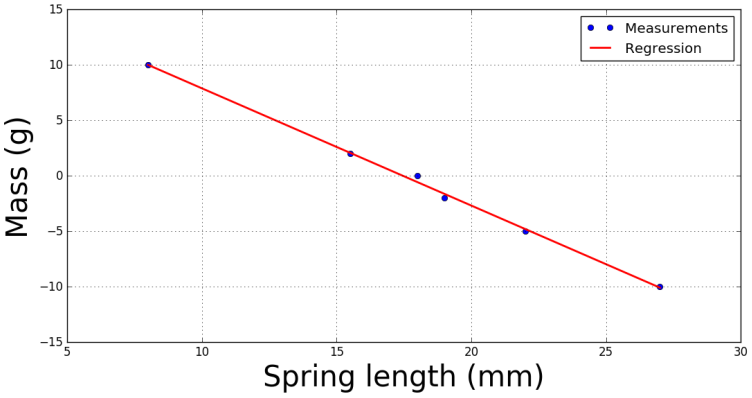

Figure 9.10 Spring compression and extension measurements to determine the spring constant.

The time taken for the spring to reopen after occlusion was calculated numerically. The spring was compressed by 13.5 mm in the fully occluded position, and moved 3 mm to reach the fully open position, where the spring was compressed 10.5 mm from it's resting position. The combined weight of the plunger and plug was

measured, and the following equation was used to model the movement of the spring from occluded position (x_0) to the spring's resting position ($x = 0$):

$$x = \frac{x_0}{m} cos\left(\sqrt{\frac{k}{m}}t\right) \tag{9.3}$$

The modelled motion of the spring is shown in figure 9.11, where the red marker indicates the time where the spring reaches the fully open position of the device.

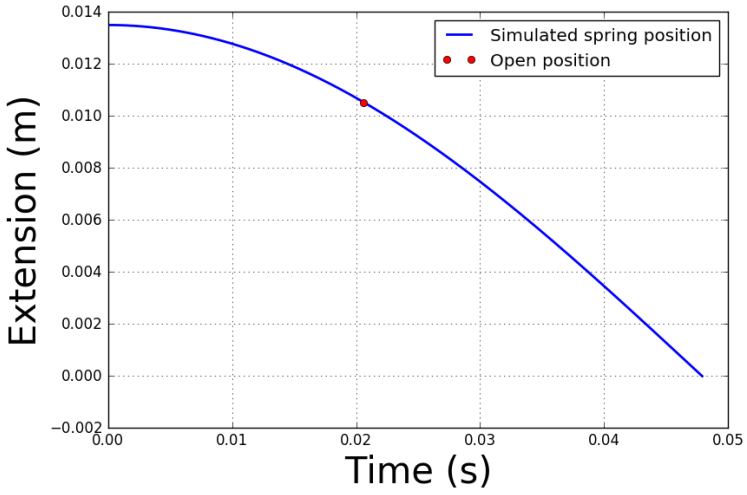

Figure 9.11 Modelled motion of the springrecoiling open given the measured spring constant and mass of the shutter.

Where x is the compression of the spring, x_0 is the initial compression of the spring, m is mass of the plunger and plug, k is the spring constant, and t is time.

Table 9.1 shows the time taken for the solenoid to completely occlude flow from the resting position, and for the spring to return the plunger to the fully open position after full occlusion. The total minimum time taken for the device to completely occlude flow and return to the resting position is 36 ms, meeting Requirement 9.2.6.

Table 9.1 Time taken for the shutter to completely occlude flow, and return to resting position.

Time to occlusion	Time to re-open
15.5 ms	20.5 ms

9.5 RAPID BREATH OCCLUSION

The circuitry controlling the behaviour of the solenoid is located on the mouthpiece, and the schematic for this circuitry is shown in Appendix A.2.1. To increase the speed at which the solenoid retracts the plunger, a voltage above the rated 5 V is briefly pulled across the solenoid. Initially, the voltage will be equal to the supply voltage, 12 V, and then drop to 5 V as a capacitor is charged. The capacitor controlling the time the increased voltage is applied is "C1" in Appendix A.2.1.

After occlusion, the solenoid should not be activated again before "C1" has been fully discharged. If "C1" remains charged, the solenoid will not perform to the same standards measured in previous sections. The time taken for the capacitor to discharge is controlled by resistors "R3" and "R5" in Appendix A.2.1. The RC time constant (τ) of the discharging circuit of "C1" is calculated using the standard equation:

$$\tau = RC \tag{9.4}$$

For this circuit, τ is 20.8 ms. After 5 time constants over 99.99% of the charge on the capacitor will have been discharged. As a result the minimum period of time permissible between occlusion events is 104 ms. This is a sufficiently short time that multiple occlusion commands can be sent per breath, meeting Requirement 9.2.7. As a use case example, if the duration of occlusion was set to 100 ms and expiration lasted 2 s, a single expiration could be occluded 9 times.

9.6 RAW RESULTS

The tests developed in this thesis focus on measurements during tidal expiration. Hence, the spirometer measurements displayed in this section were taken during expiration in normal tidal breathing. This section presents the raw data produced by the spirometer, without any additional filtering or manipulation. Further testing and analysis of this device will be completed in a collaboration between the University of Canterbury, New Zealand, and Furtwangen University, Germany, due to delays introduced by the 2020 Covid-19 pandemic.

To occlude breathing, a signal is sent from the control board to the solenoid. When

the solenoid receives this signal, the plunger will be in the fully open position. The solenoid will retract the plunger, occluding airflow, and hold this position for as long as the signal is present. As a result, the time taken for the plunger to retract must be subtracted from the total signal time to calculate how long breathing was occluded. In the case of a 150 ms signal, breathing will be occluded for 135.5 ms. The trace of pressure and flow during a 150 ms occlusion is shown in Figure 9.12.

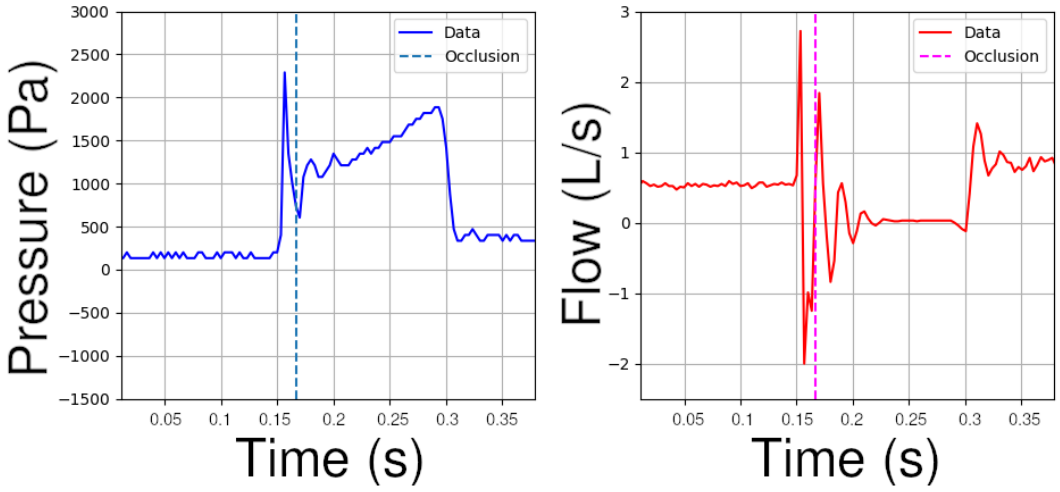

Figure 9.12 Pressure (Pa) and flow (L/s) measured by the spirometer while a 150 ms long signal to occlude expiration is sent to the device. Large oscillations are presents at shutter closure in both the pressure and flow signals. The vertical bars show the point in time full airflow occlusion is reached.

Large oscillations are present in the measured pressure and flow at the start of occlusion. These oscillations are sufficiantly large that they obscure the underlying pressure and flow waveforms, and will likely require heavy filtering to remove. The oscillations last for approximately 50 ms.

The time taken for the solenoid to occlude breathing was 15.5 ms. Some air turbulence in airflow would be caused during shutter closure. However, the turbulence lasts for closer to 50 ms. The turbulence observed after airflow is occluded was likely caused by wave reflection off the plug, and damping. The point airflow is fully occluded is clearly identifiable in the pressure waveform, occuring at the minimum pressure after the large pressure spike caused by the movement of the plug. This point is identified by the vertical dashed lines in Figure 9.12.

The waveforms on Figure 9.12 are as expected for a brief occlusion of expiration. The pressure initially jumps as mouth pressure equalises with alveolar pressure,

followed by a slow rise in pressure over the remaining time expiration is occluded. The airflow drops to 0 L/s, and remains at this value until the plunger is removed. It is clear from Figure 9.12 that airflow is able to be completely occluded by this device without noticeable air leakage.

Requirement 9.2.6 specified a minimum breath occlusion time of 75 ms. Both a 75 ms and a 100 ms duration signal were sent to the solenoid to compare performance. An occlusion of 100 ms is more typically used for breath occluding lung function tests (Panagou et al. [2004]). The pressure and flow traces of the 75 ms and 100 ms occlusions are shown in Figure A.3.

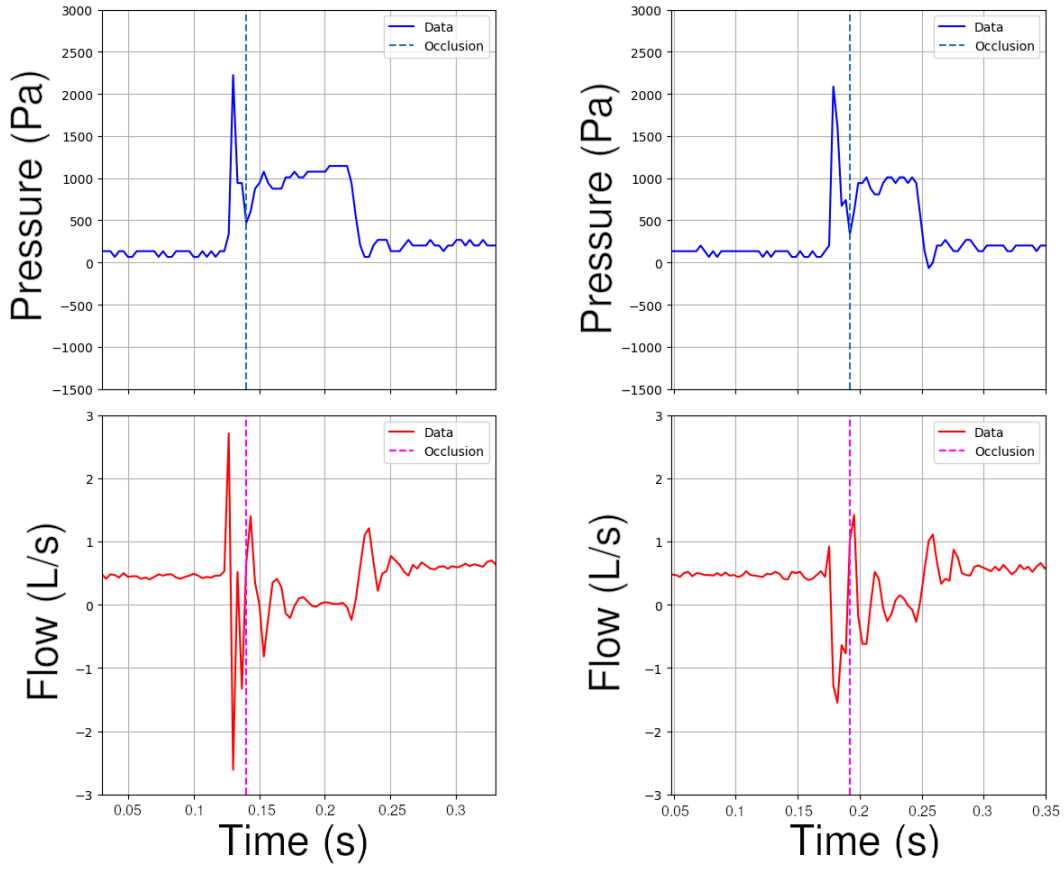

(a) 100 ms total

(b) 75 ms total

Figure 9.13 Two signals to occlude breathing were sent to the solenoid. The first signal was 100 ms long, the second was 75 ms long. These times include the time for the solenoid plunger to move to the occlusion position (15.5 ms). The plot of flow at 75 ms does not stabilise at 0 L/s, indicating that 75 ms may be too short a time-frame for pressure to equalise in the total system. The vertical bars show the point in time full airflow occlusion is reached.

Due to the relatively long time for oscillations in pressure and flow to stop compared to the total time breathing is occluded, a significant proportion of all signals in Figure A.3 are obscured by the oscillations. At 75 ms, the measured

flow does not settle at 0 L/s before the occlusion ends. The gradual increase in pressure (needed to accurately calculate airway resistance) is also not visible. However, the increase in pressure over such a short duration would be minimal. At 100 ms, flow does briefly settle at 0 L/s during occlusion, and the increasing pressure is visible. The results of this comparison indicate that the minimum viable time to occlude breathing with this device during a breath occluding lung function test will likely be between 75-100 ms.

9.7 SUMMARY

The spirometer designed for this thesis was able to measure mouth pressure and airflow at a sufficient level required for development and validation of novel breath occluding lung function tests during tidal breathing. For use outside of a research environment, or for higher flow rates than found in normal tidal breathing, the spirometer design described in this chapter will need modification. Table 9.2 shows future changes to be considered in future development of the design.

Table 9.2 Updates to consider for future spirometer designs.

System	Changes
High pressure sensor	Lower maximum pressure
Flow sensor	Lower resistance (<0.5 cmH_2Os/L)
	Higher Maximum flow rate (14 L/s)
Solenoid	Push type solenoid
Physical design	Remove any bends in spirometer airway

Chapter 10

CONCLUSION

Respiratory disease is a major public health problem globally. In New Zealand alone, 1 in 6 people are affected by respiratory disease, and it costs the economy 5.5 billion NZD per annum (∼1.8% GDP). Affected individuals must undergo lung function testing to diagnose the type and severity of respiratory disease and to regularly monitor disease progression. Spirometry is the most commonly performed lung function test in out-patient care. However, information provided by spirometry is limited.

In particular, spirometry provides no information about the underlying mechanics of the lungs, which change as disease progresses, providing a true, potentially more accurate assessment of lung condition. Additionally, the results of spirometry are highly dependent on the patient's ability to cooperate or participate in the test. Patient management is thus difficult, often ending in misdiagnosis, if the breathing manoeuvres required by spirometry are performed poorly or are unable to be repeated reliably.

Respiratory diseases can be classified as either obstructive or restrictive. Obstructive lung disease is characterized by airway obstruction or increased resistance in the airways, where restrictive lung disease is characterised by an inability to inhale due to an increase in lung elastance (a stiff lung), weakness in the muscles controlling respiration, or due to external pressure on the lungs. Examples of obstructive lung diseases include asthma, COPD, and cystic fibrosis. Restrictive diseases include fibrotic diseases of the lung, neuromuscular disorders and obesity. The different effect the two classes of respiratory disease have on breathing implies a need to assess lung function in terms of both airway resistance and lung elastance.

Lung diseases are often not homogeneous, with some regions of the lung being

affected by disease, while other regions remain healthy. As such, monitoring average lung mechanics may not provide the detailed level of insight needed clinically, with large and small airways responding at differently as the lung tissue expands and contracts during breathing.

Respiratory disease management thus faces two main issues. The first is a lack of fully relevant or timely information. The second is the patient-bases hetrogeneity of disease, and the patient-specific, time-varying response to care. Combined, these factors reduce the efficacy of management and care, and increase the social and economic costs of respiratory disease.

This thesis followed the development of a novel, model-based lung function test, and an associated testing device, all designed for use in monitoring outpatients with chronic respiratory disease. This test and device were designed to address three identified problems in current pulmonary testing:

- Lack of easy lung mechanics measurement in spontaneous tidal breathing, which gives deeper insight into lung condition and is relevant to patient lifestyle.
- High cost and lack of accessibility to specialised testing equipment
- Difficulty of obtaining accurate measurements in peak effort lung testing, especially in patients with insufficient expiratory ability, which affects their ongoing care.

Seventeen (8 Female, 9 Male) healthy subjects were recruited to validate the novel lung function test approach and device. Lung elastance and occlusion resistance measurements were as expected for healthy subjects. When external resistance was added to the spirometer inlet, measured resistance would increase as expected, and elastance would remain the same or increase slightly as work of breathing increased. This outcome is the expected response to simulated mild upper airway obstruction, and captures lung expiratory elastance as a patient-specific metric independent of test conditions. The results of this test validation showed the test was able to identify reasonable lung mechanics values, providing new insight into lung health.

The single compartment lung model was chosen to measure lung mechanics in this test. This choice of lung mechanics model was due to the model's simplicity, both mathematically and in understanding and interpreting the results, as well as significant prior clinical validation in other cohorts. The use of this model in this

research was first validated with data from fully sedated, mechanically ventilated patients in intensive care. This validation suggested real-time, breath-to-breath mechanics of expiration could be estimated by analysing the decay rate airflow. However, further testing showed monitoring decay rate in spontaneous breathing cannot capture information about airway resistance. Thus, monitoring airflow decay rate overtime could only give information about lung elastance trends, which could be useful to monitor disease progression, but do not produce direct values to assess severity.

An identified limitation of the new lung function test was its inability to capture the mechanics of small airways resistance and lung viscoelasticity. This limitation was due to the simplicity of the single compartment lung model. As a result, using the new lung function test alone to monitor changes in lung condition over time may miss information about changes in condition of small airways and lung tissue. In normal lungs, small airways do not contribute significantly to total airway resistance. It has been estimated that a 75% obstruction of all small airways is needed before changes can be detected by routine pulmonary function tests (e.g. forced expiratory volume in 1 s (FEV1)) (Burgel et al. [2013]). As such, a method to monitor any changes in small airways condition could have impact clinically.

A novel method described in this thesis to monitor these deep lung mechanics measured the rate of change of pressure during expiratory breath-occlusion. Two-compartment lung models show this pressure measurement is highly dependent on small airways resistance and elasticity. Hence, monitoring this metric alongside other lung function testing may provide useful insight into lung condition.

Typically, cheeks are supported during breath occluding lung function tests. When cheek support is missing, measurements of airway resistance are known to be underestimated. This thesis also analysed the effect of cheek support on elastance and viscoelastic lung mechanics measures. All mechanics were found to be underestimated when cheek support was missing. The error in lung mechanics measurements was subject dependent, meaning no rule-of-thumb could be applied to data to account for missing cheek support. To obtain correct lung mechanics measurements during breath-occluding lung tests, patients must have adequate cheek support, or risk significant added variability to measured results. Importantly, the support is easily provided.

All test results for human subjects presented in this thesis were obtained using a

plethysmograph. This device provides the "gold standard" for the measurement of specific airway resistance. However, regular use of a plethysmograph for model development and validation was not possible, due to the heavy clinical demand for use of these devices. Additionally, these devices are not widely used in outpatient care due to their high cost, heavy use, and large size.

To address these problems, a simple spirometer was built for model development. The spirometer was able to measure mouth pressure and airflow at a sufficient level required for development and validation of novel breath occluding lung function tests during tidal breathing. This spirometer is a first prototype for potential use in outpatient care. For use outside of a research environment, or for higher flow rates than found in normal tidal breathing, the spirometer designed in this thesis would need modification.

Overall, the results of the novel lung function test in human trials are promising. Clinically, this lung function test could impact current practice. Due to the lower levels of cooperation required from the subject, a wider cohort of patients could be assessed, and assessment could be more regular, improving monitoring, care and outcomes. Additionally, this test can be simply implemented in a small standalone device, as shown by the specialised spirometer designed for this project, or with standard lung function testing equipment such as a plethysmograph.

Chapter 11

FUTURE WORK

11.1 CLINICAL TESTING

All analysis of the novel lung function test in humans to date involved a cohort of healthy subjects. As such, the ability of this test to measure lung mechanics in the presence of lung disease is unknown. Further clinical trials are needed to determine the accuracy of the novel test for a wide range of disease types (eg COPD, asthma, pulmonary fibrosis) and for differing levels of disease severity. These trials would give insight into whether monitoring lung mechanics in outpatient care could be used as a predictor for disease type, with different diseases expected to have varying effect on lung elastance and resistance.

If successful, this novel lung function test would be a break-through for outpatient respiratory care, providing clinically important information during tidal breathing, while significantly reducing stress for both patient and clinician. These clinical trials will likely require close cooperation and support from respiratory specialists and patients with respiratory disease to be successful.

11.2 MODELS AND METHODS

Further work could develop the model used in the novel lung function test. The single compartment lung model used by the lung function test is extremely simplistic. The model could miss important lung mechanics, as shown in this thesis when viscoelastic lung mechanics were assessed. More detailed insight into lung condition could be obtained by modifying the lung function test for use with more complex lung models, while still retaining identifiability. The additional information provided by a more detailed model could provide essential insight into lung condition not provided by the current test.

The lung function test developed in this thesis occluded breathing once briefly during normal expiration. This provides insight into lung mechanics at only one point in the breathing cycle. Future work could assess whether occluding multiple times during a breath could provide further insight into how lung mechanics vary over time during the breathing cycle.

11.3 DEVICE

Further development of the specialised spirometer device created will likely be needed for future model changes and validation. The changes required to develop a lower resistance device, and more accurate device are described in Chapter 9. In its current design, the spirometer is capable of measuring pressure and flow during normal, quiet tidal breathing. In future work, if monitoring of elevated breathing rates is required, for example during exercise or peak breathing effort, the design will require updates to accommodate a higher flow rate..

Appendix A

APPENDICES

A.1 DERIVATION OF NATURAL RESPONSE OF LUNG

The single compartment lung model is defined:

$$P_{aw}(t) = R_{rs}Q(t) + E_{rs}V(t) + P_0 \tag{A.1}$$

where P_{aw} is airway pressure, t is time, R_{rs} is resistance of the conducting airways, Q is airflow, E_{rs} is respiratory elastance (inverse of compliance), V is inspired volume, and P_0 is positive end expiratory pressure (PEEP) (Bates [2009]).

This model does not account for any patient breathing effort. Thus, any changes in pressure or flow caused by muscular breathing efforts can result in incorrect measurements of underlying respiratory mechanics (Brochard et al. [2012], Grinnan and Truwit [2005], Kannangara et al. [2016], Newberry et al. [2015]). In this derivation, R_{rs} and E_{rs} are assumed to be constant at all times.

P_{aw} is equal to the total driving pressure. This pressure can be supplied by the respiratory muscles or a ventilator for Subjects in respiratory failure. During passive expiration, all airflow can be attributed to elastic recoil of the lung and diaphragm. The supplied pressure supports both the pressure driving airflow and the pressure needed to prevent lung collapse at the end of expiration, PEEP. Thus, the pressure required just to drive airflow, P_d, can be defined:

$$P_d(t) = R_{rs}Q(t) + E_{rs}V(t) \tag{A.2}$$

Any airflow into or out of the lung will create a change in lung pressure, dependent

on the lung elastance. A more elastic lung will resist airflow, resulting in a slower rate of change of lung pressure. The relationship between airflow and lung pressure is defined:

$$Q(t) = \frac{1}{E_{rs}} \frac{dP_{lung}(t)}{dt} \tag{A.3}$$

Substituting, equation A.3 into equation A.2 results in a non-homogeneous ordinary differential equation (ODE) relating the driving pressure supplied by the ventilator and lung pressure:

$$P_d(t) = \frac{R_{rs}}{E_{rs}} \frac{dP_{lung}(t)}{dt} + P_{lung}(t) \tag{A.4}$$

During passive expiration no driving pressure is supplied by respiratory muscles or a ventilator, $P_d = 0$. Solving equation A.4 for $P_d = 0$, the modeled lung pressure during expiration becomes:

$$P_{lung}(t) = P_{lung}(0) e^{\frac{-tE_{rs}}{R_{rs}}} \tag{A.5}$$

The expected flow measured in expiration can now be found by substituting P_{lung} from Equation A.5, into Equation A.3 yielding:

$$Q = \frac{-P_{lung}(0)}{R_{rs}} e^{\frac{-tE_{rs}}{R_{rs}}} \tag{A.6}$$

Equation A.6 shows that during passive expiration, the expected air flow out of the lung would be exponentially decaying. This response is observed in expiration for MV patients, confirming that this model is appropriate for passive expiration. Additionally, this response shows that for passive expiration the model becomes structurally non-identifiable, because E_{rs} and R_{rs} have a combined affect on the exponential decay rate.

A.2 SCHEMATICS

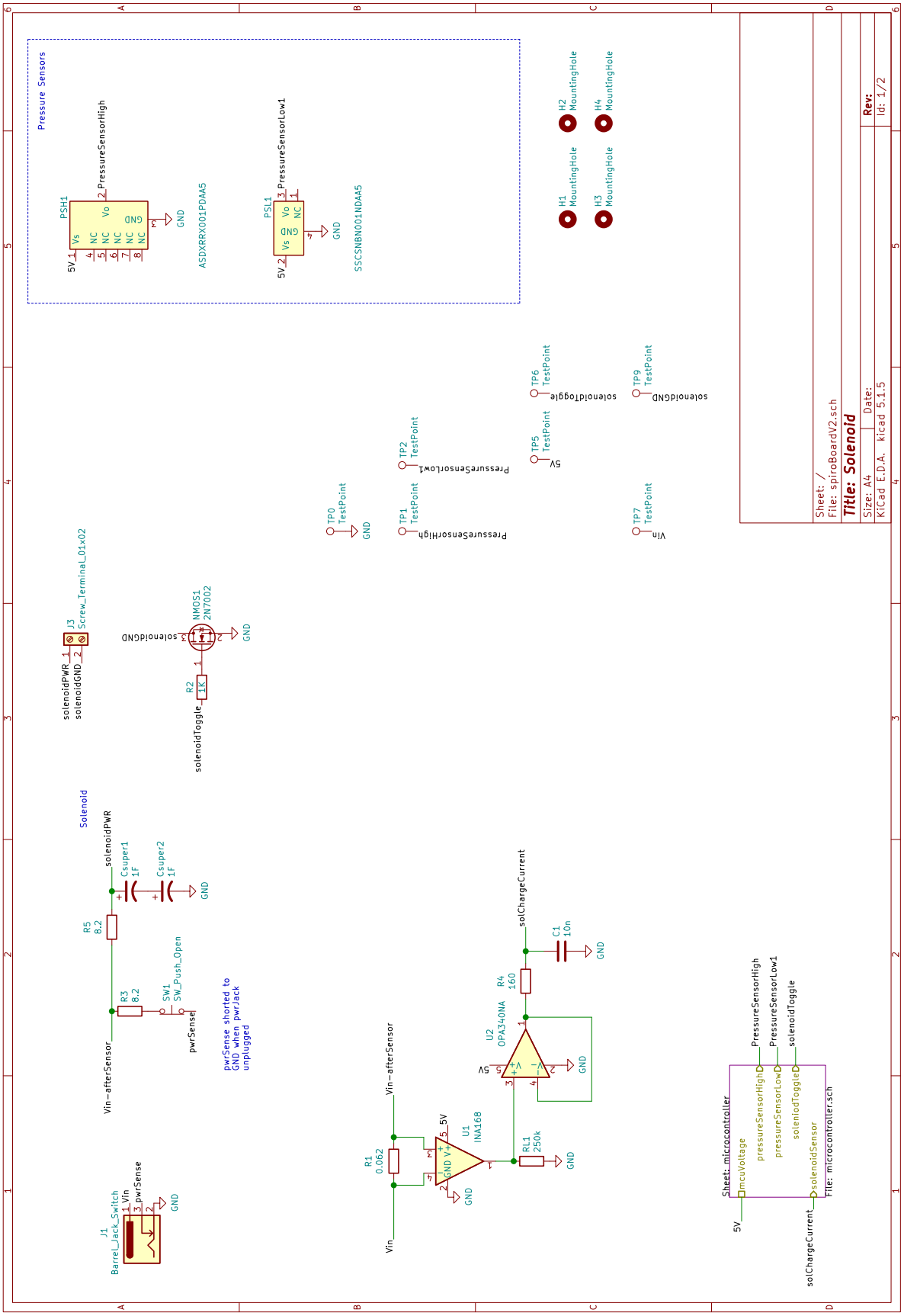

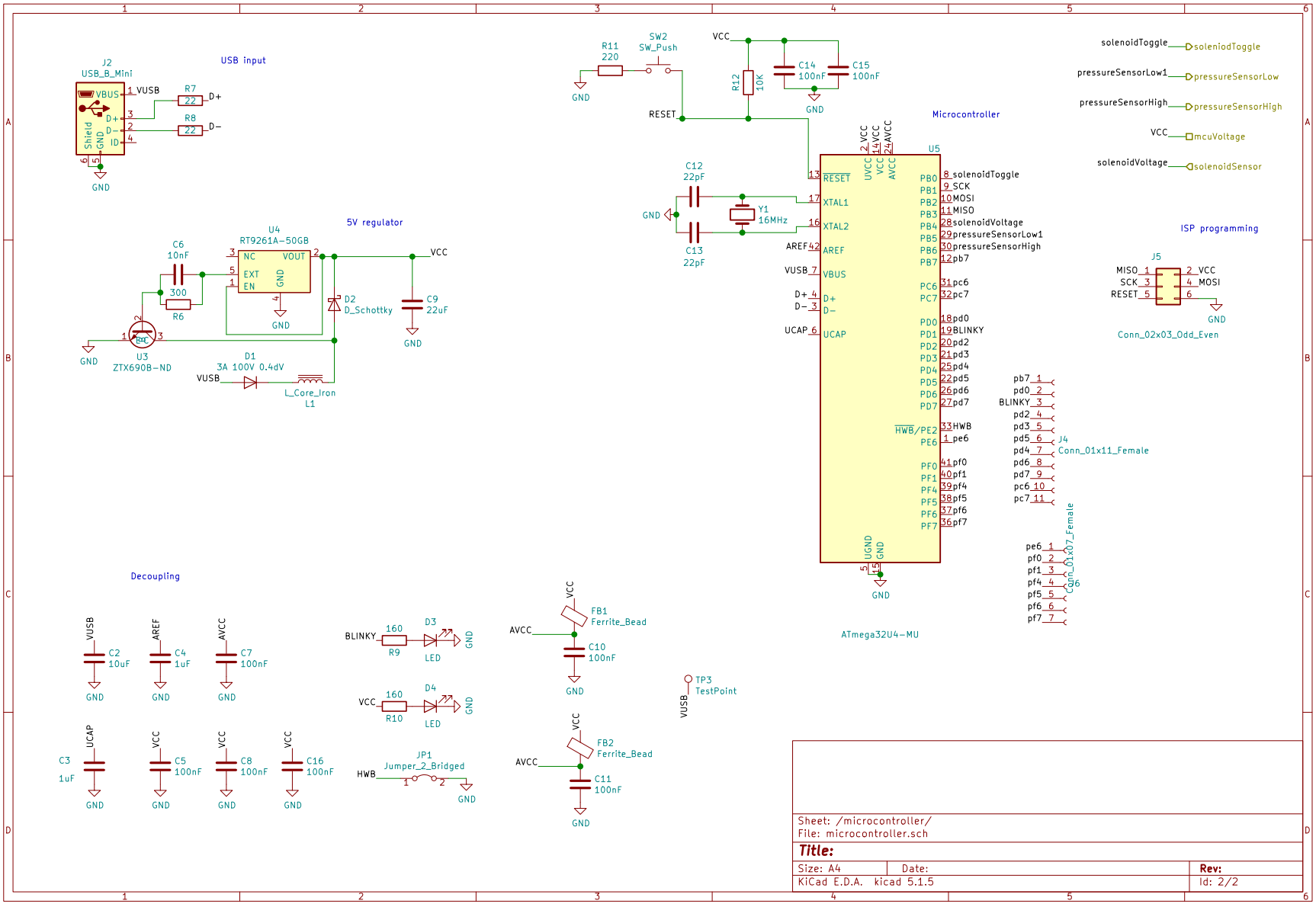
USB input
J2
USB_B_Mini
VBUS
D+
D-
ID
Shield
GND
VUSB
R7
22
D+
R8
22
D-
GND
5V regulator
U4
RT9261A-50GB
NC
VOUT
EXT
EN
GND
C6
10nF
300
R6
U3
ZTX690B-ND
D2
D_Schottky
C9
22uF
VCC
D1
3A 100V 0.4dV
VUSB
L_Core_Iron
L1
Microcontroller
U5
RESET
XTAL1
XTAL2
AREF
VBUS
D+
D-
UCAP
UVCC
VCC
AVCC
UGND
PB0 solenoidToggle
PB1 SCK
PB2 MOSI
PB3 MISO
PB4 solenoidVoltage
PB5 pressureSensorLow1
PB6 pressureSensorHigh
PB7 pb7
PC6 pc6
PC7 pc7
PD0 pd0
PD1 BLINKY
PD2 pd2
PD3 pd3
PD4 pd4
PD5 pd5
PD6 pd6
PD7 pd7
HWB/PE2 HWB
PE6 pe6
PF0 pf0
PF1 pf1
PF4 pf4
PF5 pf5
PF6 pf6
PF7 pf7
ATmega32U4-MU
R11
220
SW2
SW_Push
R12
10K
C14
100nF
C15
100nF
C12
22pF
C13
22pF
Y1
16MHz
solenoidToggle
pressureSensorLow1
pressureSensorHigh
VCC
solenoidVoltage
solenoidToggle
pressureSensorLow
pressureSensorHigh
mcuVoltage
solenoidSensor
ISP programming
J5
MISO
SCK
RESET
VCC
MOSI
Conn_02x03_Odd_Even
J4
Conn_01x11_Female
J6
Conn_01x07_Female
Decoupling
C2
10uF
C4
1uF
C7
100nF
C3
1uF
C5
100nF
C8
100nF
C16
100nF
BLINKY
160
R9
D3
LED
VCC
160
R10
D4
LED
JP1
Jumper_2_Bridged
HWB
FB1
Ferrite_Bead
C10
100nF
FB2
Ferrite_Bead
C11
100nF
AVCC
TP3
TestPoint
Sheet: /microcontroller/
File: microcontroller.sch
Title:
Size: A4
Date:
Rev:
KiCad E.D.A. kicad 5.1.5
Id: 2/2

A.2.1 Electronics located on mouthpiece

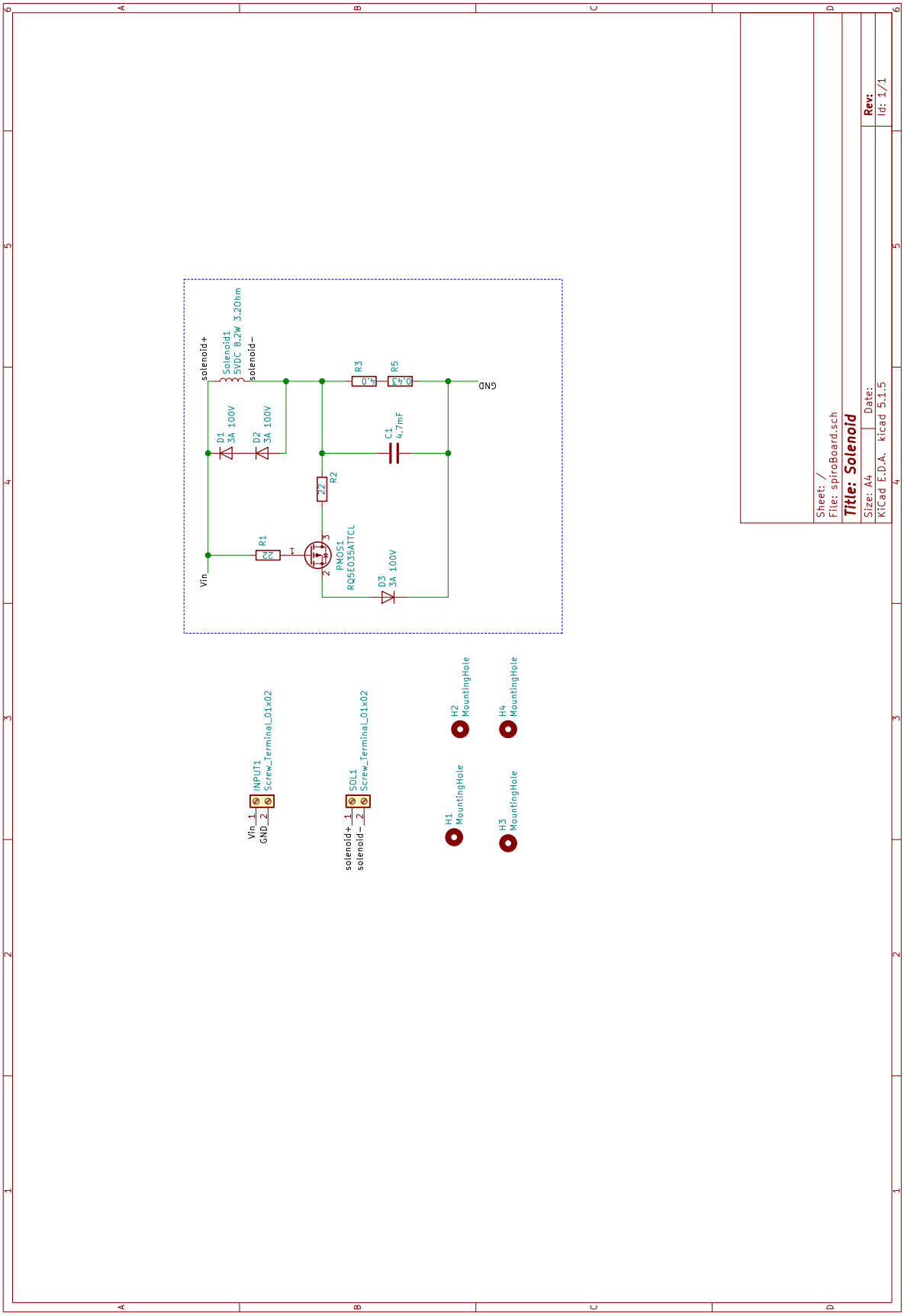

A.3 SPIROMETER BODY AND HOUSING

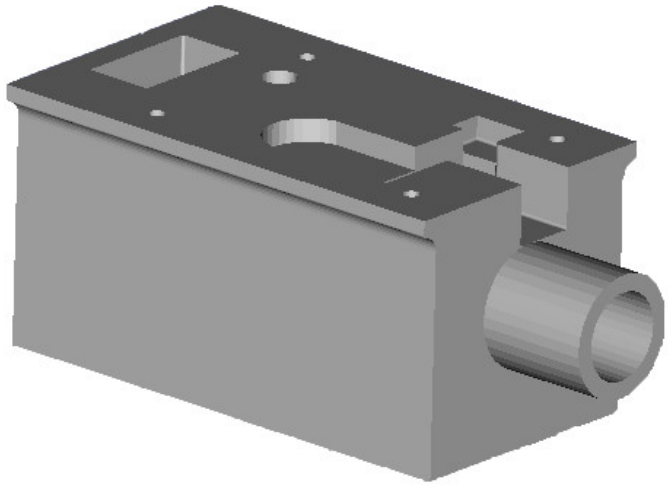

Figure A.1 Body of the prototype spirometer. The PCB containing the solenoid is mounted on top of the body. Air flows through the device, and up through the rectangular hole located at the back of the body. A housing is mounted over this hole to allow airflow occlusion by the solenoid.

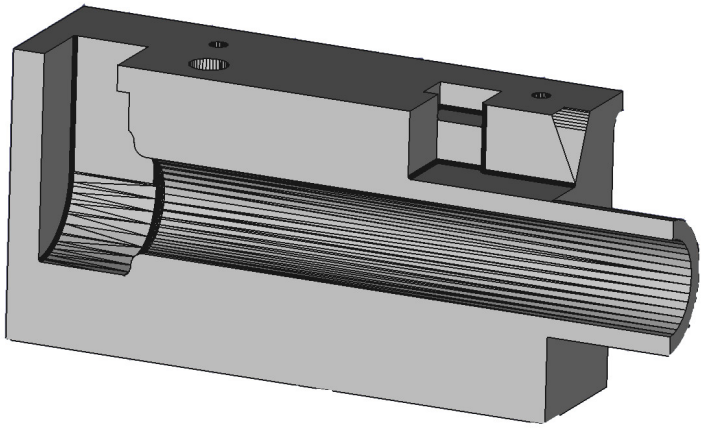

Figure A.2 A cross section of the prototype spirometer body showing the internal airways.

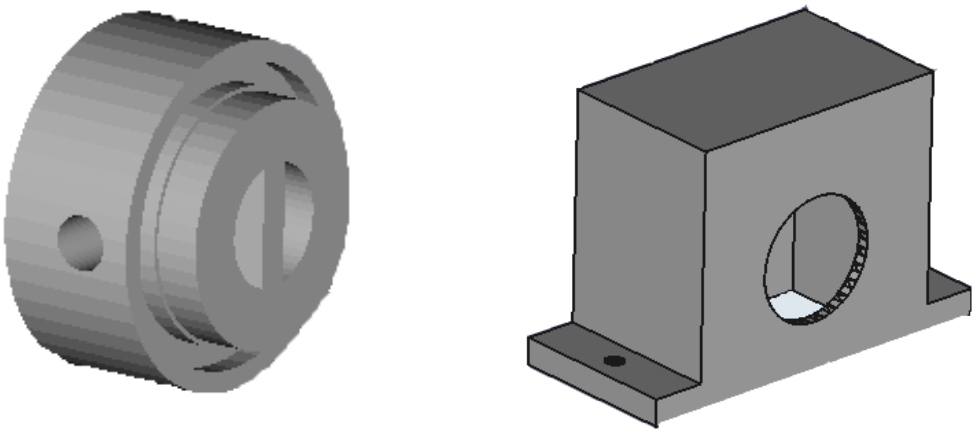

(a) Plug

(b) Housing for airflow outlet

Figure A.3 The plug to occlude airflow (a) and housing which was placed over the airflow outlet of the base (b). The plug is placed inside the housing and is attached to the end of the solenoid plunger. A groove in the front of the plug holds an o-ring. The o-ring creates a seal around the outlet hole in the housing, preventing airflow. The housing is secured to the base by 2 screws, located on the flanges either side of the main housing body. A gasket may be placed under the housing to create a better seal with the base.

REFERENCES

Adam, O., Cohen, I., Yip, W.K., Shiner, R.J., Calverley, P., Peles, Z., LaPrad, A., Dagan, Y., Brown, R., Solway, J. and Fredberg, J.J. (2018), 'Total lung capacity without plethysmography', *bioRxiv*, p. 395160.

Al-Rawas, N., Banner, M.J., Euliano, N.R., Tams, C.G., Brown, J., Martin, A.D. and Gabrielli, A. (2013), 'Expiratory time constant for determinations of plateau pressure, respiratory system compliance, and total resistance', *Critical Care*, Vol. 17, No. 1, p. R23.

Amato, M.B.P., Barbas, C.S.V., Medeiros, D.M., Magaldi, R.B., Schettino, G.D.P.P., Lorenzi-Filho, G., Kairalla, R.A., Deheinzelin, D., Munoz, C., Oliveira, R., Takagaki, T.Y. and Carvalho, C.R.R. (1998), 'Effect of a protective-ventilation strategy on mortality in the acute respiratory distress syndrome', *The New England Journal of Medicine*, Vol. 338, No. 6, pp. 347–354.

Ambrosino, N., Carpenè, N. and Gherardi, M. (2009), 'Chronic respiratory care for neuromuscular diseases in adults', *European Respiratory Journal*, Vol. 34, No. 2, pp. 444–451.

Antus, B. (2013), 'Pharmacotherapy of Chronic Obstructive Pulmonary Disease: A Clinical Review', *International Scholarly Research Notices*, Vol. 2013, p. e582807.

Arne, M., Lisspers, K., Ställberg, B., Boman, G., Hedenström, H., Janson, C. and Emtner, M. (2010), 'How often is diagnosis of COPD confirmed with spirometry?', *Respiratory Medicine*, Vol. 104, No. 4, pp. 550–556.

Balakrishnan, M. and Navaneeth, K.N. (2015), 'Detection of Plunger Movement in DC Solenoid', Tech. rep., Texas Instruments Incorporated.

Baoshun, M. and Bates, J.H.T. (2010), 'Modeling the Complex Dynamics of Derecruitment in the Lung', *Annals of Biomedical Engineering*, Vol. 38, No. 11, pp. 3466–77.

Barrow, A. and Pandit, J.J. (2017), 'Lung ventilation and the physiology of breathing', *Surgery (Oxford)*, Vol. 35, No. 5, pp. 227–233.

Bates, J.H., Baconnier, P. and Milic-Emili, J. (1988), 'A theoretical analysis of interrupter technique for measuring respiratory mechanics', *Journal of Applied Physiology*, Vol. 64, No. 5, pp. 2204–2214.

Bates, J.H.T. (2009), *Lung Mechanics: an Inverse Modeling Approach.*, Cambridge University Press, Leiden, oCLC: 609842956.

Ben-Tal, A. (2006), 'Simplified models for gas exchange in the human lungs', *Journal of Theoretical Biology*, Vol. 238, No. 2, pp. 474–495.

Benditt, J.O. (2005), 'Esophageal and Gastric Pressure Measurements', *Respiratory Care*, Vol. 50, No. 1, pp. 68–77.

Bijaoui, E., Champagne, V., Baconnier, P., Kimoff, R. and Bates, J. (2002), 'Mechanical Properties of the Lung and Upper Airways in Patients with Sleep-disordered Breathing', *American Journal of Respiratory and Critical Care Medicine*, Vol. 165, No. 8, pp. 1055–1061.

Brashier, B. and Salvi, S. (2015), 'Measuring lung function using sound waves: role of the forced oscillation technique and impulse oscillometry system', *Breathe*, Vol. 11, No. 1, pp. 57–65.

Brochard, L., Martin, G.S., Blanch, L., Pelosi, P., Belda, F.J., Jubran, A., Gattinoni, L., Mancebo, J., Ranieri, V.M., Richard, J.C.M., Gommers, D., Vieillard-Baron, A., Pesenti, A., Jaber, S., Stenqvist, O. and Vincent, J.L. (2012), 'Clinical review: Respiratory monitoring in the ICU - a consensus of 16', *Critical Care*, Vol. 16, No. 2, p. 219.

Burgel, P.R., Bergeron, A., Blic, J.d., Bonniaud, P., Bourdin, A., Chanez, P., Chinet, T., Dalphin, J.C., Devillier, P., Deschildre, A., Didier, A., Kambouchner, M., Knoop, C., Laurent, F., Nunes, H., Perez, T., Roche, N., Tillie-Leblond, I. and Dusser, D. (2013), 'Small airways diseases, excluding asthma and COPD: an overview', *European Respiratory Review*, Vol. 22, No. 128, pp. 131–147, publisher: European Respiratory Society Section: Review.

Caronia, J.R. (2016), 'Restrictive Lung Disease Treatment & Management: Medical Care, Surgical Care, Consultations', .

Chase, J.G., Preiser, J.C., Dickson, J.L., Pironet, A., Chiew, Y.S., Pretty, C.G., Shaw, G.M., Benyo, B., Moeller, K., Safaei, S., Tawhai, M., Hunter, P. and Desaive, T. (2018), 'Next-generation, personalised, model-based critical care medicine: a state-of-the art review of in silico virtual patient models, methods, and cohorts, and how to validation them', *BioMedical Engineering OnLine*, Vol. 17, No. 1, p. 24.

Cherniak, R.M. and Brown, E. (1965), 'A simple method for measuring total respiratory compliance; normal values for males', *Journal of applied Physiology*, Vol. 20, No. 1, pp. 87–91.

Chiew, Y.S. (2013), *Model-Based Mechanical Ventilation for the Critically Ill*, PhD thesis, University of Canterbury.

Chiew, Y.S., Chase, J.G., Shaw, G.M., Sundaresan, A. and Desaive, T. (2011), 'Model-based PEEP optimisation in mechanical ventilation', *BioMedical Engineering OnLine*, Vol. 10, p. 111.

Chiew, Y.S., Poole, S.F., Redmond, D.P., van Drunen, E.J., Damanhuri, N.S., Pretty, C., Docherty, P.D., Lambermont, B., Shaw, G.M., Desaive, T. and Chase, J.G. (2014), 'Time-Varying Respiratory Elastance for Spontaneously Breathing Patients', *IFAC Proceedings Volumes*, Vol. 47, No. 3, pp. 5659–5664.

Chiew, Y.S., Pretty, C., Docherty, P.D., Lambermont, B., Shaw, G.M., Desaive, T. and Chase, J.G. (2015a), 'Time-Varying Respiratory System Elastance: A Physiological Model for Patients Who Are Spontaneously Breathing', *PLOS ONE*, Vol. 10, No. 1, p. e0114847.

Chiew, Y.S., Pretty, C.G., Shaw, G.M., Chiew, Y.W., Lambermont, B., Desaive, T. and Chase, J.G. (2015b), 'Feasibility of titrating PEEP to minimum elastance for mechanically ventilated patients', *Pilot and Feasibility Studies*, Vol. 1, p. 9.

Coates, A.L., Tamari, I.E. and Graham, B.L. (2014), 'Role of spirometry in primary care', *Canadian Family Physician*, Vol. 60, No. 12, pp. 1069–1070.

Criée, C.P., Sorichter, S., Smith, H.J., Kardos, P., Merget, R., Heise, D., Berdel, D., Köhler, D., Magnussen, H., Marek, W., Mitfessel, H., Rasche, K., Rolke, M., Worth, H. and Jörres, R.A. (2011), 'Body plethysmography – Its principles and clinical use', *Respiratory Medicine*, Vol. 105, No. 7, pp. 959–971.

Damanhuri, N.S., Docherty, P.D., Chiew, Y.S., van Drunen, E.J., Desaive, T., Chase, J.G., Damanhuri, N.S., Docherty, P.D., Chiew, Y.S., van Drunen, E.J., Desaive, T. and Chase, J.G. (2014), 'A Patient-Specific Airway Branching Model for Mechanically Ventilated Patients, A Patient-Specific Airway Branching Model for Mechanically Ventilated Patients', *Computational and Mathematical Methods in Medicine, Computational and Mathematical Methods in Medicine*, Vol. 2014, 2014, p. e645732.

Damanhuri, N.S., Chiew, Y.S., Othman, N.A., Docherty, P.D., Pretty, C.G., Shaw, G.M., Desaive, T. and Chase, J.G. (2016), 'Assessing respiratory mechanics using pressure reconstruction method in mechanically ventilated spontaneous breathing patient', *Computer Methods and Programs in Biomedicine*, Vol. 130, pp. 175–185.

Das, A., Menon, P.P., Hardman, J.G. and Bates, D.G. (2013), 'Optimization of Mechanical Ventilator Settings for Pulmonary Disease States', *IEEE Transactions on Biomedical Engineering*, Vol. 60, No. 6, pp. 1599–1607.

de Ryk, J., Thiesse, J., Namati, E. and McLennan, G. (2007), 'Stress distribution in a three dimensional, geometric alveolar sac under normal and emphysematous conditions', *International Journal of Chronic Obstructive Pulmonary Disease*, Vol. 2, No. 1, pp. 81–91.

Delacourt, C., Lorino, H., Herve-Guillot, M., Reinert, P., Harf, A. and Housset, B. (2000), 'Use of the forced oscillation technique to assess airway obstruction and reversibility in children', *American journal of respiratory and critical care medicine*, Vol. 161, No. 3, pp. 730–736.

Desai, J.P. and Moustarah, F. (2019), 'Pulmonary Compliance', In *StatPearls*, StatPearls Publishing, Treasure Island (FL).

Di Mango, A.M.G.T., Lopes, A.J., Jansen, J.M. and Melo, P.L. (2006), 'Changes in respiratory mechanics with increasing degrees of airway obstruction in COPD: detection by forced oscillation technique', *Respiratory Medicine*, Vol. 100, No. 3, pp. 399–410.

Docherty, P.D., Chase, J.G., Lotz, T.F. and Desaive, T. (2011), 'A graphical method for practical and informative identifiability analyses of physiological models: A case study of insulin kinetics and sensitivity', *BioMedical Engineering OnLine*, Vol. 10, p. 39.

DuBois, A.B., Botelho, S.Y. and Comroe, J.H. (1956), 'A new method for measuring airway resistance in man using body plethysmography: Values in normal subjects and in patients with respiratory disease', *Journal of Clinical Investigation*, Vol. 35, No. 3, pp. 327–335.

Eric Yat-Tung Chan (2007), 'Use of the interrupter technique in assessment of lung function', *Journal of Paediatric Respirology and Critical Care*, Vol. 3, No. 4, pp. 6–8.

Freezer, N.J., Nicholai, T. and Sly, P.D. (1993), 'Effect of volume history on measurements of respiratory mechanics using the interrupter technique', *Pediatric Research*, Vol. 33, No. 3, p. 6.

Galetke, W., Feier, C., Muth, T., Ruehle, K.H., Borsch-Galetke, E. and Randerath, W. (2007), 'Reference values for dynamic and static pulmonary compliance in men', *Respiratory Medicine*, Vol. 101, No. 8, pp. 1783–1789.

Gong, B., Krueger-Ziolek, S., Moeller, K., Schullcke, B. and Zhao, Z. (2015), 'Electrical impedance tomography: functional lung imaging on its way to clinical practice?', *Expert Review of Respiratory Medicine*, Vol. 9, No. 6, pp. 721–737.

Grinnan, D.C. and Truwit, J.D. (2005), 'Clinical review: Respiratory mechanics in spontaneous and assisted ventilation', *Critical Care*, Vol. 9, No. 5, pp. 472–484.

Guo, Y.F., Herrmann, F., Michel, J.P. and Janssens, J.P. (2005), 'Normal values for respiratory resistance using forced oscillation in subjects >65 years old', *European Respiratory Journal*, Vol. 26, No. 4, pp. 602–608.

Gólczewski, T., Lubiński, W. and Chciałowski, A. (2012), 'A mathematical reason for FEV1/FVC dependence on age', *Respiratory Research*, Vol. 13, p. 57.

Hadjikoumi, I., Hassan, A. and Milner, A.D. (2003), 'Effects of respiratory timing and cheek support on resistance measurements, before and after bronchodilation in asthmatic children using the interrupter technique', *Pediatric Pulmonology*, Vol. 36, No. 6, pp. 495–501.

Hill, K., Goldstein, R.S., Guyatt, G.H., Blouin, M., Tan, W.C., Davis, L.L., Heels-Ansdell, D.M., Erak, M., Bragaglia, P.J., Tamari, I.E., Hodder, R. and Stanbrook, M.B. (2010), 'Prevalence and underdiagnosis of chronic obstructive pulmonary disease among patients at risk in primary care', *CMAJ : Canadian Medical Association Journal*, Vol. 182, No. 7, pp. 673–678.

Hofmann, G., Haan, L. and Anderson, J. (2016), 'Esophageal Pressure Measurements in Patients With Acute Respiratory Distress Syndrome', *Critical Care Nurse*, Vol. 36, No. 5, pp. 27–35.

Howe, S.L., Chase, J.G., Redmond, D.P., Morton, S.E., Kim, K.T., Pretty, C., Shaw, G.M., Tawhai, M.H. and Desaive, T. (2020), 'Inspiratory respiratory mechanics estimation by using expiratory data for reverse-triggered breathing cycles', *Computer Methods and Programs in Biomedicine*, Vol. 186, p. 105184.

Ignacio-Garcia, J.M. and Gonzalez-Santos, P. (1995), 'Asthma self-management education program by home monitoring of peak expiratory flow.', *American Journal of Respiratory and Critical Care Medicine*, Vol. 151, No. 2, pp. 353–359.

Jaeger, M.J. (1982), 'Effect of the cheeks and the compliance of alveolar gas on the measurement of respiratory variables', *Respiration Physiology*, Vol. 47, No. 3, pp. 325–340.

Johnson, J.D. and Theurer, W.M. (2014), 'A Stepwise Approach to the Interpretation of Pulmonary Function Tests - American Family Physician', *American Family Physician*, Vol. 89, No. 5, pp. 359–366.

Kaczka, D.W. and Dellacá, R.L. (2011), 'Oscillation mechanics of the respiratory system: Applications to lung disease', *Critical reviews in biomedical engineering*, Vol. 39, No. 4, pp. 337–359.

Kaminsky, D.A. (2012), 'What Does Airway Resistance Tell Us About Lung Function?', *Respiratory Care*, Vol. 57, No. 1, pp. 85–99.

Kannangara, D.O., Newberry, F., Howe, S., Major, V., Redmond, D., Szlavecs, A., Chiew, Y.S., Pretty, C., Benyo, B., Shaw, G.M. and Chase, J.G. (2016), 'Estimating the true respiratory mechanics during asynchronous pressure controlled ventilation', *Biomedical Signal Processing and Control*, Vol. 30, pp. 70–78.

Khirani, S., Polese, G., Aliverti, A., Appendini, L., Nucci, G., Pedotti, A., Colledan, M., Lucianetti, A., Baconnier, P. and Rossi, A. (2010), 'On-line monitoring of lung mechanics during spontaneous breathing: a physiological study', *Respiratory Medicine*, Vol. 104, No. 3, pp. 463–471.

Kim, K.T., Chiew, Y.S., Pretty, C., Shaw, G.M., Desaive, T. and Chase, J.G. (2015), 'Breath-to-breath respiratory mechanics variation: how much variation should we expect?', *Critical Care*, Vol. 19, No. 1, p. P260.

Kim, K.T., Redmond, D.P., Morton, S.E., Howe, S.L., Chiew, Y.S. and Chase, J.G. (2017), 'Quantifying patient effort in spontaneously breathing patient using negative component of dynamic Elastance', *IFAC-PapersOnLine*, Vol. 50, No. 1, pp. 5486–5491.

Kim, K.T., Howe, S., Chiew, Y.S., Knopp, J. and Chase, J.G. (2018), 'Lung Mechanics in Premature infants: Modelling and clinical validation', *IFAC-PapersOnLine*, Vol. 51, No. 27, pp. 225–230.

Kitaoka, H., Nieman, G.F., Fujino, Y., Carney, D., DiRocco, J. and Kawase, I. (2007), 'A 4-dimensional model of the alveolar structure', *The journal of physiological sciences: JPS*, Vol. 57, No. 3, pp. 175–185.

Kress, J.P., Pohlman, A.S., O'Connor, M.F. and Hall, J.B. (2000), 'Daily Interruption of Sedative Infusions in Critically Ill Patients Undergoing Mechanical Ventilation', *New England Journal of Medicine*, Vol. 342, No. 20, pp. 1471–1477.

Krueger-Ziolek, S., Schullcke, B., Gong, B., Müller-Lisse, U. and Moeller, K. (2017), 'EIT based pulsatile impedance monitoring during spontaneous breathing in cystic fibrosis', *Physiological Measurement*, Vol. 38, No. 6, pp. 1214–1225.

Lai-Fook, S.J. and Rodarte, J.R. (1991), 'Pleural pressure distribution and its relationship to lung volume and interstitial pressure', *Journal of Applied Physiology (Bethesda, Md.: 1985)*, Vol. 70, No. 3, pp. 967–978.

Lucangelo, U., Bernabè, F. and Blanch, L. (2007), 'Lung mechanics at the bedside: make it simple', *Current Opinion in Critical Care*, Vol. 13, No. 1, pp. 64–72.

M. B. McIlroy and E. S. Thomlinson (1955), 'The mechanics of breathing in newly born babies', *Thorax*, Vol. 10, No. 1, pp. 58–61.

Magnoni, M.S., Caminati, M., Senna, G., Arpinelli, F., Rizzi, A., Dama, A.R., Schiappoli, M., Bettoncelli, G. and Caramori, G. (2015), 'Asthma under/misdiagnosis in primary care setting: an observational community-based study in Italy', *Clinical and Molecular Allergy : CMA*, Vol. 13.

Major, V., Corbett, S., Redmond, D., Beatson, A., Glassenbury, D., Chiew, Y.S., Pretty, C., Desaive, T., Szl{\'\a}vecz, \., Beny{'\o}, B., Shaw, G.M. and Chase, J.G. (2016), 'Respiratory mechanics assessment for reverse-triggered breathing cycles using pressure reconstruction', *Biomedical Signal Processing and Control*, Vol. 23, pp. 1–9.

Mavili, E., Büyükoğlan, H., Çomu, N.B. and Güleç, M. (2010), 'Expiratory CT: Correlation With Pulmonary Function Tests And Value For Discriminating Lung Diseases', *European Journal of General Medicine*, Vol. 7, No. 1, pp. 56–62.

McCann, U.G., Schiller, H.J., Carney, D.E., Gatto, L.A., Steinberg, J.M. and Nieman, G.F. (2001), 'Visual Validation of the Mechanical Stabilizing Effects of Positive End-Expiratory Pressure at the Alveolar Level', *Journal of Surgical Research*, Vol. 99, No. 2, pp. 335–342.

Mead, J. and Whittenberger, J.L. (1953), 'Physical Properties of Human Lungs Measured During Spontaneous Respiration', *Journal of Applied Physiology*, Vol. 5, No. 12, pp. 779–796.

Miller, M.R., Hankinson, J., Brusasco, V., Burgos, F., Casaburi, R., Coates, A., Crapo, R., Enright, P., Grinten, C.P.M.v.d., Gustafsson, P., Jensen, R., Johnson, D.C., MacIntyre, N., McKay, R., Navajas, D., Pedersen, O.F., Pellegrino, R., Viegi, G. and Wanger, J. (2005), 'Standardisation of spirometry', *European Respiratory Journal*, Vol. 26, No. 2, pp. 319–338.

Miller, M.R., Quanjer, P.H., Swanney, M.P., Ruppel, G. and Enright, P.L. (2011), 'Interpreting lung function data using 80% predicted and fixed thresholds misclassifies more than 20% of patients', *Chest*, Vol. 139, No. 1, pp. 52–59.

Mohamed Hoesein, F.A.A., Zanen, P. and Lammers, J.W.J. (2011), 'Lower limit of normal or FEV1/FVC <0.70 in diagnosing COPD: An evidence-based review', *Respiratory Medicine*, Vol. 105, No. 6, pp. 907–15.

Morton, S.E., Dickson, J.L., Chase, J.G., Docherty, P.D., Howe, S.L., Shaw, G.M. and Tawhai, M. (2018a), 'Basis function identification of lung mechanics in mechanical ventilation for predicting outcomes of therapy changes: A first virtual patient', *IFAC-PapersOnLine*, Vol. 51, No. 15, pp. 299–304.

Morton, S.E., Knopp, J.L., Chase, J.G., Docherty, P.D., Howe, S.L., Shaw, G.M. and Tawhai, M. (2018b), 'Development of a Predictive Pulmonary Elastance Model to Describe Lung Mechanics throughout Recruitment Manoeuvres', *IFAC-PapersOnLine*, Vol. 51, No. 27, pp. 215–220.

Möller, K., Zhao, Z., Stahl, C., Schumann, S. and Guttmann, J. (2009), 'On the separate determination of lung mechanics in in-and expiration', In *4th European Conference of the International Federation for Medical and Biological Engineering*, Springer, pp. 2049–2052.

Navajas, D. and Farré, R. (2001), 'Forced oscillation assessment of respiratory mechanics in ventilated patients', *Critical Care*, Vol. 5, No. 1, pp. 3–9.

Newberry, F., Kannangara, O., Howe, S., Major, V., Redmond, D., Szlavecz, A., Chiew, Y.S., Pretty, C., Benyo, B., Shaw, G.M. and Chase, J.G. (2015), 'Iterative Interpolative Pressure Reconstruction for Improved Respiratory Mechanics Estimation During Asynchronous Volume Controlled Ventilation', In *SpringerLink*, Springer, Singapore, pp. 133–139.

Officer, T.M., Pellegrino, R., Brusasco, V. and Rodarte, J.R. (1998), 'Measurement of pulmonary resistance and dynamic compliance with airway obstruction', *Journal of Applied Physiology*, Vol. 85, No. 5, pp. 1982–1988.

Otis, A.B. (1954), 'The work of breathing', *Physiological reviews*, Vol. 34, No. 3, pp. 449–458.

Owens, M.W., Anderson, W.M. and George, R.B. (1991), 'Indications for spirometry in outpatients with respiratory disease', *Chest*, Vol. 99, No. 3, pp. 730–734.

Pakhale, S., Sumner, A., Coyle, D., Vandemheen, K. and Aaron, S. (2011), '(Correcting) misdiagnoses of asthma: a cost effectiveness analysis', *BMC Pulmonary Medicine*, Vol. 11, p. 27.

Panagou, P., Kottakis, I., Tzouvelekis, A., Anevlavis, S. and Bouros, D. (2004), 'Use of interrupter technique in assessment of bronchial responsiveness in normal subjects', *BMC Pulmonary Medicine*, Vol. 4, p. 11.

Patton, K.T. and Thibodeau, G.A. (2010), *Anatomy & Physiology*, Mosby Elsevier, 7th ed.

Pellegrino, R., Viegi, G., Brusasco, V., Crapo, R.O., Burgos, F., Casaburi, R., Coates, A., Grinten, C.P.M.v.d., Gustafsson, P., Hankinson, J., Jensen, R., Johnson, D.C., MacIntyre, N., McKay, R., Miller, M.R., Navajas, D., Pedersen, O.F. and Wanger, J. (2005), 'Interpretative strategies for lung function tests', *European Respiratory Journal*, Vol. 26, No. 5, pp. 948–968.

Rabe, K.F., Hurd, S., Anzueto, A., Barnes, P.J., Buist, S.A., Calverley, P., Fukuchi, Y., Jenkins, C., Rodriguez-Roisin, R., van Weel, C. and Zielinski, J. (2007), 'Global Strategy for the Diagnosis, Management, and Prevention of Chronic Obstructive Pulmonary Disease (ATS Journals)', *American Thoracic Society*, Vol. 176, No. 6, pp. 532–555.

Ranu, H., Wilde, M. and Madden, B. (2011), 'Pulmonary Function Tests', *The Ulster Medical Journal*, Vol. 80, No. 2, pp. 84–90.

Reddy, P.I., Al-Jumaily, A.M. and Bold, G.T. (2011), 'Dynamic surface tension of natural surfactant extract under superimposed oscillations', *Journal of Biomechanics*, Vol. 44, No. 1, pp. 156–163.

Redmond, D., Chiew, Y.S., Major, V. and Chase, J.G. (2016), 'Evaluation of model-based methods in estimating respiratory mechanics in the presence of variable patient effort', *computer methods and programs in biomedicine*, Vol. 171, pp. 67–79.

Redmond, D.P., Major, V., Corbett, S., Glassenbury, D., Beatson, A. and Chiew, Y.S. (2014), 'Pressure reconstruction by eliminating the demand effect of spontaneous respiration (PREDATOR) method for assessing respiratory mechanics of reverse-triggered breathing cycles', Vol. 1, Kuala Lumpur, pp. 332–337.

Redmond, D.P., Kim, K.T., Morton, S.E., Howe, S.L., Chiew, Y.S. and Chase, J.G. (2017), 'A Variable Resistance Respiratory Mechanics Model**The authors acknowledge the support of the Health Research Council (HRC) of New Zealand', *IFAC-PapersOnLine*, Vol. 50, No. 1, pp. 6660–6665.

Richard, J.C., Maggiore, S.M., Jonson, B., Mancebo, J., Lemaire, F. and Brochard, L. (2001), 'Influence of Tidal Volume on Alveolar Recruitment', *American Journal of Respiratory and Critical Care Medicine*, Vol. 163, No. 7, pp. 1609–1613.

Ruppel, G.L. and Enright, P.L. (2012), 'Pulmonary Function Testing', *Respiratory Care*, Vol. 57, No. 1, pp. 165–175.

Schena, E., Massaroni, C., Saccomandi, P. and Cecchini, S. (2015), 'Flow measurement in mechanical ventilation: A review', *Medical Engineering & Physics*, Vol. 37, No. 3, pp. 257–264.

Schifano, E.D., Hollenbach, J.P. and Cloutier, M.M. (2014), 'Mismatch between Asthma Symptoms and Spirometry: Implications for Managing Asthma in Children', *The Journal of Pediatrics*, Vol. 165, No. 5, pp. 997–1002.

Schirrmann, K., Mertens, M., Kertzscher, U., Kuebler, W.M. and Affeld, K. (2010), 'Theoretical modeling of the interaction between alveoli during inflation and deflation in normal and diseased lungs', *Journal of Biomechanics*, Vol. 43, No. 6, pp. 1202–1207.

Schranz, C., Docherty, P.D., Chiew, Y.S., Möller, K. and Chase, J.G. (2012), 'Iterative integral parameter identification of a respiratory mechanics model', *Biomedical engineering online*, Vol. 11, No. 1, p. 1.

Stanbrook, M.B. and Kaplan, A. (2008), 'The error of not measuring asthma', *Canadian Medical Association Journal*, Vol. 179, No. 11, pp. 1099–1100.

Stanojevic, S., Wade, A. and Stocks, J. (2010), 'Reference values for lung function: past, present and future', *The European Respiratory Journal*, Vol. 36, No. 1, pp. 12–19.

Stocks, J., Godfrey, S., Beardsmore, C., Bar-Yishay, E. and Castile, R. (2001), 'Plethysmographic measurements of lung volume and airway resistance', *European Respiratory Journal*, Vol. 17, No. 2, pp. 302–312.

Sundaresan, A. and Chase, J.G. (2012), 'Positive end expiratory pressure in patients with acute respiratory distress syndrome – The past, present and future', *Biomedical Signal Processing and Control*, Vol. 7, No. 2, pp. 93–103.

Sundaresan, A., Yuta, T., Hann, C.E., Chase, J.G. and Shaw, G.M. (2009), 'A minimal model of lung mechanics and model-based markers for optimizing ventilator treatment in ARDS patients', *Computer Methods and Programs in Biomedicine*, Vol. 95, No. 2, pp. 166–180.

Szlavecz, A., Chiew, Y.S., Redmond, D., Beatson, A., Glassenbury, D., Corbett, S., Major, V., Pretty, C., Shaw, G.M., Benyo, B., Desaive, T. and Chase, J.G. (2014), 'The Clinical Utilisation of Respiratory Elastance Software (CURE Soft): a bedside software for real-time respiratory mechanics monitoring and mechanical ventilation management', *BioMedical Engineering OnLine*, Vol. 13.

Talmor, D., Sarge, T., Malhotra, A., O'Donnell, C.R., Ritz, R., Lisbon, A., Novack, V. and Loring, S.H. (2008), 'Mechanical Ventilation Guided by Esophageal Pressure in Acute Lung Injury', *New England Journal of Medicine*, Vol. 359, No. 20, pp. 2095–2104.

Tawhai, M.H. and Bates, J.H.T. (2011), 'Multi-scale lung modeling', *Journal of Applied Physiology (Bethesda, Md.: 1985)*, Vol. 110, No. 5, pp. 1466–1472.

Tawhai, M.H., Hunter, P., Tschirren, J., Reinhardt, J., McLennan, G. and Hoffman, E.A. (2004), 'CT-based geometry analysis and finite element models of the human and ovine bronchial tree', *Journal of Applied Physiology (Bethesda, Md.: 1985)*, Vol. 97, No. 6, pp. 2310–2321.

Tepper, R.S., Pagtakhan, R.D. and Taussig, L.M. (1984), 'Noninvasive determination of total respiratory system compliance in infants by the weighted-spirometer method', *American Review of Respiratory Disease*, Vol. 130, No. 3, pp. 461 – 466.

Ulmer, W.T. and Schäfer, T. (2004), 'New insights into physiology and pathophysiology by resistance-volume recordings', *Journal of Physiology and Pharmacology*, Vol. 55, No. 3, pp. 149–153.

van Drunen, E.J., Chiew, Y.S., Chase, J.G., Shaw, G.M., Lambermont, B., Janssen, N., Damanhuri, N.S. and Desaive, T. (2013), 'Expiratory model-based method to monitor ARDS disease state', *BioMedical Engineering OnLine*, Vol. 12, No. 57.

van Drunen, E.J., Chiew, Y.S., Pretty, C., Shaw, G.M., Lambermont, B., Janssen, N., Chase, J.G. and Desaive, T. (2014), 'Visualisation of time-varying respiratory system elastance in experimental ARDS animal models', *BMC Pulmonary Medicine*, Vol. 14, No. 1, pp. 1–9.

Vicario, F., Albanese, A., Karamolegkos, N., Wang, D., Seiver, A. and Chbat, N. (2015), 'Noninvasive Estimation of Respiratory Mechanics in Spontaneously Breathing Ventilated Patients: A Constrained Optimization Approach.', *IEEE Transactions on Biomedical Engineering*, Vol. 83, pp. 775–787.

Vieira, S.R.R., Puybasset, L., Richecoeur, J., Lu, Q., Cluzel, P., Gusman, P.B., Coriat, P. and Rouby, J.J. (1998), 'A Lung Computed Tomographic Assessment of Positive End-Expiratory Pressure–induced Lung Overdistension', *American Journal of Respiratory and Critical Care Medicine*, Vol. 158, No. 5, pp. 1571–1577.

Vollmer, W.M., Gíslason, P., Burney, P., Enright, P.L., Gulsvik, A., Kocabas, A. and Buist, A.S. (2009), 'Comparison of spirometry criteria for the diagnosis of COPD: results from the BOLD study', *European Respiratory Journal*, Vol. 34, No. 3, pp. 588–597.

Ward, J. (2005), 'Physiology of breathing I', *Surgery (Oxford)*, Vol. 23, No. 11, pp. 419–424.

West, J.B. (1974), *Respiratory Physiology - The essentials*, The Williams & Wilkins Company.

Yang, I.A., Brown, J.L., George, J., Jenkins, S., McDonald, C.F., McDonald, V.M., Phillips, K., Smith, B.J., Zwar, N.A. and Dabscheck, E. (2017), 'COPD-X Australian and New Zealand guidelines for the diagnosis and management of chronic obstructive pulmonary disease: 2017 update', *The Medical Journal of Australia*, Vol. 207, No. 10, pp. 436–442.

Zhao, Z., Pulletz, S., Frerichs, I., Müller-Lisse, U. and Möller, K. (2014), 'The EIT-based global inhomogeneity index is highly correlated with regional lung opening in patients with acute respiratory distress syndrome', *BMC Research Notes*, Vol. 7, No. 1, p. 82.